Appendix A

Details of the Basic Reductions of the Photometry

A.1 Bias

There are 55 bias exposures, taken on 6 different nights, as listed in Table A.1.

Table A.1: The Bias Exposures

set #	night	#frames	dfsc #
1	2	10	1514–1526 (not: 1516 & 1518)
2	5	10	1909–1918
3	6	5	1921–1925
4	8	10	2192–2201
5	10	10	2499–2508
6	12	10	2558–2567

Notes: The names of the raw images from the DFOSC are in the form `dfsc`*nnnn*.

The frames within each set were combined. In this process, values in pixels affected by cosmic-ray-events were excluded. The bias level is around 124.2 ADU, but it is not the same in the 6 sets, it varies within ± 0.5 ADU. There is a positive gradient in the y-direction, but the slope is not the same for the 6 sets, it ranges from 0 to 0.5 ADU over the length of the chip (1024 pixels). There is no simple relation between the change of level and gradient, and time. These two phenomena are illustrated in Figure A.1.

As can also be seen in Figure A.1 (left), there are some stripes which run along y (i.e., across x). They are the same in the 6 frames, and are part of the bias image.

All the 6 frames were combined into one (weighting by the number of frames they had been made from). No further processing was done. We would have liked to smooth the image to remove the pixel-to-pixel noise, but since we believe the stripes to be part of the bias image, we could not do that. The mean bias level is 124.2 ADU/pixel. The standard deviation on the final bias image in areas between the vertical stripes is 0.31 ADU/pixel.

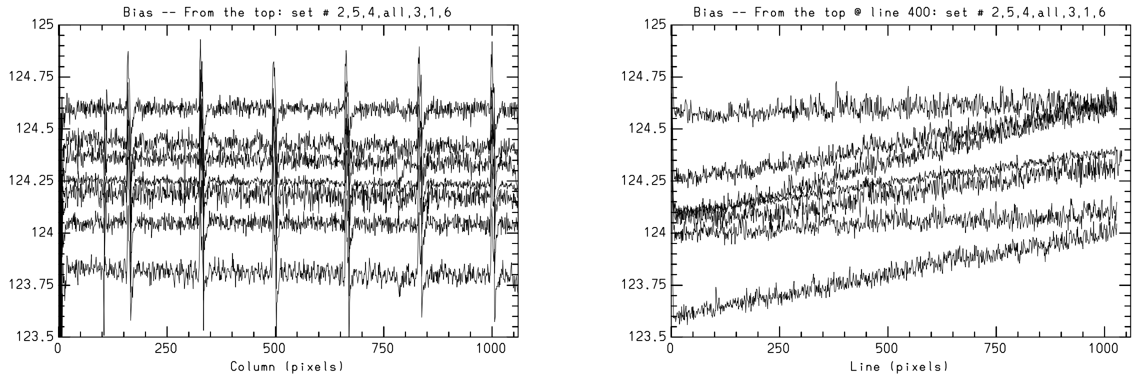

Figure A.1: The bias images from the 6 nights, and the mean bias image. Left: Along x (columns). Right: Along y (Lines). From the top (at $y = 400$): set 2, 5, 4, mean, 3, 1, and 6, corresponding to night 5, 10, 8, mean, 6, 2, and 12. All the images all have dimension 1060×1028, except the set 3 image (from night 6), which have dimension 1080×1040 (this image is extended only at large x and y, so that when trimming using the same section as for the rest of the images, one gets the same physical part of the CCD).

A.2 Dark

There are 22 dark exposures, all with exposure time 1 hour, taken on 7 different nights, as listed in Table A.2.

Table A.2: The Dark Exposures

image #	dfsc #	night	level
1	1511	2	5.09
2	1512	2	5.70
3	1513	2	7.51
4	1642	3	4.58
5	1643	3	5.04
6	1644	3	5.76
7	2057	6	16.13
8	2058	6	17.07
9	2059	6	23.15
10	2189	7	17.89
11	2190	7	25.09
12	2191	7	40.16
13	2353	8	23.83
14	2354	8	20.96
15	2355	8	22.77
16	2415	9	16.63
17	2416	9	17.90
18	2417	9	22.47
19	2418	9	32.98
20	2509	10	21.68
21	2510	10	31.07
22	2511	10	47.11

Notes: "level" is the median value (after bias subtraction). The median is approximated by `midpt` from `imstat`, using an upper cut of 200 to avoid most of the cosmic-ray-events.

The level histograms of the 22 images is shown in Figure A.2.

As is evident from Table A.2 and Figure A.2, the levels in the 22 images are *not* the same. Two effects are seen:

1. There is a big difference of the levels before and after the change of CCD temperature, which happened between night 5 and 6.

2. Within each night, there is a tendency towards higher levels for later times. Since the dark exposures were made in the morning, this indicates a light leak in the camera.

From this it was decided to make two dark frames, one for night 1–5, and one for night 6–14. The following frames were considered not affected by the light-leak, and therefore usable for constructing the two final dark images: 1, 2 (night 1), 4, 5, 6 (night 2), which were combined to the image dark1; and 7, 8 (night 6), 16, 17 (night 9), which were combined to the image dark2. The combination was done using a 2 sigma clipping (avsigclip) with a grow radius of 1. The images from night 8

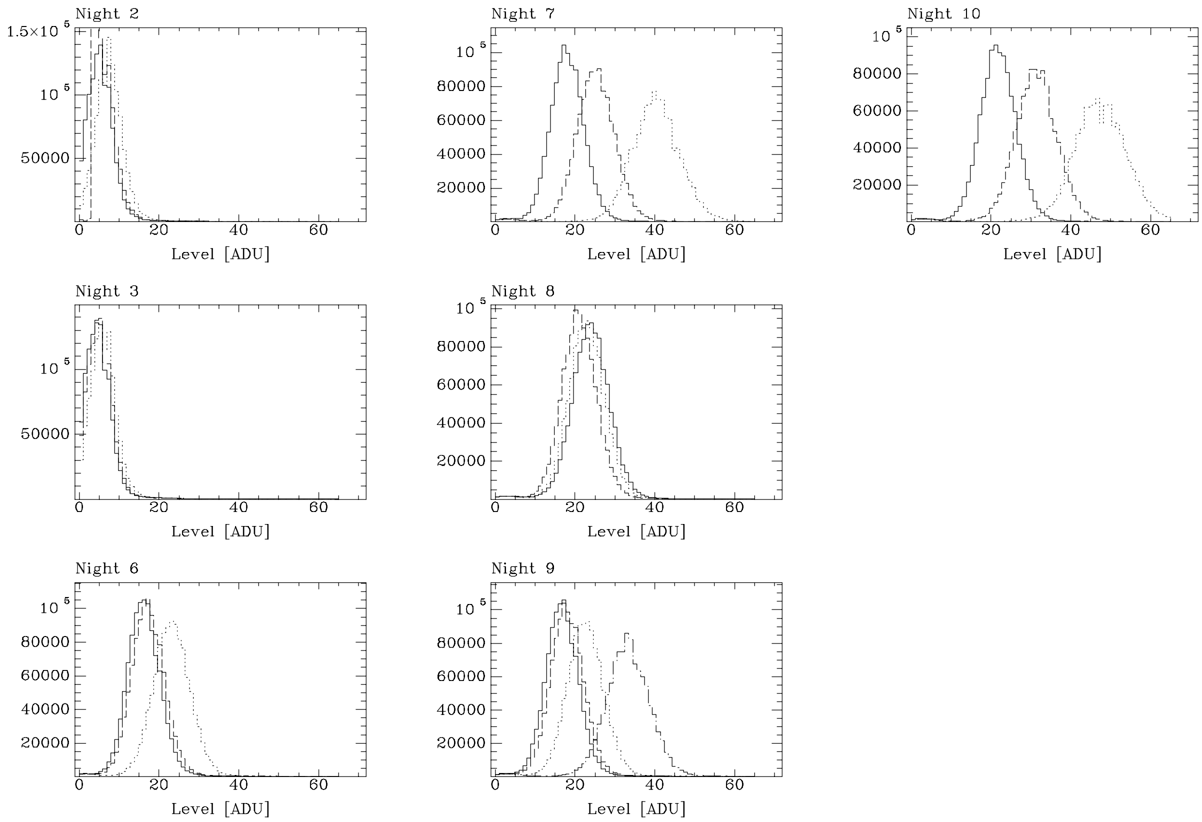

Figure A.2: The histograms for the 22 raw dark images. Within each night, the time order of the 3 or 4 frames are marked as solid, dashed, dotted, and dot-dashed.

was not used, since they all had a higher level, even though they did not show the time evolution the other did.

To get rid of the cosmic-ray-events, the values in the tails of the two combined images (dark1 and dark2) were replaced (using `imreplace`) by the median value, using the following values: dark1: values outside [INDEF,20.] replaced by 5.457, dark2: values outside [7.,27.] replaced by 17.14.

The two images (especially dark1) had a number of columns with higher or lower levels (the lower ones being fat zero, the higher ones probably being remanence), which were removed by linear interpolation of the unaffected neighboring pixels (using `fixpix`).

The dark images had now two kinds of structure left: some smooth variations, and a discontinuity between $y = 512$ and 513 (in the coordinates of the final 1024×1024 trimmed image). The two images, dark1 and dark2, where cut in halves according to the discontinuity, and to each of these 4 pieces a Legendre polynomial of third order in x and y with cross terms was fitted. Afterwards, the corresponding halves were joined. It was tested that these two new dark1 and dark2 images did not have any residuals or large scale gradients with respect to the "unsmoothed" ones. The two final dark images are shown in Figure A.3.

The two images do not exactly scale, the relative standard deviation on the quotient of the two is 2%. Given the low absolute counts, this is a small difference.

The mean dark levels the final two dark images are: dark1: 5.6 ADU/hour, dark2: 17.3 ADU/hour. The low frequency pattern, characterized by the standard deviation of the two images, is 0.12 (dark1) and 0.24 (dark2). Since they are smooth legendre polynomials, there is no

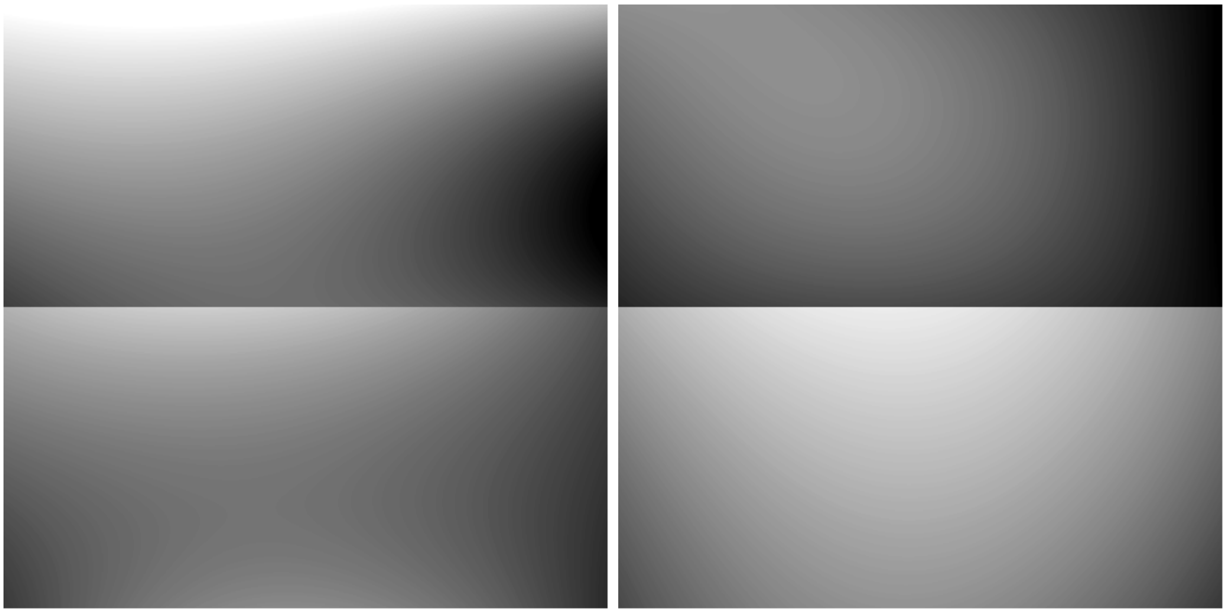

Figure A.3: The two final dark images. Left: dark1 (nights 1–5). Right: dark2 (nights 6–14). The display cuts for both images are ±2.5 standard deviations around the mean. The values from low to high are color coded as white to black.

pixel-to-pixel noise in them.

A.3 Shutter

If we ask the data acquisition system to make an exposure of time t, and it instead makes one of time $t + \delta$ (with $\delta \neq 0$), we have to make a *shutter correction*, where we multiply the image with $t/(t+\delta)$. δ can be a scalar (i.e. be the same for all the pixels), or it can an image (i.e. vary across the CCD), depending on what kind of shutter the system has.

δ can be determined from two images with different "apparent" exposure time t_1 and t_2, as follows: Since the CCD is a linear detector, when it is exposed to the intensity I in the time t_{real}, the level we read out N for a given pixel is proportional to the product of the two,

$$N_1 \propto I_1 \cdot t_{real,1} \tag{A.1}$$

$$N_2 \propto I_2 \cdot t_{real,2} \tag{A.2}$$

If we keep the intensity constant, and since we have $t_{real} = t + \delta$, we get

$$\frac{N_1}{N_2} = \frac{t_1 + \delta}{t_2 + \delta}, \quad t_1 \neq t_2, \tag{A.3}$$

from which we can determine δ.

One can use more images to get a better determination. We used the temporal sequence of one 10 sec, ten 1 sec, and one 10 sec exposure. If we let N_1' denote the sum of the levels in the ten 1 sec exposures, and N_2' the sum of the levels of the two 10 sec exposures, we get

$$\frac{N_1'}{N_2'} = \frac{10 \cdot (1\ \text{sec} + \delta)}{2 \cdot (10\ \text{sec} + \delta)} \tag{A.4}$$

which yields

$$\delta = \frac{10(2N_1'/N_2' - 1)}{10 - 2N_1'/N_2'}\ \text{sec} \tag{A.5}$$

For the determination of the shutter correction, a number of dome flats were taken, using the same lamp with constant voltage, thereby hoping to get a constant intensity. The images are listed in Table A.3.

The images in Table A.3 were corrected for bias and dark. The delta image was then computed using equation A.5 for each of the four (1×10 sec, 10×1 sec, 1×10 sec) sequences. The mean of the four was also calculated. The results are in Table A.4.

A visual inspection of the four delta images showed, that they were all almost flat, as the low standard deviations also suggest. There was, however, a small gradient in the x direction of about 0.001 sec, but since it was much lower than our estimated uncertainty of 0.02 sec (see below), we decided to neglect it.

Therefore, we decided to use a *scalar* delta value instead of a delta image. We set this delta value to the (scalar) mean of the mean delta image, which amounts to 0.41 sec. We estimate the uncertainty on this value to be half of the maximum difference between the four individual determinations, i.e. 0.02 sec.

The differences between the four is probably due to the light not being constant. The symmetric sequence (1×10 sec, 10×1 sec, 1×10 sec) makes the determination insensitive to a light variation which is linear in time, so the light variations was probably more ill-behaved than that.

A cl-script `b_dcorr` was written to implement the scalar shutter correction.

Table A.3: The Images Used to Determine the Shutter Correction

dfsc #	#frames	exp. time [sec]
2233	1	10
2234	1	10
2235–2244	10	1
2245	1	10
2246	1	10
2247–2256	10	1
2257	1	10
2258	1	10
2259–2268	10	1
2269	1	10
2270	1	10
2271–2280	10	1
2281	1	10
2282	1	10

Notes: All images are from night 8. The first and the last image in the table were not used.

Table A.4: Statistics of the four Individual Delta Images and the Mean Delta Image

image	mean	median	stddev
1	0.3999	0.3997	0.01101
2	0.4093	0.4090	0.01051
3	0.4004	0.4004	0.01065
4	0.4325	0.4323	0.01073
mean	0.4105	0.4105	0.00682

Notes: "median" is the `midpt` from `imstat`.

A.4 Linearity Test

We want to test, whether our CCD is linear, i.e. whether the level we read out (when bias has been subtracted, of course), N, is proportional to the integration time, t, times the intensity of the light reaching the CCD, I.

We envisioned that we could do two tests of the linearity of the CCD. An *indirect* test where we would test whether the conversion factor was constant with level, and a *direct* test where we would test whether the level per unit time was constant with level. Results from these two test are reported in Sect. A.4.1 and A.4.2 below.

For both purposes, 68 dome flats were taken, with an attempted constant light source. 2 filters were used: Johnson B (JB) and Gunn r (GR). Only the section `[1:1060,300:700]` (in untrimmed coordinates) was read out (this should not affect the results). All the images were taken in pairs with equal exposure time. The exposure time was varied in on order to span the full range of the CCD (0 – 65535 ADU). In between every one or two pairs of exposures with varying exposure time, a pair of exposures with exposure time 10 sec was taken. The sequence of exposure times is shown in Table A.5.

Table A.5: Exposure Times for the 34 Pairs of Images used for the Linearity Test

Johnson B:	10, 1, 2, 10, 4, 7, 10, 15, 20, 10, 30, 45, 10, 60, 10, 80, 10, 100, 10, 120, 10
Gunn r:	10, 2, 4, 7, 10, 15, 20, 10, 30, 45, 10, 55, 10

Notes: The exposure times are in seconds. The images are dfsc2284–2325 (JB) and dfsc2327–2352 (GR).

A.4.1 Conversion factor vs. level

`findgain` was used to determine the conversion factor (CF) and the read-out noise (RON) for the 34 pairs of images. The bias images dfsc1922 and 1925 (using the same section: `[1:1060,300:700]`) were used. These are from night 6 (whereas the dome flats used were from night 8). The bias images from night 6 are the ones which resembles the mean bias image the most.

`findgain` was used at the section `[480:0600,160:280]` (center of CCD) and `[910:1030,080:200]` (right hand side of CCD). It was suspected, that the CCD would behave strange in the right hand side. The result is shown in Figure A.4. It it seen that apparently CF increases with level. However, this can not be the case since the CCD found to be linear in the direct test, cf. Sect. A.4.2 below. More probable a malfunction in the read-out electronics caused RON to vary with the exposure level.

A direct way to calculate the RON in ADU is the fact, that the standard deviation on a bias image is the RON in ADU. The standard deviation of 5 raw bias images (dfsc1921–1925) was found to be 2.25 ADU (using `imstat` with an upper limit of 150 to cut cosmic-ray-events).

If we use only flat field images with levels above 1000 ADU and without severe cosmic-ray-events, we get CF = 1.95 e^{-}/ADU and RON = 2.25 ADU. These are the values that have been used hereafter.

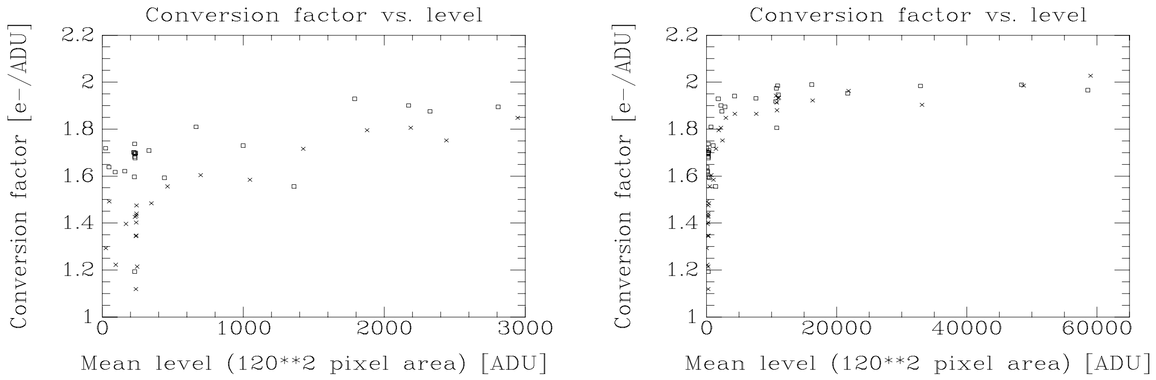

Figure A.4: Conversion factor versus level. Boxes: center of CCD, crosses: right hand side of CCD. Left: levels from 0 to 3000 ADU. Right: levels from 0 to 65000 ADU.

A.4.2 The direct test

A direct way of checking the linearity of the CCD is to plot level pr. unit time versus level, since if we have $N \propto I \cdot t$, and I is constant, then N/t is constant.

The level used before (e.g. in Figure A.4) was computed using `imstat` with a suitable upper cut to avoid cosmic-ray-events. To get more precise level, `fitsky` was used. This task fits a Gaussian to the histogram of the sky values and determines the mean level from the fit. The center area was defined as $(x, y) = (500, 200)$, and the right hand side area as $(x, y) = (995, 300)$, both with an inner radius (`annulus`) of 2.5 pixels and an outer radius (`dannulus`) of 40.0 pixels.

Since we have a number of images with the same exposure time (10 sec, see Table A.5), we can check whether the intensity really was constant by plotting the level versus the (clock) time. This is shown in Fig. A.5. It is seen that the illumination level was *not* constant.

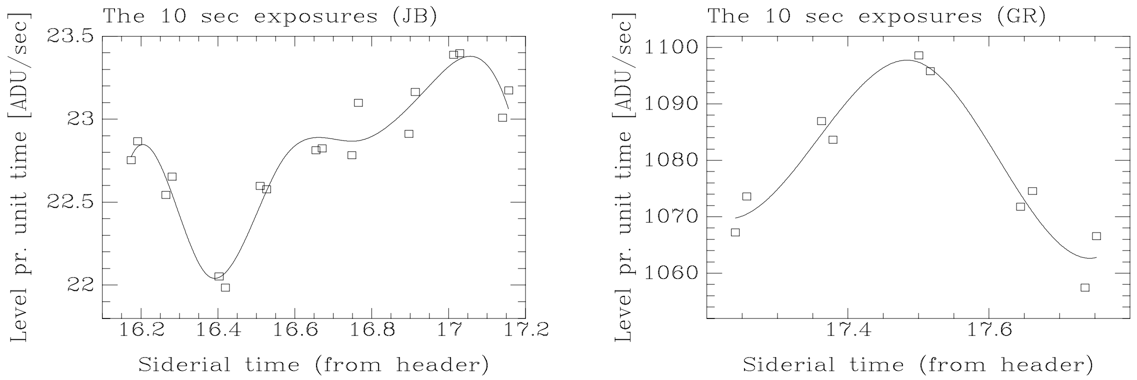

Figure A.5: The light variation with time. Left: Johnson B, the first sequence. Right: Gunn r, the second sequence. The levels shown are the ones in the center area; the right hand side area levels are different, but by a constant factor.

The points shown in Figure A.5 were fitted with a 5 piece (JB) / 2 piece (GR) cubic spline using `gfit1d`, as also shown in the figure.

All the N/t values for the 68 images were now divided by the fit to the time variation. Now N/t vs. t could be plotted, as shown in Figure A.6.

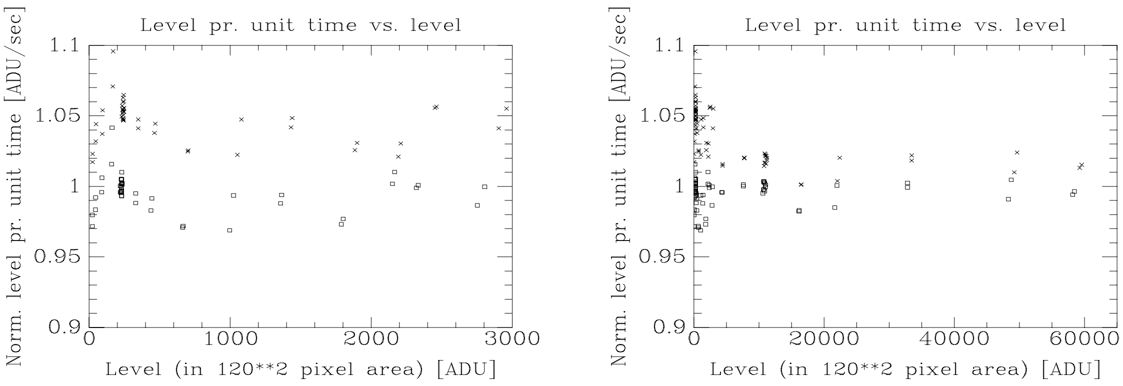

Figure A.6: The level pr. unit time normalized by the lamp time variation, versus the level. Boxes: center of CCD, crosses: right hand side of CCD. Note, that the center and right hand side values are normalized by the same function. The time dependence is the same in the two areas, but since the levels are not the same, there is an offset between the two in this graph. Left: levels from 0 to 3000 ADU. Right: levels from 0 to 65000 ADU.

As Figure A.6 shows, the CCD is in fact linear up to the very highest levels.

The rms standard deviation of all the data with levels > 100 ADU is 1.1%. The rms for the first sequence (JB) and the second sequence (GR) separately, is 1.4% and 0.7%, respectively. The reason for the difference is probably the more ill-behaved lamp variation for the first sequence, as seen in Figure A.5. We conclude, that the CCD is linear within 0.7%.

A.5 Fat Zero

Though the CCD on the overall is linear, it nevertheless turned out, that 20 of the 1024 columns were *not* linear – they were affected by the so-called fat zero effect.

The fat zero affected columns can be seen in the 2 dimensional images images as vertical stripes with (usually) lower level than the background.

This phenomenon was investigated using the dome flats used for the linearity test (with levels in the range 22 – 58437 ADU) and an extra sequence of dome flats with very low levels (with levels in the range 1 – 48 ADU). The very low level dome flats are dfsc2597–2616, from night 13 (filter: Johnson B). These were also corrected for bias, dark current, and shutter effect.

We have the following 3 sequences of images:

1. The very low level images, with exposure times 1, 2, 4, 7, 10, 13, 16, 20, 25, 30 sec, and levels in the range 1 – 48 ADU (filter: JB).

2. The low level images from the linearity test, with exposure times 1, 2, 4, 7, 10, 15, 20, 30, 45, 60, 80, 100, 120 sec, and levels in the range 22 – 2700 ADU (filter: JB).

3. The high level images from the linearity test, with exposure times 2, 4, 7, 10, 15, 20, 30, 45, 55 sec, and levels in the range 2100 – 58000 (filter: GR).

Within each of the 3 sequences, all the images with the same exposure time (usually this number is 2, except for the 10 sec images in the 2 last sequences, which were more numerous) and thus same level, were combined. That yielded 32 $(10 + 13 + 9)$ images.

These 32 images were now made 1 dimensional by averaging in the y-dimension using `blkavg`. This is because the fat zero effect only varies from column to column (x), not from line to line (y).

To find the columns affected by fat zero, the following was done: All the exposures in sequence 1 and all the non 10 sec exposures in sequence 2 was divided by the 10 sec exposure from sequence 2, and all the non 10 sec exposures in sequence 3 was divided by the 10 sec exposure from sequence 3. Since the 10 sec exposure from sequence 2 were made from 18 images, and the one from sequence 3 from 10 images, they both had better signal-to-noise (S/N) than the other ones.

If we did not have any fat zero columns, the plot of the quotients should be flat (within the noise and cosmic-ray-events), since the flat field pattern (which also is seen even in the 1 dimensional images) is divided out. By inspecting the 30 $(10 + 12 + 8)$ quotient plots, 44 fat zero column candidates were noted. The columns were in 6 "locations", with each location having a number of fat zero columns next to each other.

The fat zero effect as function of the level in the non-affected neighbor column was now measured as follows: In a 25 pixel wide area on each side of the given fat zero location the median value was calculated, and the mean of these 2 medians was defined as the background level. The level in each of the suspected fat zero columns together with the level in a test column on each side was measured, and the difference between the background level and the level in the given column calculated. This procedure is implemented in the cl-script `calc_fatzero`.

If the images had been flat fielded, the plot of a non fat zero column would be flat and zero (diff $= 0\cdot$background). When not flat fielded, one gets a straight line (diff $= k\cdot$background).

In the case of a fat zero column, one does not get a straight line, but a more complicated non-linear behavior. If the image has not been flat fielded, there might be a flat field effect of the form diff $= k\cdot$background superimposed, which will show up at high levels. Two examples are shown in Figure A.7.

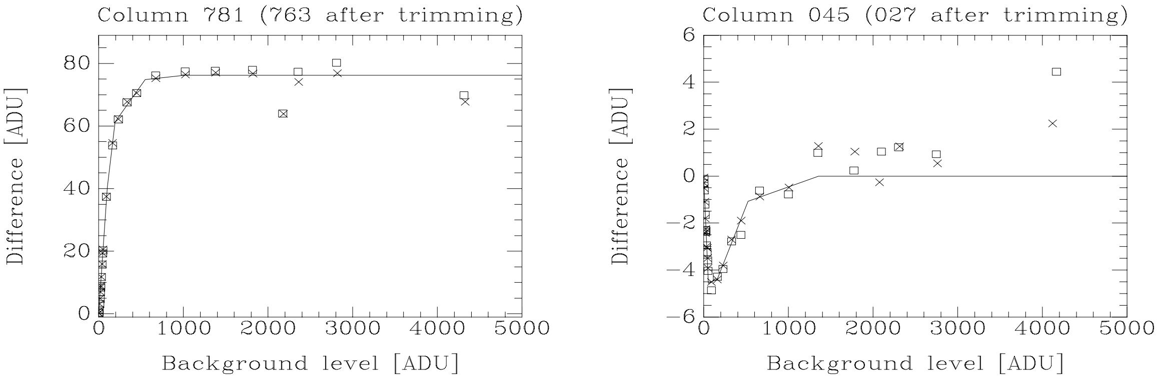

Figure A.7: 2 of the 20 fat zero columns. Boxes: before flat fielding, using a 2×25 pixel background area. Crosses: after flat fielding, using a 2×2 pixel background area. The fit to the flat fielded points is overplotted.

Table A.6: The 20 Fat Zero Columns

044, 045, 046; 098; 176, 177; 290, 291, 292; 781, 782, 783, 784, 785, 786, 787, 788; 949, 950, 951

Notes: The column numbers are in the untrimmed frame, after trimming subtract 18 pixels.

The plot similar to the ones shown in Figure A.7 were investigated for the 44 fat zero column candidates. Of these, 20 were actually fat zero columns with an effect > 1 ADU. The 20 columns are listed in Table A.6.

It was not possible to find any simple analytical function that fitted the fat zero effect as function of the background level, so it was decided to use the following piecewise linear function

$$f(x) = \begin{cases} (y_1 - 0)/(x_1 - 0) \cdot (x - 0) + 0 & ; \quad 0 \leq x < x_1 \\ (y_2 - y_1)/(x_2 - x_1) \cdot (x - x_1) + y_1 & ; \quad x_1 \leq x < x_2 \\ (y_3 - y_2)/(x_3 - x_2) \cdot (x - x_2) + y_2 & ; \quad x_2 \leq x < x_3 \\ (y_4 - y_3)/(x_4 - x_3) \cdot (x - x_3) + y_3 & ; \quad x_3 \leq x < x_4 \\ y_4 & ; \quad x_4 \leq x \end{cases} \tag{A.6}$$

where f is the difference and x is the background level. This is just a straight line between the following points: $(0,0)$, (x_1, y_1), (x_2, y_2), (x_3, y_3), (x_4, y_4), and (∞, y_4). The function has 8 free parameters: (x_i, y_i), $i = 1, \ldots, 4$. Two examples of the 8 fitted parameters are shown in Table A.7

Table A.7: Two examples of fat zero fit parameters.

Column	(x_1, y_1)	(x_2, y_2)	(x_3, y_3)	(x_4, y_4)
045 (027 after trimming)	(53.7,−4.57)	(160,−4.39)	(523,−1.07)	(1353,0)
781 (763 after trimming)	(100,40.4)	(193,61.3)	(548,74.8)	(1013,76.2)

The actual fitting was done using the task `nfit1d`, which uses least squares fitting implemented by a downhill simplex minimization algorithm ("amoeba").

In some cases we decided, that the asymptotic level should be zero (i.e. $y_4 = 0$), even though when fit y_4 might not turn out to be zero. An example is column 045, shown in Figure A.7.

The method requires an initial guess on the free parameters (x_i, y_i). The problem is not very well constrained, and is therefore quite sensitive to the initial conditions. Nevertheless, it produces a quite good fit, with lower residuals than the initial guess.

A cl-script `b_fatzero` was written. This procedure corrects a 2 dimensional image for the fat zero effect in the 20 columns, using equation (A.6) and the corresponding 20×8 coefficients. The background level is determined locally, i.e. it is not the same for the entire column.

We wanted to have our images flat fielded before we determined the fat zero correction. However, we could not make any flat fields as long as we were not able to correct for fat zero. Therefore, the above determination of the fat zero effect on the non flat fielded images is only a first approximation. We can now use this to make fat zero corrected flat fields, which we can then use to flat field our images, after which we can get a second approximation to the fat zero effect.

The 10 JB dome flats dfsc1670–1679 (night 4) and the 10 GR dome flats dfsc1808–1817 (night 5) were corrected for bias, dark, shutter, and fat zero as determined from the first iteration as mentioned above, and then combined. The two 2 dimensional images (using the same section as the fat zero images) were made 1 dimensional, and the 32 1 dimensional fat zero images were then flat fielded.

Now the measuring of the fat zero effect using `calc_fatzero` could be repeated, this time using areas for background level determination only 2 pixels wide (this is the width we want to use for the science images).

Hereafter, the fat zero functions could be fitted again. As seen in Figure A.7, the change from no flat fielding and 25 pixel background areas to flat fielding and 2 pixel background areas is not that big on small levels (< 5000 ADU). On larger levels (up to 65000 ADU), a bigger difference can be seen, with the flat fielded images indeed being more flat that the non flat fielded images.

`b_fatzero` was updated to use the new coefficients. The maximum correction for the 20 columns ranges from 1 to 76 ADU).

A.5.1 The Extra Correction

When all the science images (from night 1, 2, 3, 4, 6, & 9) were reduced using the fat correction mentioned above, it turned out, that it did not remove the fat zero stripes for the images from night 1–4. The fat zero effect had changed with the CCD temperature change between night 5 and 6, and since the images used to determine the fat zero effect were from night 8 and 13 (i.e. both after the temperature change), the established correction worked only for night 6–14.

Since we did not have the same type of calibration images taken before the temperature change, the extra correction needed to remove the fat zero effect from the night 1–5 images needed to be modeled from the science images.

The approach was the following: For all the science images from night 1–4: for all the 20 fat zero columns, and for the 6 background areas, the level (one number) representing the sky background (not the objects, such as galaxies and stars, which happens to be in that column somewhere) was calculated. This was done by a 3 step process: First guess, N_1, was `midpt` from `imstat` using no cuts. Second guess, N_2, was `midpt` using cuts $\pm 5\sigma$, with σ being the theoretical standard deviation corresponding to that level, $\sigma = (N/\mathrm{CF} + \mathrm{RON}^2_{\mathrm{ADU}})^{1/2}$, with $N = N_1$ in this step. Third and final guess, N_3, was `midpt` using cuts $\pm 3\sigma$, with σ being calculated using $N = N_2$. When having the level in the background and in the fat zero column, the difference can be calculated. This process was implemented in the cl-script `extra_fat`.

An example of the extra fat effect can be seen in Figure A.8.

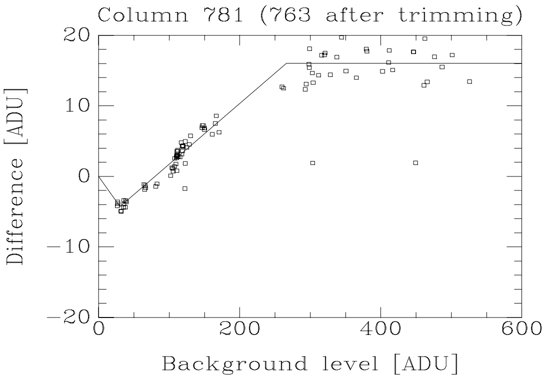

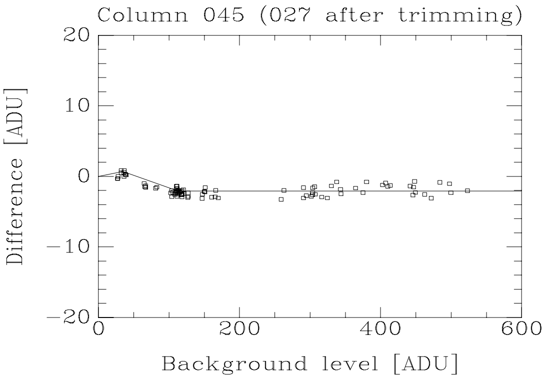

Figure A.8: The extra fat zero effect for the nights before the CCD temperature change, shown for 2 of the 20 fat zero columns. "Difference" is background level minus value in the given fat zero column. Also the 3 piece linear by eye fit is shown.

The data were fit by eye with a 3 piece linear function (example of fit also shown in Figure A.8). 13 out of the 20 fat column had a significant (> 2 ADU) extra effect. `b_fatzero.cl` was modified to be able to make the extra correction.

A.6 Flat Fields

A number of sky and dome flats had been taken, as listed in Table A.8. Additional data, such as exposure time and level, can be found in Table A.9, A.10, and A.11, although the ordering of the images in the JB and JU tables is not chronological, i.e. the dfsc numbers can not be inferred from them.

Table A.8: The Available Photometry Flat Fields

Type	Filter	#frames	dfsc numbers	night(s)
Sky flat	Gunn r	14	1362–1364, 1498–1501, 2175–2181	1, 2, 7
Sky flat	Johnson B	14	1365–1366, 1502–1505, 2048–2052, 2182–2184	1, 2, 6, 7
Sky flat	Johnson U	16	1367–1369, 1506–1510, 2053–2056, 2185–2188	1, 2, 6, 7
Sky flat	Johnson V	0		
Dome flat	Gunn r	10	1808–1817	5
Dome flat	Johnson B	10	1670–1679	4
Dome flat	Johnson U	20	1649–1668	4
Dome flat	Johnson V	14	2515–2528	11

The 44 sky flats were corrected for bias, dark, shutter, and fat zero. The images from before the CCD temperature change (i.e. the flat fields from night 1 and 2) did *not* get the extra fat zero correction, since it was not known at that time.

A thorough comparison of the flat fields from the different nights showed, that they were not the same, there were gradients in their quotients. While the flats within night 2+ (i.e. night 2, 6, and 7) agreed well (within 0.2% in GR and $< 0.1\%$ in JB and JU), the agreement between night 2+ and night 1 was not good, 0.4% in GR and 0.15% in JB and JU. Therefore it was decided to make one set (GR, JB, JU) of flats for night 1, and one set for night 2+.

In each of the 3 filters, the images from night 1 and 2+ were combined separately (weighting by the level in the images, and using a 2 sigma clipping) into a night 1 and 2+ flat, respectively. Care was taken that objects (stars) did not make it to the combined flat.

Since the night 1 flats are made from only 2 or 3 images, the noise in them are too big. Therefore we do the following: we assume, that the pixel-to-pixel variation does not change from night 1 to 2+, but only the large-scale variation. We therefore make the 3 quotients between the night 1 and the night 2+ flats, and fit the large-scale pattern in this using a many piece (6 in x and 10 in y) cubic spline. This fit is then multiplied with the flat from night 2+, thereby getting flats with the pixel-to-pixel variation from night 2+, and the large-scale variation from night 1.

A.6.1 The Uncertainty on the Flat Fields

We would like to calculate how well we are able to flat field our science images, i.e. what the uncertainty (or noise) on the flat fields are.

Given the read out noise in ADU, $\mathrm{RON_{ADU}}$, the conversion factor in $\mathrm{e^-/ADU}$, CF, and the number of counts, $\mathrm{N_{ADU}}$, the uncertainty on $\mathrm{N_{ADU}}$ is given by

$$\sigma_{N_{\mathrm{ADU}}} = \left(\frac{N_{\mathrm{ADU}}}{\mathrm{CF}} + \mathrm{RON}^2_{\mathrm{ADU}} \right)^{1/2} . \tag{A.7}$$

If we make an unweighted average of n images with individual uncertainties σ_i, the uncertainty on the combined image is

$$\sigma = \frac{1}{n}\left(\sigma_{x_1}^2 + \ldots + \sigma_{x_n}^2\right)^{1/2} . \tag{A.8}$$

The Gunn r night 2+ flats (of which there are 11), where combined in one round. The combination was made using `combine` with the following parameters different from the default: `lsigma` = 2, `hsigma` = 2, `scale` = `mean`, `weight` = `mean`, `nkeep` = 1, `grow` = 2. *The intention* with scaling was, that the different flats, which have different levels, should be scaled to a common level, so that sigma rejection can be used, after which they should be scaled back, and then made into a weighted average. Unfortunately, it seems that `combine` does *not* scale back, leading to the output being just an unweighted mean. The uncertainty should not be much higher due to this, since the individual flat field images have similar levels (within a factor of less than 4 at worst). It also means, that the uncertainty on the combined image is very easy to calculate.

Table A.9 lists the levels in ADU, N_i, and the uncertainties on the individual flats, σ_i, with σ_i is calculated from Eq. (A.7) (using $N = N_i$). They also lists the scale factors, s_i, and the weights, a_i, but these quantities do not enter the uncertainty equations.

Table A.9: The levels and uncertainties on the individual Gunn r night 2+ flat fields.

i	exptime	N_i	s_i	a_i	σ_i
1	30	2896.5	1.289	0.071	38.6
2	25	4046.9	0.922	0.099	45.6
3	20	5307.4	0.703	0.129	52.2
4	10	4127.3	0.905	0.101	46.1
5	60	3029.7	1.232	0.074	39.5
6	45	4004.2	0.932	0.098	45.4
7	25	3737.3	0.999	0.091	43.8
8	15	3447.3	1.083	0.084	42.1
9	10	3388.5	1.102	0.083	41.7
10	7	3500.6	1.066	0.085	42.4
11	5	3579.7	1.043	0.087	42.9

Notes: exptime is in seconds. N_i, s_i, and a_i, are the level (mean) in ADU, the scale factor, and weight, respectively, as reported from `combine`. σ_i was calculated from Eq. (A.7) using CF = 1.95 e^-/ADU and RON = 2.25 ADU.

To calculate the uncertainty on the combined GR flat, we apply Eq. (A.8) to the individual uncertainties, σ_i (calculated from Eq. A.7), which yields

$$\sigma_{\mathrm{GR}} = 13.21\,\mathrm{ADU} . \tag{A.9}$$

What we really want is the relative uncertainty, σ/N, and since the Gunn r combined flat had a level before normalization of 3723 ADU, we get

$$\left(\frac{\sigma}{N}\right)_{\mathrm{GR}} = \frac{13.21\,\mathrm{ADU}}{3723\,\mathrm{ADU}} = 0.35\% . \tag{A.10}$$

The Johnson B and U night 2+ flats (of which there are 12 and 13, respectively), were combined in two rounds: first in 3 groups of 4 or 5 images, and then these 3 images were combined. The combination on both levels were made with `combine` using the same parameters as for Gunn r (the so-called scaled weighted mean). The two-level combination was used to make sure that no objects (stars) would make it to the final flat field, since there was not applied any offset of the telescope between the individual flats from night 6 (where only JB and JU flats were taken). Table A.10 and Table A.11 lists the levels in ADU, N_{ij}, and the uncertainties on the individual flats, σ_{ij}, with σ_{ij} calculated from Eq. (A.7) (using $N = N_{ij}$). They also lists the scale factors, t_{ij}, and the weights, b_{ij}, but these quantities do not enter the uncertainty equations.

Table A.10: The levels and uncertainties on the individual Johnson B night 2+ flat fields.

i	j	exptime	N_{ij}	t_{ij}	b_{ij}	σ_{ij}
1	1	15	5665.3	0.844	0.296	53.9
1	2	30	4348.0	1.099	0.227	47.3
1	3	5	4840.9	0.987	0.253	49.9
1	4	17	4264.5	1.121	0.223	46.8
2	1	7	5064.0	0.871	0.287	51.0
2	2	30	2305.3	1.914	0.131	34.5
2	3	20	5632.8	0.783	0.319	53.8
2	4	10	4649.1	0.949	0.263	48.9
3	1	20	2174.1	2.271	0.110	33.5
3	2	20	3982.4	1.240	0.202	45.2
3	3	15	7823.4	0.631	0.396	63.4
3	4	7	5767.3	0.856	0.292	54.4

Notes: exptime is in seconds. N_{ij}, t_{ij}, and b_{ij}, are the level (mean) in ADU, the scale factor, and weight, respectively, as reported from `combine`. σ_{ij} was calculated from Eq. (A.7) using CF = 1.95 e^-/ADU and RON = 2.25 ADU.

To calculate the uncertainty the combined JB flat, we apply Eq. (A.8) to the individual uncertainties, σ_{ij}, in each of the 3 groups, which yields

$$\sigma_{\mathrm{JB},1} = 24.8\,\mathrm{ADU} \tag{A.11}$$

$$\sigma_{\mathrm{JB},2} = 23.8\,\mathrm{ADU} \tag{A.12}$$

$$\sigma_{\mathrm{JB},3} = 25.2\,\mathrm{ADU} \tag{A.13}$$

Using Eq. (A.8) one more time, we get

$$\sigma_{\mathrm{JB}} = \frac{1}{3}\left(\sigma^2_{\mathrm{JB},1} + \sigma^2_{\mathrm{JB},2} + \sigma^2_{\mathrm{JB},3}\right)^{1/2} = 14.20\,\mathrm{ADU}\ . \tag{A.14}$$

The relative uncertainty is:

$$\left(\frac{\sigma}{N}\right)_{\mathrm{JB}} = \frac{14.20\,\mathrm{ADU}}{4645\,\mathrm{ADU}} = 0.31\%\ . \tag{A.15}$$

To calculate the uncertainty the combined JU flat, we follow the same procedure as for JB:

$$\sigma_{\mathrm{JU},1} = 25.0\,\mathrm{ADU} \tag{A.16}$$

$$\sigma_{\mathrm{JU},2} = 25.1\,\mathrm{ADU} \tag{A.17}$$

$$\sigma_{\mathrm{JU},3} = 20.2\,\mathrm{ADU} \tag{A.18}$$

and

$$\sigma_{\mathrm{JU}} = \frac{1}{3}\left(\sigma^2_{\mathrm{JU},1} + \sigma^2_{\mathrm{JU},2} + \sigma^2_{\mathrm{JU},3}\right)^{1/2} = 13.61\,\mathrm{ADU}\ . \tag{A.19}$$

Table A.11: The levels and uncertainties on the individual Johnson U night 2+ flat fields.

i	j	exptime	N_{ij}	t_{ij}	b_{ij}	σ_{ij}
1	1	25	4645.9	1.047	0.239	48.9
1	2	15	5130.9	0.948	0.264	51.3
1	3	18	4618.8	1.053	0.237	48.7
1	4	7	5065.0	0.961	0.260	51.0
2	1	8	4833.0	1.018	0.246	49.8
2	2	5	4935.4	0.997	0.251	50.4
2	3	9	4014.5	1.226	0.204	45.4
2	4	14	5898.6	0.834	0.300	55.0
3	1	3	4685.0	0.851	0.235	49.1
3	2	5	3731.4	1.068	0.187	43.8
3	3	3	3544.5	1.125	0.178	42.7
3	4	20	4546.8	0.877	0.228	48.3
3	5	3	3426.9	1.163	0.172	42.0

Notes: exptime is in seconds. N_{ij}, t_{ij}, and b_{ij}, are the level (mean) in ADU, the scale factor, and weight, respectively, as reported from `combine`. σ_{ij} was calculated from Eq. (A.7) using CF = 1.95 e^-/ADU and RON = 2.25 ADU.

The relative uncertainty is:

$$\left(\frac{\sigma}{N}\right)_{\mathrm{JU}} = \frac{13.61\,\mathrm{ADU}}{4384\,\mathrm{ADU}} = 0.31\% \ . \tag{A.20}$$

The levels used to calculate the relative uncertainties (Eq. A.10, A.15, and A.20), are the levels in the section `[25:800,25:925]`. This section is in some sense "normal", as opposed to the right and upper edge, which is more sensitive in the blue than the rest of the chip. The levels in the entire frames are 3733 ADU (GR), 4710 ADU (JB), and 4591 ADU (JU). If these values are used for calculating the relative uncertainty, we get 0.35% (GR), 0.30% (JB), and 0.30% (JU), so there is only a small difference.

Even though the chip is more blue-sensitive in the right and upper side, it is still linear in that area. This was checked using 10 JU dome flats with levels of $\sim$ 13000 ADU (dfsc1649–1658, exptime 10 sec), and 10 with levels of $\sim$ 6000 ADU (dfsc1659–1663, exptime 5 sec; dfsc1664–1668, exptime 7 sec). The high and the low level images were separately combined, and the quotient of the 2 resulting images was made. This quotient images had a gradient in the x-direction of $<$ 0.05%, and in the y-direction of $<$ 0.1%, which is very small. The quoted numbers are (maximum – minimum)/2.

The relative uncertainties are summarized in Table 3.6 (p. 32).

A.6.2 Illumination Correction

Even though we use (twilight) *sky* flats, there still seems to be a large-scale difference between the (sky) flat field and the sky background in the science frames. Since the color of the morning sky (where the sky flats are taken) and of the night sky is different, a large-scale gradient in the quotient of the flat field at different wavelengths (colors) will give an effect that behaves like the above mentioned illumination effect. The problem might be accentuated by a red leak in the Gunn r filter that we used, see Stetson (1989) for a discussion of read leaks.

To determine the illumination correction, one could observe parts of the sky without (or with few) objects. Indeed, two such *empty fields* were observed; the field SPKS04 was observed in GR and JB (dfsc2413 and 2414), and SPKS10 was observed in GR (dfsc2487). Unfortunately (and surprisingly), these images were not useful since a) the large-scale variation in the two GR empty fields did *not* match (relative difference on their quotient was up to ± 1.5%), and b) the large-scale variation in the empty fields did not match that in the science frames. It was checked that the moon was not up when these images were taken (the moon *could* have caused scattered light problems).

Instead it was tried to determine the illumination correction directly from the science images. A number (48 out of 118) of the GR and JB science images were read from tape and corrected for bias, fat zero, dark, shutter, and flat field (the sky flat fields without any illumination correction were used). The images with few bright objects were found; which was images of the following fields: 214, 21 (two exposures), 22, 36, and 44.

The objects (stars and galaxies) in the images were now removed in the following two step procedure: First all values outside $\pm 5\sigma$ from the median were replaced by the median value, with σ calculated from equation (A.7). The median was estimated as the `midpt` from `imstat` in two steps, first with no cuts, and then with cuts $\pm 5\sigma$, calculating σ from the first `midpt`. Second, `imsurfit` was used to fit a legendre polynomial in x and y (with cross terms) of order 4 in x and 3 in y (using the IRAF definition of *order*), and applying a sigma rejection with a lower sigma of 3 and an upper sigma of 2, using 3 iterations.

The agreement between the large-scale sky background variation in the above mentioned 6 science frames was not that good. In some cases objects had not been totally removed, and in some cases there was no straightforward explanation.

It was decided to use the derived large-scale sky background variation in the two field 21 frames and the field 44 frame (i.e. the mean of the 3) as the illumination correction. These two illumination images (one in GR and one in JB) were normalized using the same section as for the sky flats, `[25:800,25:925]`.

The size of the illumination can be characterized as follows (values for the entire frame): (min,max) is (0.9807,1.013) for GR and (0.9869,1.012) for JB. The standard deviation is 0.62% for GR and 0.47% for JB.

How well the illumination correction is determined is hard to say. If we look at the abovementioned 7 or 8 images (that is, 6 science frames with all objects removed, and 2 (for JB 1) empty field(s)), and we exclude the field 36 science frame because there is an unremoved object in it, and the SPKS10 (GR only) empty field because it is just strange, we can get an estimate of how well we do. The mean standard deviation of the 6 individual GR large-scale patterns is 0.62%. When making the quotient with the decided final illumination correction mentioned above (which is the mean of 3 of the 6 images), the mean standard deviation of the 6 quotients is 0.42%. For JB the numbers are 0.50% and 0.34%

So far, no remaining large-scale pattern has been noticed in the science frames reduced with the abovementioned illumination correction.

For JU, where we only have 5 science frames and no empty fields (though they did not prove useful for GR and JB), no illumination correction could be established, since the 5 frames were full of objects, and the background levels were low.

A.6.3 The Final Photometry Flats

To make the final flats, the illumination correction was multiplied to the flats. To summarize in a hopefully understandable notation:

$$\text{flat(GR,1)} = \text{sky\_flat(GR,2+)} * \text{ill.\_corr.(GR)} * \text{smooth}\left(\frac{\text{sky\_flat(GR,1)}}{\text{sky\_flat(GR,2+)}}\right) \tag{A.21}$$

$$\text{flat(GR,2+)} = \text{sky\_flat(GR,2+)} * \text{ill.\_corr.(GR)} \tag{A.22}$$

$$\text{flat(JB,1)} = \text{sky\_flat(JB,2+)} * \text{ill.\_corr.(JB)} * \text{smooth}\left(\frac{\text{sky\_flat(JB,1)}}{\text{sky\_flat(JB,2+)}}\right) \tag{A.23}$$

$$\text{flat(JB,2+))} = \text{sky\_flat(JB,2+)} * \text{ill.\_corr.(JB)} \tag{A.24}$$

$$\text{flat(JU,1)} = \text{sky\_flat(JU,2+)} * \text{smooth}\left(\frac{\text{sky\_flat(JU,1)}}{\text{sky\_flat(JU,2+)}}\right) \tag{A.25}$$

$$\text{flat(JU,2+))} = \text{sky\_flat(JU,2+)} \tag{A.26}$$

A.7 Overflow and Remanence

When there is a very bright object (star) in the frame, there will be so much charge build up in the corresponding pixels, that the potential well can not hold on to it, and it overflows. For this CCD, it flows upwards (i.e. towards higher y's) along the column(s) (typically 1-5 columns, but it can be even more). To have such an overflow stripe is in itself a problem.

But the real problem comes in the following frames, where one can now see a *remanence* stripe going downwards from where the star was in the last frame (say, we are now looking at another field without any star at the point where the bright star was in the last frame). In approximately 20 frames (not including a similar number of frames used only for pointing the telescope) after the exposure of the bright star, this remanence stripe can be seen, only fading slowly. The strength of the remanence stripe increases with exposure time. We do not fully understand the physical processes involved with this phenomenon.

It is possible to measure how much extra signal there is in an overflow or remanence affected column compared to the background. For the remanence effect, this signal is (to a good approximation) a linear function of y, although sometimes 2 (or more) linear pieces are needed, with an abrupt jump usually at $y = 512$. The overflow signal falls off much faster than a linear function in y, but it is not easily approximated by a simple function. A many-piece cubic spline works satisfactory.

The remanence and overflow stripes were removed using the cl-script `remanence`, written by IJ. It works like this: On the displayed image, the user marks the position of all the stripes and their widths in pixels (only the interval 1–9 is supported, since the width is marked just by pressing one of the keys 1 to 9). Thereafter, for each stripe, the program plots the level along the stripe (i.e. along y). The user then marks a number of intervals in y where a correction needs to be applied. The choices are fitting a linear function, `l`, or a many-piece cubic spline, `s`. The appropriate key is pressed at the endpoints of the interval. The program then fits the appropriate function to the stripe, and fits the background on each side of the stripe using a linear function. After this, the difference between the stripe fit and the sky fit can be subtracted from the original image (if this difference is less than zero, no action is taken), and one has the cleaned image.

As the above might indicate, the process involves a lot of manual work, and is rather time consuming. However, it works remarkably well in most cases.

114 of the 123 images were corrected for one or (usually) more remanence and/or overflow stripes. No of the 5 JU images needed correction. 6 of the images had also horizontal stripes (very strong overflow), and this was removed by rotating the images 90 degrees, running `remanence` on it, and rotating them back again.

A.8 Removal of Spectroscopy Calibration Lamp Signature

The DFOSC spectroscopy calibration lamp was accidentally left on while taking 8 of the photometry science images, i.e. with the DFOSC in imaging mode. These images are listed in Table A.12.

Table A.12: Images affected by the spectroscopy calibration lamp.

Image	Filter	Field
d1549	GR	00
d1550	JB	00
d1552	GR	14
d1553	JB	14
d1555	GR	15
d1556	JB	15
d1558	GR	13
d1559	GR	13

It was not possible to see the lamp signature in the Johnson B images – the lamp must have been very red – so only the 5 Gunn r images needed to have the lamp signature removed.

By coincidence, an image, dfsc1205, had been taken earlier, also with the lamp on. This image was binned 4×4. This image was expanded to full size using `blkavg`, had bias subtracted, had some cosmic-ray-events removed, and was trimmed. It is shown in Figure A.9 (left).

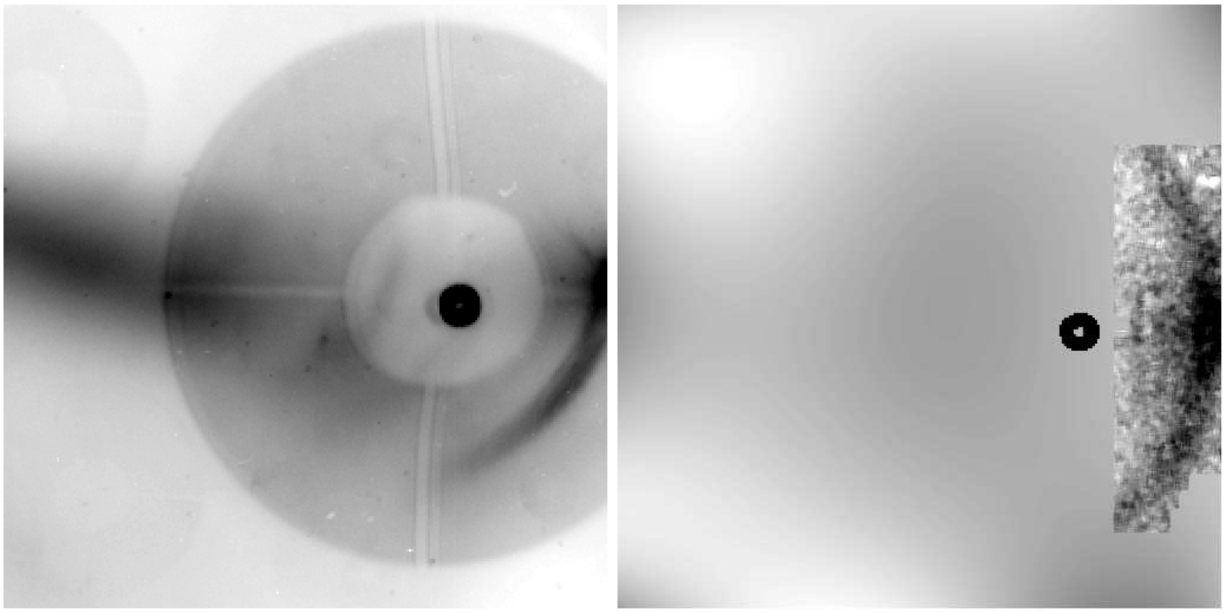

Figure A.9: The spectroscopy lamp signature. Left: the image `d1205` (see text). Right: the image `lamp_5mGR`, which is the applied correction for the lamp signature. The values from low to high are color coded as white to black.

However, the lamp signature in the science images did not look exactly like d1205. The bright small ring in the middle right hand side of the image matched well if it was shifted, but the arcs in the right hand side was symmetric in the science images, whereas it was asymmetric in d1205.

The lamp correction image was constructed as follows:

- The ring was cut out of d1205, and shifted in x and y, and scaled in intensity.
- The symmetric arc was taken from the science image d1555 of field 15, where the arc is free of galaxies in the image. Unfortunately, field 15 is next to the central field, field 00, so at the position of the arc, there was a contribution from (especially) the very bright galaxy R256/NGC3309 A model of this was made by simply taking the corresponding part from the field 00 image d1278 (since the fields overlap), translating it to the corresponding location in d1555, and subtracting the d1278 background level to get only the galaxy contribution. The shift was computed using 3 stars in common to the two images.

  The arc could now be cut out of d1555. The d1555 background was subtracted to get only the arc contribution. A number (~ 50) of weak objects was removed by replacing the affected pixels by a linear interpolation of the neighbor values, using `fixpix`. The image was then median filtered using a 11×11 box, using the task `median`.
- The low frequency variation was fitted to d1555 with the ring and the arc subtracted, using `imsurfit`. The objects (stars and galaxies) in d1555 was excluded from the fit by specifying the parts of the image not affected by galaxies, and by doing a sigma-rejection for the rest (setting `low`=3, `up`=2, and `niter`=3). The function used was a 2×2 piece cubic spline.

The three parts were put together to the image `lamp_5mGR`, which is shown in Figure A.9 (right). This image has a maximum value of 46 and a minimum value of -7. It was subtracted from the 5 affected Gunn r science images mentioned in Table A.12 – no scaling was necessary. The correction worked remarkably well.

A.9 Astrometry

Astrometry was done on all 68 focused standard star images (cf. Table C.1, p. 181 further on), using tasks in the package `finder`. The main purpose was to determine the CCD pixel scale, since that had not been determined before with sufficient accuracy.

First, the task `tfinder` was run on the images. It is given the epoch and the center coordinates of the image, the intended orientation of the CCD (in our case north at the bottom, and east to the right), and a good guess on the CCD ("plate") scale (in our case 0.51 ″/pixel). It then uses the Hubble Guide Star Catalog (GSC; on CD-ROM) to find the GSC stars present in the given CCD image. The GSC stars are drawn as rings on top of the image, which is displayed in SAOimage. The user does the coarse centering, after which the task does the real centering, and outputs a catalog *image*`.tab`, in which the following columns are of particular interest: `RA_DEG`, `DEC_DEG`, `X_CENTER`, and `Y_CENTER`.

A note should be made about the two coordinate systems involved. (x, y) are the *ideal plate coordinates*, in radians. They are given in the columns `RA_DEG` and `DEC_DEG`, with a conversion from degrees to radians. The x-axis points towards east, and the y-axis points towards north, making it a left-handed system. (x', y') are the CCD coordinates, in pixels. They are given in the columns `X_CENTER` and `Y_CENTER`. In our case, the x'-axis points approximately towards east, and the y'-axis points approximately towards south, making it a usual right-handed system. See Figure A.10.

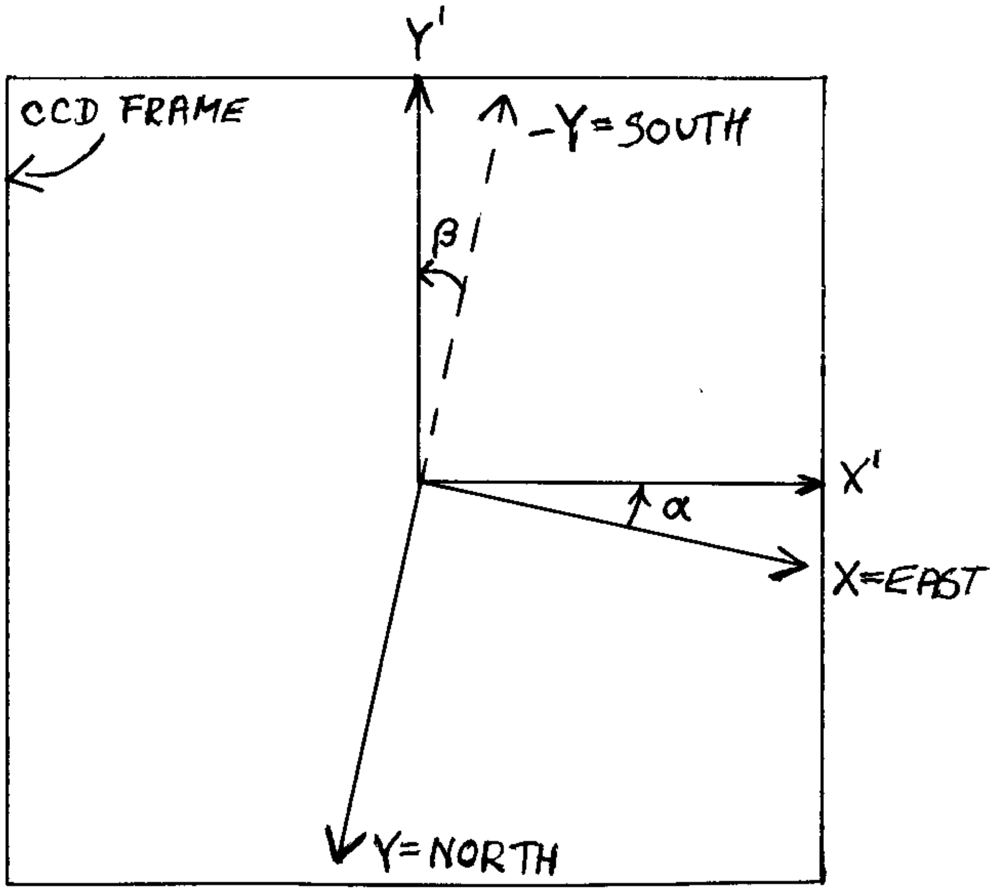

Figure A.10: Coordinate systems. Note, that for simplicity, the two coordinate systems are shown to have coinciding origins, i.e. with the offset vector $\mathbf{b} = \mathbf{0}$ (cf. Eq. A.27).

The task `tastrom` takes the catalog *image*`.tab` produced by `tfinder` and computes a 6 coefficient co-called plate solution of the form

$$\begin{pmatrix} x \\ y \end{pmatrix} = \begin{pmatrix} a_{11} & a_{12} \\ a_{21} & a_{22} \end{pmatrix} \begin{pmatrix} x' \\ y' \end{pmatrix} + \begin{pmatrix} b_1 \\ b_2 \end{pmatrix}. \tag{A.27}$$

These 6 coefficients, a_{ij} and b_i, are written to the ASCII file *image*`.ast`, along with a number of other informations. An example of the lines giving the 6 coefficients from `d1318.ast` is:

```
1PLATE SOLUTION - EMPIRICAL, 6-COEFF
 --------------   -----------------

     X,Y = IDEAL PLATE COORDINATES (RADIANS)

     X =   -0.001269                                       Y =    0.001301
       +   0.2458474E-05 * XMEAS                             +  -0.2458925E-05 * YMEAS
       +  -0.1837236E-07 * YMEAS                             +  -0.1840916E-07 * XMEAS
```

We identify a_{ij} and b_i as

$$\begin{array}{rcl} x & = & b_1 \\ & + & a_{11} \cdot x' \\ & + & a_{12} \cdot y' \end{array} \qquad \begin{array}{rcl} y & = & b_2 \\ & + & a_{22} \cdot y' \\ & + & a_{21} \cdot x' \end{array} \tag{A.28}$$

The transformation matrix $\mathbf{A}$ can be written in terms of the following geometrical quantities

1. α: The angle from the x-axis (east) to the x'-axis (CCD abscissa), measured counterclockwise
2. β: The angle from the $-y$-axis (south) to the y'-axis (CCD ordinate), measured counterclockwise
3. $s_{x'}$: The CCD scale in the x' direction
4. $s_{y'}$: The CCD scale in the y' direction

as

$$\mathbf{A} = \begin{pmatrix} s_{x'} \cos\alpha & -s_{y'} \sin\beta \\ -s_{x'} \sin\alpha & -s_{y'} \cos\beta \end{pmatrix}, \tag{A.29}$$

where the minus signs on a_{21} and a_{22} are due to the fact that we have a usual right-handed coordinate system being rotated with respect to a *left-handed* coordinate system, cf. Figure A.10.

A.9.1 CCD Orientation

The angles α and β were calculated from the extracted elements of $\mathbf{A}$ as

$$\tan\alpha = -\frac{a_{21}}{a_{11}} \tag{A.30}$$

and

$$\tan\beta = +\frac{a_{12}}{a_{22}}. \tag{A.31}$$

Figure A.11 shows the values of α and β as function of a chronological image serial number for the 68 images. Vertical dashed lines demarcates the different nights. The observations come in sets of 4 images, one in each filter. These sets are labeled with the field name, with "PG" being PG1633+099, and "SA" being SA110–503.

The observation history is, that on night 1 there was no encoder on the rotator. After images with serial numbers 1 to 8 had been observed, the rotator was turned, and therefore it is expected that images with serial number 9 to 12 have a different orientation than the above. On night 2, an encoder was available.

It is seen, that for all the PG images, α and β agree well. $\alpha = \beta$ is expected, since it means that the CCD is right-angled. However, for all the SA image, there is a systematic difference between α and β of about 0.1°. This is probably due to the fact, that the 18 GSC stars in the SA field comes from two different Schmidt plates, with 9 stars from plate 0192, and 9 stars from plate 050T. For the PG field, all 12 stars come from one plate, 006K. This can be seen from the `PLATE_ID` column in the *image*`.tab` tables. The hardcopy documentation for `finder` actually warns against using data from more than one plate at the time, so it seems justified to exclude the SA data.

The PG data only is plotted in Figure A.12. The horizontal dotted-dashed line shows the mean of these data of +0.29°. The data points scatter around this value within ±0.3° (min-max). The step size of the encoder is 0.2°, which almost explains the scatter.

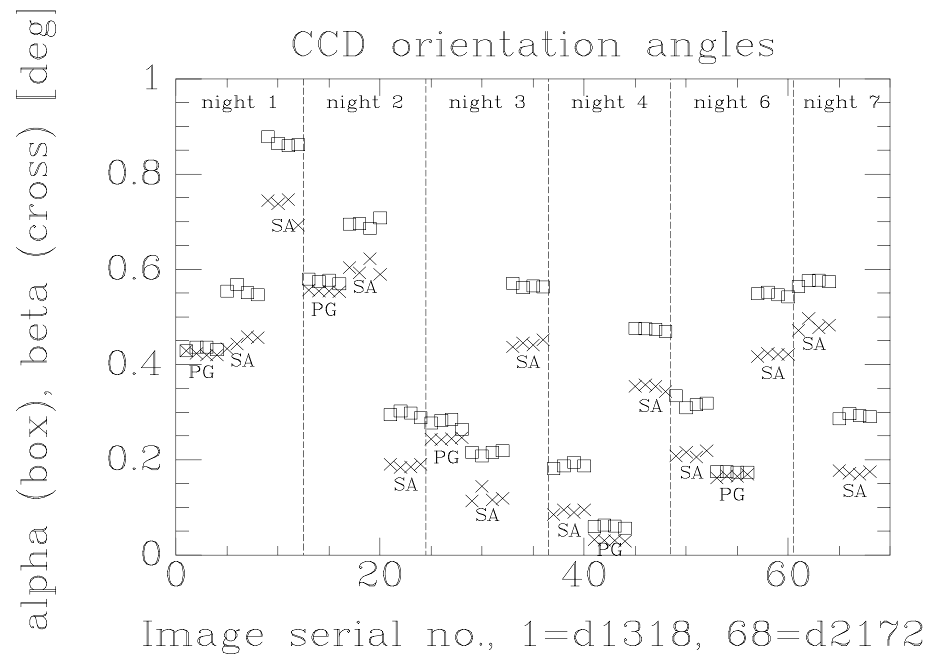

Figure A.11: CCD orientation angles. Each set of four observations is labeled by the field name.

A.9.2 CCD Scale

`tastrom` directly outputs the CCD scales in the x and y direction, $s_{x'}$ and $s_{y'}$, in the *image*`.ast` file, with 4 decimal places. A manual calculation using the found values of α and β and equation (A.29) gives the same result. The scales are shown in Figure A.13. There seems to be a small difference between the x scale and the y scale. This is small enough to be ignored.

The horizontal dotted-dashed line shows the adopted value of the CCD scale of 0.5073 ″/pixel. This is actually not a mean of all the data, but only of 6 images on which astrometry was done at an earlier point. However, this value is very representative for all the data, as the figure shows.

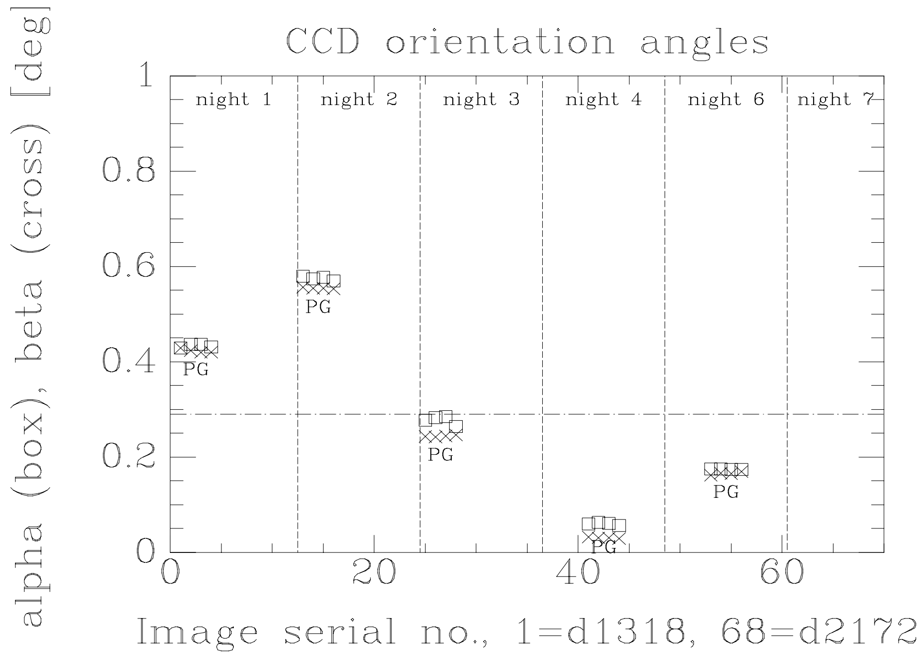

Figure A.12: CCD orientation angles, PG images only. The horizontal dotted-dashed line is at $+0.29°$.

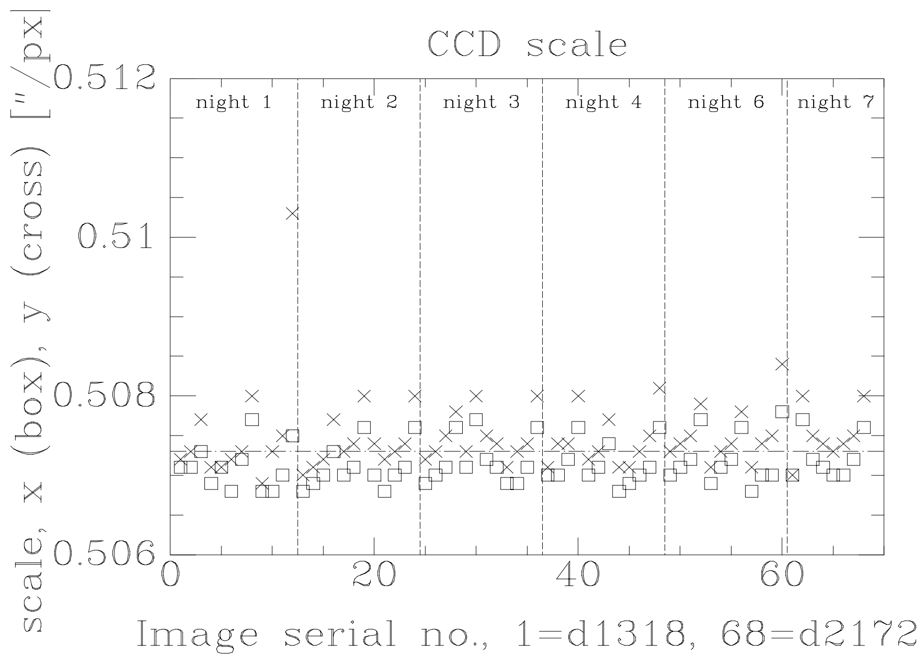

Figure A.13: CCD scale in the x and y direction. The horizontal dotted-dashed line is at 0.5073 $''$/pixel.

Appendix B

Details of the Surface Photometry

B.1 Details on How to Fit Ellipses

This section gives a more detailed description of the things that is needed to consider when fitting ellipses using the current implementation of GALPHOT. Since the description in the main text (Sect. 4.1, p. 35) was kept in general terms, we start by introducing the terminology specific to GALPHOT and its implementation. In the following '*galaxy*' is a generic name for a galaxy observation. An example is `r214_GR_1`, which is a Gunn r (GR) observation of the galaxy R214. Since this galaxy has been observed more than once in Gunn r, it is given a serial number, in this case 1.

`classify` is the task that does the classification of objects into 'stars' and cosmic-ray-events. It outputs the positions and flagging radii of the two types of objects in the two files *galaxy*`.star` and *galaxy*`.cosmic`. In addition, the center coordinates of the program galaxy is put in the file *galaxy*`.gal`.

`harmfit` is the task that does the harmonic expansion along concentric circles. It outputs the radial profiles of the Fourier coefficients from the expansion and their uncertainties in the STSDAS table *galaxy*`.har.tab`, and also produces a residual image called *galaxy*`.resh.imh`.

`deviate` is the task that flags the pixels that deviate by more than (say) 5 sigma in the above residual image. The output is a list of additional pixels to be flagged called *galaxy*`.pos.del`.

`ellipfit` is the task that does the ellipse fitting. The radial profiles are output in the STSDAS table *galaxy*`.prf.tab`, and the residual image is called *galaxy*`.res.imh`. `ellipfit` has some parameters that sometimes need to be fine tune. `errcen` and `errshap` are the uncertainties that the first and second order coefficients from `harmfit` needs to be below to keep the center and shape as free parameters, respectively. As default values for both we used 0.02 for Gunn r and Johnson B, and 0.04 for Johnson U. `rcen` and `rshap` can be used to explicitly set $r_{\mathrm{free-center}}$ and $r_{\mathrm{free-shape}}$ and thus overriding the automatic determination using `errcen` and `errshap`. The parameters `dposmax`, `dellmax`, and `dangmax` control how much the center position, the ellipticity, and the position angle, respectively, are allowed to change at a given radius per iteration step. These need to be increased when the initial guess on the profiles computed from the `harmfit` output are far from the actual values for some reason.

`model` is a task that can construct a model image from the ellipse fit.

Finally, the task `galfit` is an 'umbrella task' that basically calls the three tasks `harmfit`, `deviate`, and `ellipfit`.

We are now ready to fit an isolated galaxy (Sect. B.1.1) or two overlapping galaxies (Sect. B.1.2).

B.1.1 Fitting a Single Galaxy

By single galaxy, we mean a galaxy, which has a large angular separation from other galaxies, i.e., no other galaxies overlap with the galaxy in question.

First, we run `galfit` on all the single galaxies using the default parameters. Most of the galaxies are so relatively small, that it is not necessary to use the entire 1024 pixel $\times$ 1024 pixel image to fit them. Usually, a 400 pixel $\times$ 400 pixel section will do. When possible, the section should be centered on the galaxy. A typical call to `galfit` is:

```
galfit d1293[096:495,517:916] infiles=r214_GR_1 output=r214_GR_1
```

where the name of the galaxy image in the example is `d1293`.

Besides the galaxy image, the input files to `galfit` are *galaxy*`.gal`, *galaxy*`.star`, and *galaxy*`.cosmic`, and the output files are *galaxy*`.har.tab`, *galaxy*`.resh.imh`, *galaxy*`.pos.del`, *galaxy*`.prf.tab`, and *galaxy*`.res.imh`.

The two images are examined to see whether the obtained fit is good. It is mostly the `ellipfit` residual image (i.e. *galaxy*`.res.imh`) that is interesting. Two typical types of problems are:

- r_{free} is wrong and/or there are overlapping ellipses. Since the center and shape parameters of the galaxy actually change with r, we want to have r_{free} as large as possible. However, when the signal to noise becomes too low, the fit is poorly constrained, and one can get overlapping ellipses, which is undesirable. In a number of cases, it is necessary to manually intervene to get the best fit:
  - If r_{free} is too low, i.e. if one can see from the `ellipfit` residual image that e.g. the ellipticity is still rising beyond r_{free}, one can try to increase `errcen` and `errshap`, or set `rcen` and `rshap` to something suitable.
  - If r_{free} is too high and one gets overlapping ellipses, one can try to set `rcen` and `rshap` to the radius just before the overlap occurs.
  - If a galaxy has a sharp isophote twist, and has been observed in good seeing, it is not possible to just decrease r_{free} to avoid the overlapping ellipses, because then the outer parts beyond the sharp isophote twist are not fitted correctly. This can be solved by making sure r_{free} is large enough to fit the entire galaxy, and then manually remove the radius/radii from *galaxy*`.prf.tab` at which the ellipses overlap (this is reported by `galfit` as e.g. 'MODELINIT: WARNING: ellipses overlapping at $r = 24.05$'). One can construct a residual image corresponding to this new profile using `model` with `residual=yes`. From this image it should be checked, that the model is well behaved in the flagged pixels, where the model values will be used when calculating aperture magnitudes. One can do that by blinking the above `cmodel` residual image with an image that has the flagged pixels marked, e.g. the residual image from `galfit`. The above procedure was done for 1 of the 147 observations that I (BMJ) fitted (`r253_JB_2`).
- Problems with flagging other objects.
  - Even though `classify` is quite good at assigning radii to the extended objects, there will still be some objects where the radius is not correct, being either too large or too small. This is particularly a problem close to the center of the galaxy, both because the non-flat background confuses `classify`, and because the flagging is more critical here. Correction of the assigned radii is done by editing *galaxy*`.star`.

- Some extended objects might not have been detected, typically faint galaxies, so they need to be added to *galaxy*`.star`.
- Some cosmic-ray-events might not have been detected, so they need to be added to *galaxy*`.cosmic`.
- In a few cases, there are cosmic-ray-events very close to the center. Flagging them using *galaxy*`.cosmic` or letting `deviate` do the job might not work, because the interpolation routine used by `ellipfit` cannot handle having such a large fraction of the ellipse flagged. One has to replace the affected pixels by the values in their symmetric counterparts, assuming symmetry around the center of the galaxy. This was done for 3 of the 147 observations which were fitted by me.

B.1.2 Fitting Overlapping Galaxies

By overlapping galaxies, we mean two (or more) galaxies, which have a small angular separation, so that it is not possible just flag the other galaxy. Therefore, the galaxies have to be fitted iteratively. GALPHOT does not support this per se, so one has to do it in a manual fashion. In the following, *image* is the original image, *gal1* is the brightest of the two overlapping galaxies, and *gal2* is the faintest.

1. (a) Using *image*, *gal1* is fitted with *gal2* flagged with a large radius. A model image based on the fit is subtracted from *image* to get *image_mod*. The background level in *image* is added to *image_mod*, so that the two has the same background levels, keeping photon statistics unaltered.
   (b) Using *image_mod*, *gal2* is fitted with *gal1* flagged with a large radius. A model image based on the fit is subtracted from *image* to get *image_gal1* – the notation is, that *gal1* is the galaxy *left* in the image *image_gal1*. The background level in *image* is added to *image_gal1*.
2. (a) Using *image_gal1*, *gal1* is fitted with *gal2* flagged with a small radius. A model image based on the fit is subtracted from *image* to get *image_gal2*. The background level in *image* is added to *image_gal2*.
   (b) Using *image_gal2*, *gal2* is fitted with *gal1* flagged with a small radius.

We found that the above 2 steps were enough. Otherwise the procedure could be continued further.

The iterative procedure were also used on galaxies with bright stars very close to the center. This gave a much better fit than if we had just flagged the star. This kind of star subtraction was done for 2 of the 34 galaxies fitted by me. Note the notation: we have 64 *galaxies* and 227 galaxy *observations*.

B.2 Corrections to the PA-profiles

Note: in this section, we will use primes to denote the CCD coordinate system, to keep the notation consistent with that of the astrometry section (Sect. A.9, p. 156). For example, we will use the term "the CCD x'-axis", or just "the x'-axis", to denote what would otherwise just be called "the CCD x-axis". Unprimed quantities will refer to the ideal plate coordinate system.

B.2.1 Transformation to the Standard System

The ellipse fitting task (`galfit`) measures the position angle from the CCD x'-axis and counterclockwise. The standard way of measuring position angles is "from north through east". The task that calculates instrumental magnitudes (`galmag`) also attempts to transform the position angles to the standard system.

In our case, the CCD x'-axis points (approximately; see Sect. B.2.2 below) towards east, and the CCD y'-axis points (approximately) towards south, so "from north through east" still means counterclockwise. However, instead of starting from the CCD x'-axis, we need to start from *minus* the CCD y'-axis. Therefore, in our case, `galmag` does the following transformation:

1. $\mathrm{PA}_{\mathtt{galmag}} = \mathrm{PA}_{\mathtt{galfit}} + 90°$
2. If $\mathrm{PA}_{\mathtt{galmag}} > 180°$ then $\mathrm{PA}_{\mathtt{galmag}} = \mathrm{PA}_{\mathtt{galmag}} - 180°$

$\mathrm{PA}_{\mathtt{galfit}}$ denotes the position angles calculated by `galfit` (found in *galaxy*`.prf.tab`), and $\mathrm{PA}_{\mathtt{galmag}}$ denotes the position angles calculated by `galmag` (found in *galaxy*`.mags.tab`).

B.2.2 Correction for the Slight CCD Misalignment

We found in the astrometry section (Sect. A.9, p. 156), that the CCD coordinate system was turned $+0.29°$ with respect to the ideal plate coordinates. Let us denote this angle by γ, i.e. $\gamma = +0.29°$. Because of this misalignment, `galmag` did not quite get us to the standard system, we are still $0.29°$ off.

Figure B.1 shows the setup. On the figure, an angle θ' is shown. θ' is measured from minus the CCD y'-axis counterclockwise, i.e. just as the position angles that `galmag` outputs. It can readily be seen, that the angle θ, measured from the true north axis and also counterclockwise, can be calculated as

$$\theta = \theta' + \gamma \ . \tag{B.1}$$

Therefore, all the PA-profiles of the galaxies from all nights where corrected for this mean $+0.29°$ CCD misalignment as

$$\mathrm{PA}_{\mathrm{corr}} = \mathrm{PA}_{\mathtt{galmag}} + 0.29° \ . \tag{B.2}$$

B.2.3 PA-profiles that Cross $0°$ or $180°$

The position angles determined from `galmag` are in the range $0°$–$180°$. They do not go all the way to $360°$, since the major axis of a galaxy does not have a positive and a negative direction, as opposed to for example a coordinate axis.

If a galaxy has an isophote twist, i.e. the position angle changes with the radius r, the position angle might cross the upper or lower limit of $180°$ or $0°$, respectively, and thereby appearing discontinuous. This is in a way a cosmetical problem. Since the position angle is only determined to within a factor of $180°$, we can add or subtract $180°$ at certain radii to make the profile look continuous. This was done using the task `pa1shift`. An example of this is shown in Figure B.2.

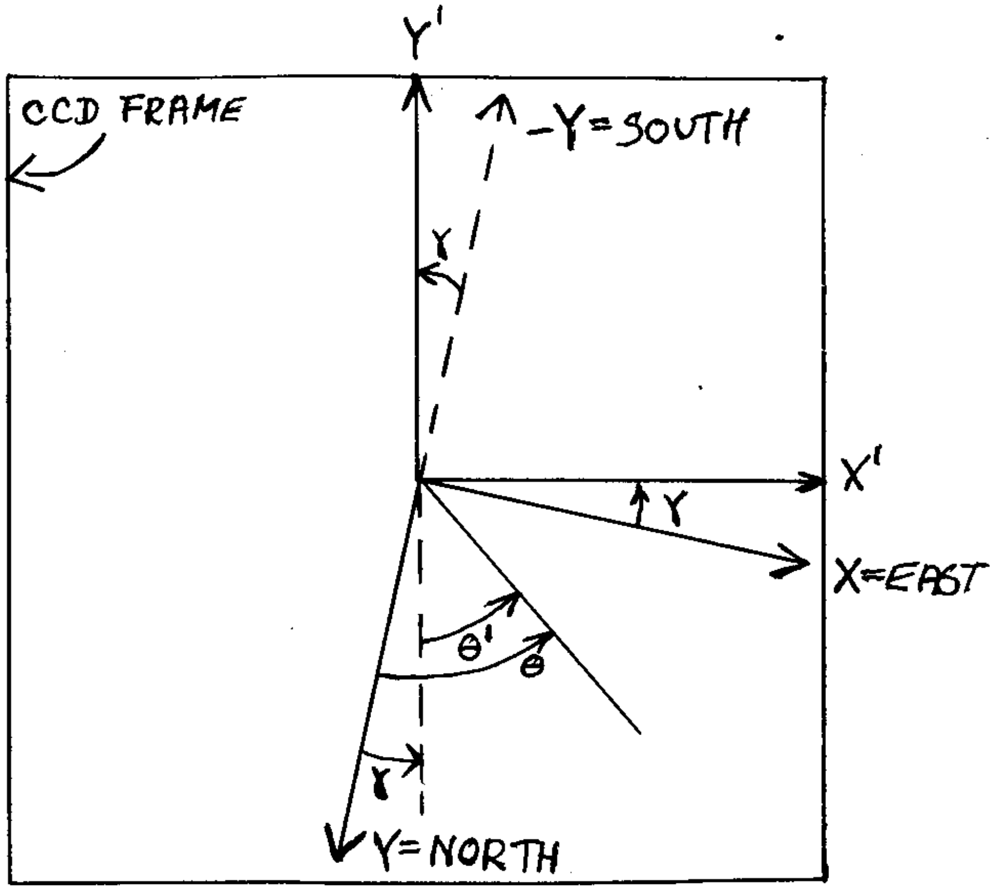

Figure B.1: Correction for the CCD orientation

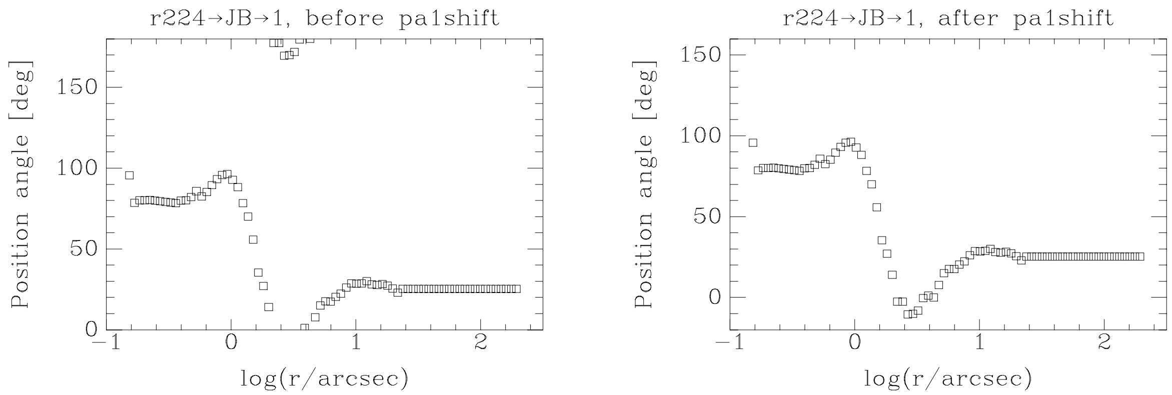

Figure B.2: Example of a PA-profile that crosses 0°/180°, and which was cosmetically changed to look continuous. The isophote twist of R224 is visible in the image on p. 219. Note that 'isophote twist' just means that the position angle is changing significantly with radius, not necessarily that it crosses 0° or 180°. The seeing for the shown observation is 1.8 arcsec, i.e. $\log(r/\mathrm{arcsec}) = 0.25$.

B.3 Corrections to Non-Photometric Observations

Unfortunately, not all the images have been taken in photometric weather. We need to identify these, and then compute offsets that will bring these images to the same system as the images observed under photometric conditions.

The observations log is shown in Table B.1. It clearly states, that the weather was non-photometric when observing field 210 on night 4, that the weather might not have been photometric when observing fields 427, 215, 28, and 33 just after this, and that there might be problems with the 5 JU fields on night 9.

One check of the photometric consistency comes from the program galaxies that have been observed more than once in a given filter. All possible pairs of such observations were formed, giving 53 pairs in GR, 42 pairs in JB, and 2 pairs in JU. The order of the two observations within the pairs was chosen to be chronological. About half of the observations are tested in this way see the "Pair" column in Table B.2 (p. 172). The number of pairs can be calculated from the numbers in Table 3.4 (p. 29) as $N_{\mathrm{pair}} = N_2 + 3N_3 + 6N_4$, where N_2, N_3, and N_4 is the number of galaxies observed twice, three times, and four times, respectively. Note, that the one pair that can be formed from a galaxy observed exactly twice can be uniquely referred to by the name of the galaxy (and the filter).

From the raw magnitudes (cf. Sect. 4.2, p. 39) instrumental magnitudes were calculated as

$$m_{\mathrm{inst}} = m_{\mathrm{raw}} - kX + n, \tag{B.3}$$

where $-kX$ is the extinction correction and $+n$ is the night shift. (This equation is described briefly in Sect. 4.3, p. 40, and in more detail in Ap. C, p. 179.) For each pair of observations, the (instrumental) magnitude difference within a circular aperture, $\Delta m_{\mathrm{circ}}(r) \equiv m_{\mathrm{circ},1}(r) - m_{\mathrm{circ},2}(r)$, was calculated at aperture radii $6.26''$ and $10.08''$.

Magnitude difference at these two apertures for the three filters are plotted in Figure B.3. Most magnitude differences are within $0\overset{\mathrm{m}}{.}02$. Only two galaxies, R336 and R337, have large magnitude differences of around $0\overset{\mathrm{m}}{.}1$. These two pairs are due to R336 and R337 being located in the overlap region between field 210 and 28. Field 210 is the one for which the observations log clearly states that the weather was non-photometric. Field 28 was observed later on night 4, where the log says that is should be checked whether the weather was photometric.

The only other pairs that have large deviations are R317 and R308. The R317 pair is due to field 33 being observed twice, on night 1 and 4. The R308 pair is due to field 16 being observed twice, on night 1 and 6.

We note that for the $6.26''$ aperture there is a small systematic offset of $\sim 0\overset{\mathrm{m}}{.}01$. This is most likely a seeing effect, as is shown in Sect. 4.4 (p. 41). It is not important for the determination of the non-photometric offsets. First of all it is a small effect, and second, the $10.08''$ aperture, which was also used, is not significantly affected.

From the above we have identified 5 field complexes that need to be checked:

Field complex	Filter	Indication of problems	
		Observations log	Galaxy $\Delta(m)$
210/28/16	GR+JB	210: yes; 28: maybe; 16: no	210/28: yes; 16: maybe
427	GR+JB	maybe	n/a
215	GR+JB	maybe	n/a
33	GR+JB	maybe	maybe
00/13/14/15/18	JU	maybe	maybe

Table B.1: The Notes in the Observations Log about the Weather

Night	Page	Weather	Galaxy fields observed
1	1	Photometric – to be checked	–
1	2	Photometric	–
1	3	Photometric	00, 16, 13, 25, 37
1	4	Photometric	37c, 18, 12, 21, 33, 45
1	5	Photometric	–
1	6	Photometric	–
1	7	Photometric	–
2	8	Photometric	214, 320
2	9	Photometric	428, 632, 29, 419, 519
2	10	Photometric	15
2	11	Photometric	–
2	12	Photometric	–
2	13	Photometric	–
3	14	[nothing written]	–
3	15	Photometric	00, 14, 15, 13
3	16	Photometric	27, 23, 43, 18, 321, 535
3	17	Photometric	535c, 35
3	17	May not be photometric right now, check this	–
3	18	Photometric (?)	–
3	19	Photometric	–
4	20	Photometric	–
4	21	Photometric	46
4	22	Photometric	47, 34, 22, 26, 24
4	22	NON-photometric	210
4	23	Photometric? check this	427, 215, 28, 33
4	24	Photometric	–
4	25	Photometric	–
4	26	Photometric	–
6	25	Photometric	–
6	26	Photometric	213, 39, 36, 44
6	27	Photometric	45, 32, 64, 66, 615, 16
6	28	Photometric	21
6	29	Photometric (?)	–
6	30	Photometric (?)	–
9	42	Photometric – but clouds may come later	–
9	43	Photometric – but clouds on their way!	00, 14, 15, 13, 18
9	44	Non-photometric!	–

Notes: The weather was noted on top of each page of the log book, except for page 17 and 22, where it was also noted further down. On night 5, the first page number was set to 21 instead of 27 as it should have been, therefore the strange page numbers for night 6. A "c" after the field number means that the observations of the given field were noted over two pages of the log.

For each field complex, aperture photometry using the task `phot` was performed on all suitable stars in the overlap regions within the complex and with at least one other field that had been observed under photometric conditions according to the observations log. From the raw magnitudes, instrumental magnitudes were calculated in the same way as for the galaxy magnitudes, i.e. using Eq. (B.3). For each overlap region, the magnitude difference for the stars, $m_1 - m_2$, was plotted

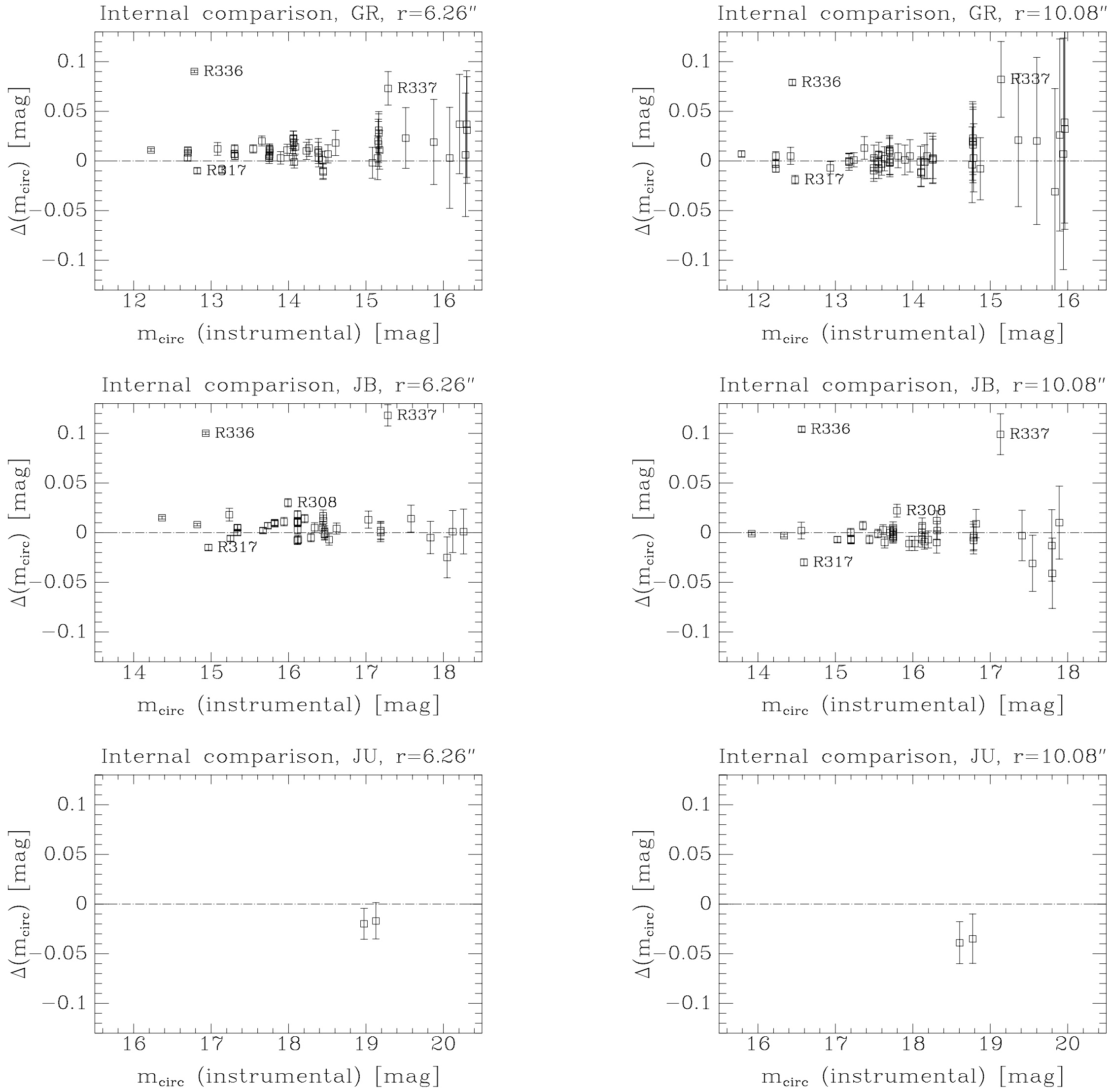

Figure B.3: Comparison of instrumental aperture magnitudes for galaxies observed more than once. From top to bottom the filters are GR, JB, and JU. The left three panels are for an aperture of 6.26″, the right three panels are for an aperture of 10.08″. The galaxies R317, R336 and R337 have been marked, and for JB also R308. The systemtic offset of $\sim 0\overset{\mathrm{m}}{.}01$ seen for the 6.26″ aperture is a seeing effect, cf. the text.

against m_1, using open boxes as the plotting symbol. These plots are referred to as *offset plots*. The first offset plots appear in Fig. B.4 (p. 173). The title of each of these plots are of the form "Overlap: *image1* (*field1*) – *image2* (*field2*)", where m_1 corresponds to *image1*, and m_2 corresponds to *image2*. The aperture radius (usually 9 pixels = 4.6″) is noted in the label of the x-axis. If there were any program galaxies in the overlap region, the magnitude differences for these at apertures 6.26″ and 10.08″ (12 and 20 pixels) were also plotted as filled triangles and boxes, respectively. The horizontal dashed line indicates the derived offset.

The offset plots for a given field complex are summarized in what is termed an *offset diagram*. The first offset diagrams appear in Fig. B.6 (p. 175). In these, each observation of a field is shown as a box, and the overlaps are indicated by arrows. Each arrow is labeled by the derived offset. The direction of the arrow indicates how the offset was calculated: if the arrow goes from field 2 to field 1 the offset was calculated as $\langle m_1 - m_2 \rangle$. The idea is, that to go in the direction of the arrow, one has to *add* the given offset.

How the fields are positioned on the sky relative to each other can be seen from Fig. 3.1 (p. 25) for GR and JB, and Fig. B.14 (p. 177; left panel) for JU.

We now summarize the overlaps studied within the 5 field complexes that we found above needed to be checked. After that, we give the conclusions.

Field 210, 28, and 16

Offset plots: Figure B.4 (GR) and B.5 (JB). Offset diagrams: Figure B.6. 8 overlaps involving 6 images pr. filter were studied:

- field 210 night 4 – field 16 night 1
- field 210 night 4 – field 16 night 6
- field 16 night 1 – field 16 night 6
- field 210 night 4 – field 28 night 4
- field 16 night 1 – field 14 night 3
- field 16 night 6 – field 14 night 3
- field 14 night 3 – field 28 night 4
- field 26 night 4 – field 28 night 4

Note, that the field 14, night 3 GR image, d1552, has scattered light, which may cause extra scatter.

Field 427

Offset plots: Figure B.7. Offset diagrams: Figure B.8. 1 overlap was studied: field 428 night 2 – field 427 night 4.

Field 215

Offset plots: Figure B.9. Offset diagrams: Figure B.10. 1 overlap was studied: field 18 night 1 – field 215 night 4.

Field 33

Offset plots: Figure B.11. Offset diagrams: Figure B.12. 1 overlap was studied: field 33 night 1 – field 33 night 4.

A strange phenomenon can be observed in the JB offset plot: $m_1 - m_2$ is not constant with m_1, it decreases with increasing m_1. If the y-axis had been extended, this would be even more clear. The sky determination in both images was checked and was found to be OK. The phenomenon may either be related to fat zero at low levels (both images have low background levels), or related to the 2 images being stacked from several (2 or 4) shorter exposures. In any case, the bright stars are believed to not be significantly influenced by this.

The 5 JU fields

Offset plots: Figure B.13. Offset diagrams: Figure B.14 (right). 4 overlaps involving 4 images all from night 9 were studied:

- field 00 – field 13
- field 00 – field 14
- field 00 – field 15
- field 13 – field 15

Note, that field 18 does not overlap with any of the other JU images.

Conclusions

Two problem areas were identified, namely the last part of night 4, and night 9. Conclusions:

Night 4

- Clearly, field 210 in both GR and JB are non-photometric.
- The offsets between field 33 night 1 and field 33 night 4 of −0.01 in GR and −0.02 in JB are well determined. Field 33 night 1 were taken to be photometric, and field 33 night 4 were taken to be non-photometric by the above amounts.
- The rest of the night 4 checked fields, 26, 24[1], 427, 215, and 28, have nominal offsets no larger than 0.02. These offsets are not determined better than that, so they were all taken to be zero.

  That the accuracy of these offsets are 0.01–0.02 can be seen from the field 210 complex offsets diagrams, Figure B.6. Different paths from one field to another give results that differ by up to 0.03.
- The adopted value of the offset for field 210 were taken as a suitable mean to be −0.10 in GR and −0.11 in JB.

Night 9

- Field 00 was taken to be the reference image, since it was the one most likely to be photometric, because it had been observed first.
- The offsets for field 14, 15, and 13 were taken to be the derived offset with field 00, namely +0.03, −0.04, and −0.06, respectively. The derived offset between field 13 and 15 is very consistent with these other offsets, the difference is only 0.01, which is less than the uncertainty of the offsets.
- That the field 00 – field 14 offset is positive means that field 14 is a better photometric reference than field 00. However, since no standard stars were observed on night 9 and hence no night coefficient is available, we will need to determine the zero point using comparison with external references anyway.

[1]No overlap photometry on stars using `phot` was done involving field 24, but for the galaxy R243 located in the overlap between field 24 night 4 and field 23 night 3, an offset Δm_{circ} is available. At the $10.08''$ aperture, it is -0.007 ± 0.006 in GR and -0.007 ± 0.003 in JB.

- Field 18, observed just after field 15, did not overlap with any of the other 4 fields. Since it was believed that it was observed under non-photometric conditions, it was assigned an offset equal to that of field 15, namely −0.06.

Other nights

- Field 16 night 1 and field 16 night 6 were both believed to be photometric. The nevertheless non-zero offsets between them of 0.01 in GR and 0.02 in JB[2] were taken to be the typical internal photometric uncertainties. No offsets should be applied to either of these images.

The correcting offsets derived above are listed in Table B.2. These offsets (where non-zero) were added to the 4 magnitude quantities, $m_{\rm ell}(r)$, $m_{\rm circ}(r)$, $\mu(r)$, and $<\mu>(r)$.

[2] To these magnitude differences at a finite aperture r, $\Delta m(r)$, should be added the difference in aperture correction induced by the difference in seeing, $\Delta\mathrm{apcor}(r)$, to get the intrinsic magnitude difference, $\Delta m_{\rm T}$; i.e. $\Delta m_{\rm T} = \Delta m(r) + \Delta\mathrm{apcor}(r)$. $\Delta\mathrm{apcor}(r)$ for those particular images and the used 9 pixel aperture is −0.002 for GR and −0.003 for JB, and thus negligible. For reference, the seeing values are listed in Table 3.5 (p. 30), the aperture correction vs. seeing is plotted in Fig. C.2 (p. 184) and C.3 (p. 184), and the pixel scale is 0.5073 ″/pixel.

Table B.2: List of Non-photometric Corrections

Night	Offset GR	Offset JB	Field	Pair	Program galaxies
1			00	x	R245, R253, R255, R256, R266, R268, R269, R273, R286, R293
1	0.00	0.00	16	x	R308
1			13	x	R209, R217, R234, R237, R241
1			25		–
1			37	x	R166, R185
1	0.00	0.00	18	x	R214, R219, R225
1			12	x	R255, R273, R278
1			21		–
1	0.00	0.00	33	x	R317
1			45		–
2			214		R261
2			320		R327
2	0.00	0.00	428		R250
2			632		–
2			29		R193
2			419		R138
2			519		R129
2			15	x	R213, R216, R224, R226, R239, R245
3			00	x	R245, R253, R255, R256, R266, R268, R269, R273, R286, R293
3	0.00	0.00	14		R316, R322
3			15	x	R213, R216, R224, R226, R239, R245
3			13	x	R209, R217, R234, R237, R241
3			27	x	R188, R194, R209
3			23	x	R243
3			43		R338, R343, R347
3			18	x	R214, R219, R225
3			321		R283, R288
3			535		R252, R295
3			35		R218, R231
4			46		R238
4			47		R202
4			34		R254
4			22		R319
4	0.00	0.00	26		R334, R359
4			24	x	R211, R212, R243
4	−0.10	−0.11	210	x	R336, R337
4	0.00	0.00	427		R305
4	0.00	0.00	215	x	R225
4	0.00	0.00	28	x	R336, R337, R340
4	−0.01	−0.02	33	x	R317
6			213		–
6			39	x	R166
6			36		–
6			44		–
6			45		–
6			32		–
6			64		R389
6			66		R307
6			615		R112, R120
6	0.00	0.00	16	x	R308
6			21		–
	JU				
9	0.00		00	x	R239, R245, R253, R255, R256, R266, R268, R269, R273, R286, R293
9	+0.03		14		R316, R322
9	−0.04		15	x	R213, R216, R224, R239, R245
9	−0.06		13		R217, R234, R237
9	−0.06		18		R214, R219, R225

Notes: The list is in chronological order. Exactly those images that appear in the offset plots in this section has a listed offset (with the exception of field 18 JU; see the text). "Pair" means that the given entry has one or more galaxies that have been observed more than once. The 64 galaxies in this table are the ones in the HydraI surface photometry sample, cf. Table 3.3 (p. 28).

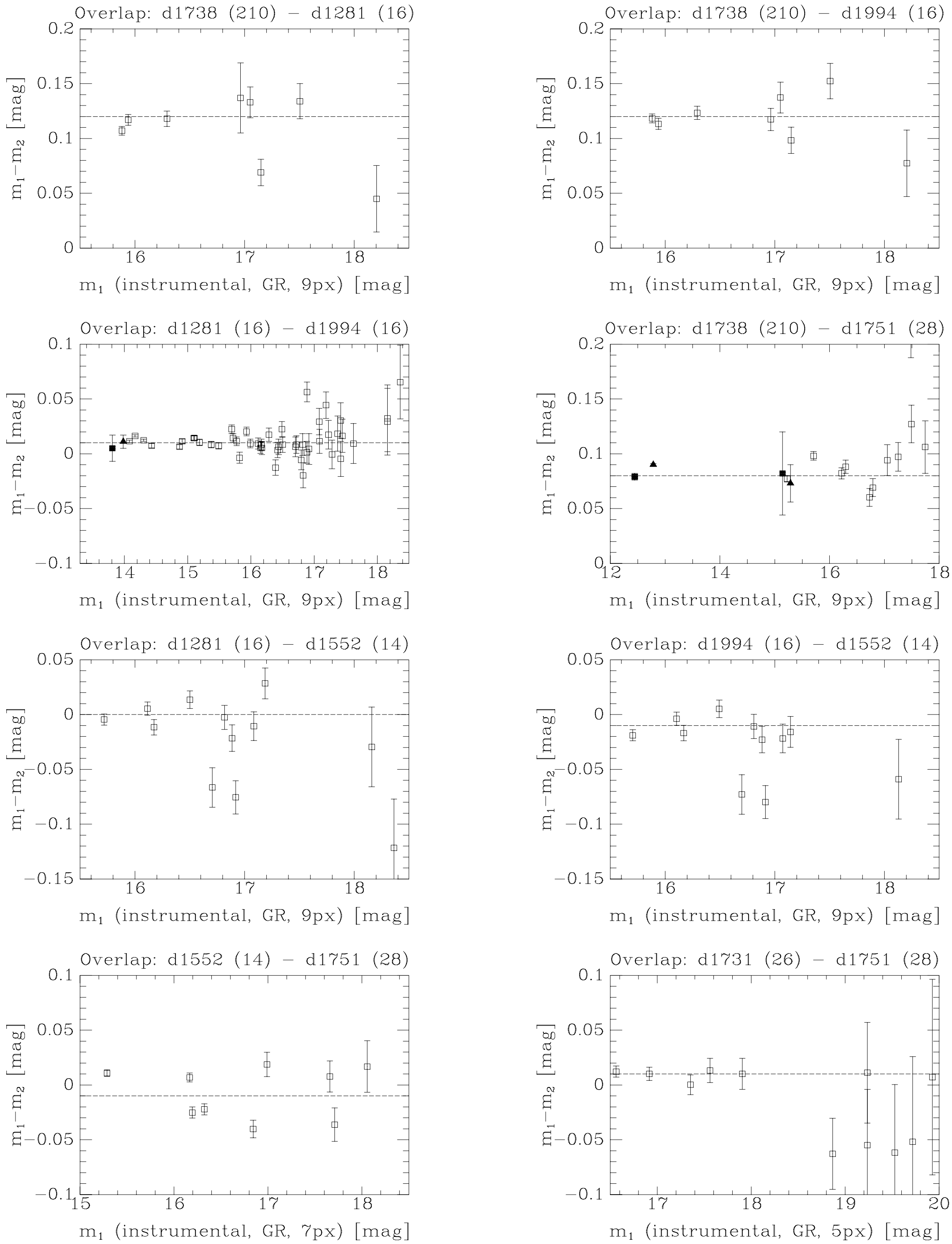

Figure B.4: Offset plots, field 210 and 28, GR. The galaxies in the overlap between field 210 and 28 are R336 (bright) and R337 (faint). The galaxy in the overlap between field 16 and 16 (sic!) is R308. Note, that the image d1552 has scattered light, which may cause extra scatter.

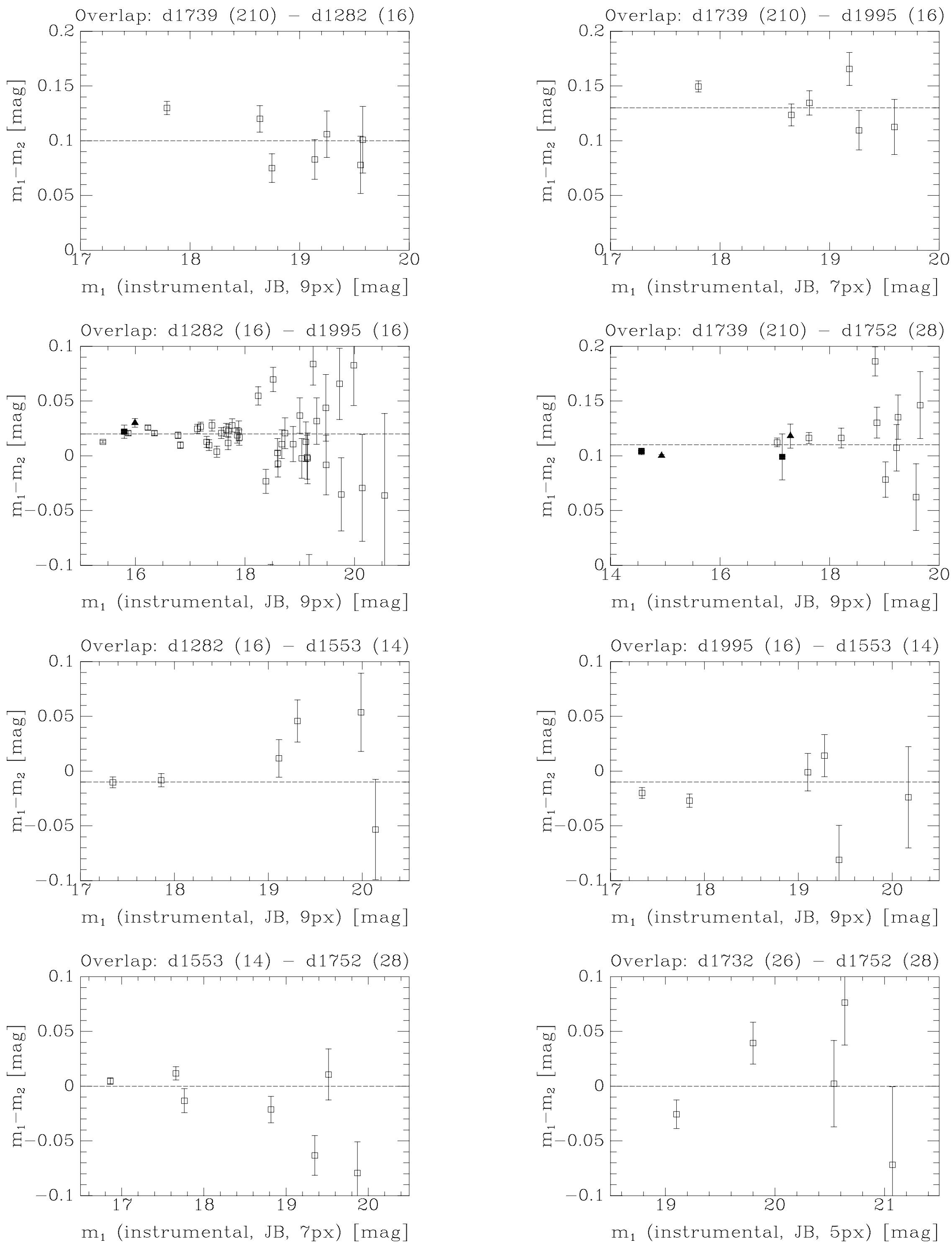

Figure B.5: Offset plots, field 210 and 28, JB. The galaxies in the overlap between field 210 and 28 are R336 (bright) and R337 (faint). The galaxy in the overlap between field 16 and 16 (sic!) is R308.

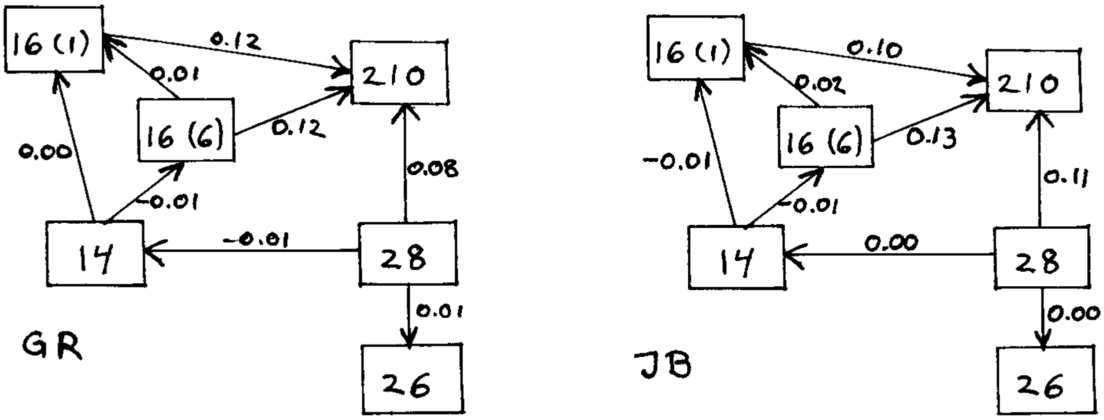

Figure B.6: Offset diagrams, field 210 and 28.

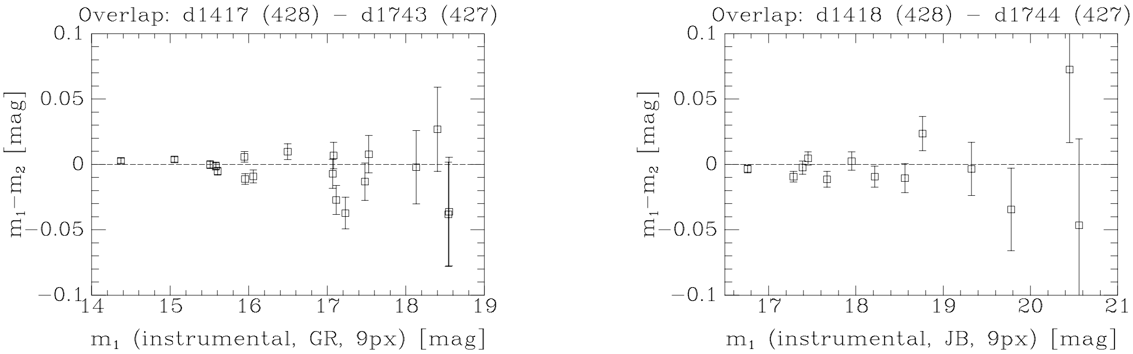

Figure B.7: Offset plots, field 427.

Figure B.8: Offset diagrams, field 427.

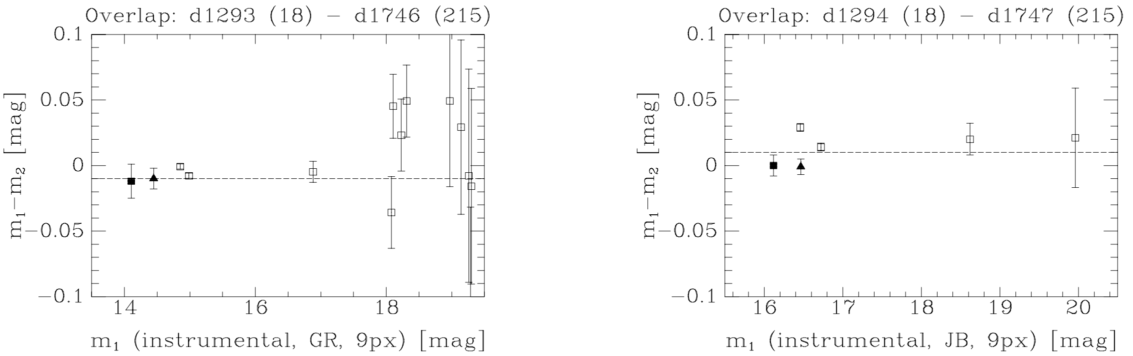

Figure B.9: Offset plots, field 215. The galaxy is R225.

Figure B.10: Offset diagrams, field 215.

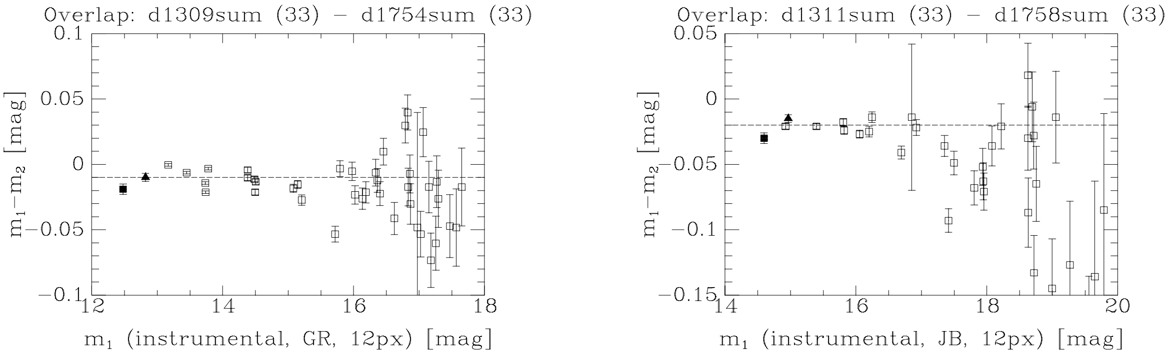

Figure B.11: Offset plots, field 33. The galaxy (seen to the very left) is R317.

Figure B.12: Offset diagrams, field 33.

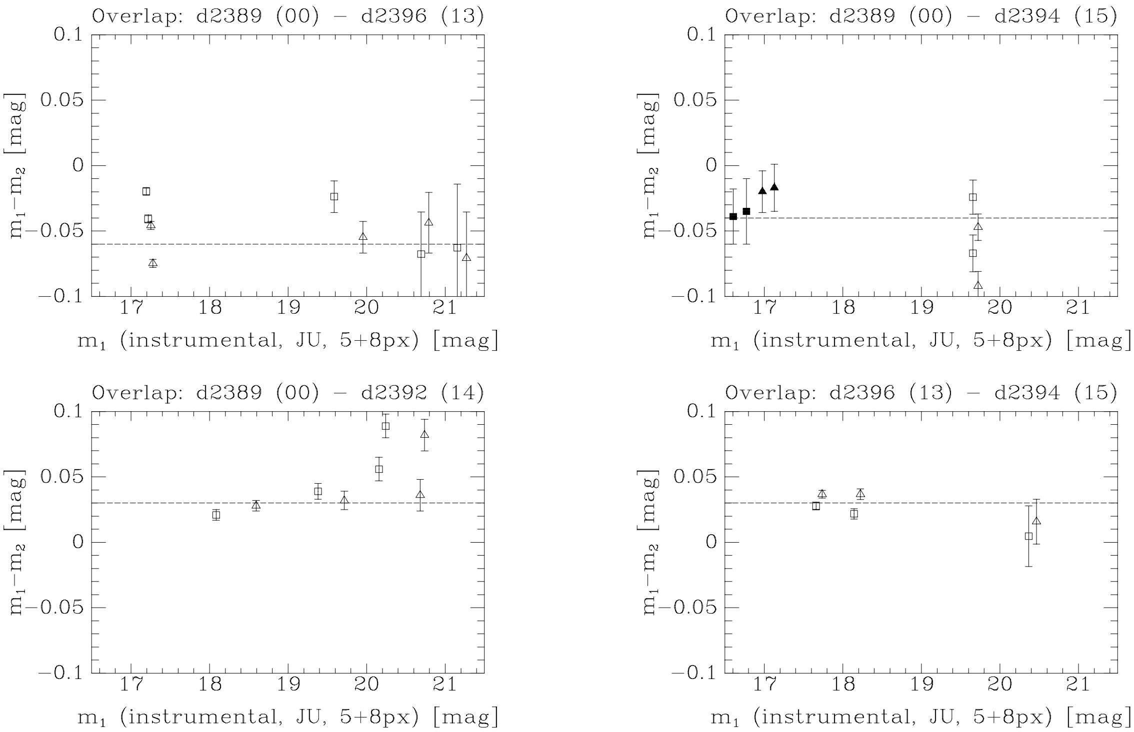

Figure B.13: Offset plots, the JU fields. The galaxies in the overlap between field 00 and 15 are R239 (faint) and R245 (bright). Here, two `phot` apertures are shown: open triangle: 5 pixels; open box: 8 pixels. The `galmag` points are as in the other offset plots: filled triangle: 6.26″; filled box: 10.08″.

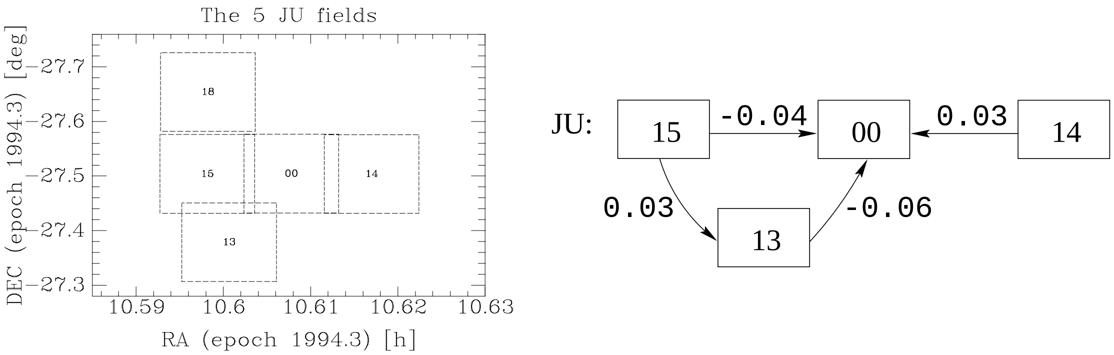

Figure B.14: Left: The position of the JU fields on the sky. Right: Offset diagrams, the JU fields.

Appendix C

The Standard Calibration

C.1 Standard Star Observations

Three standard star fields were observed: M67, PG1633+099, and SA110 centered on star 503 (hereafter SA110–503). The M67 field was observed with the telescope defocused, since the stars in that field are very bright; the other two fields were observed with the telescope focused. Examples of the visual appearance of a defocused and a focused star are shown in Figure C.1. four passbands were used: Gunn r, and Johnson V, B, and U. Standard stars were observed on all the nights that the Hydra galaxies were observed in Gunn r and Johnson B (night 1, 2, 3, 4, & 6), but not the night that the Hydra galaxies were observed in Johnson U (night 9). In addition, standard stars were observed on night 7. Details of the standard star observations are in Table C.1 and C.2.

Two naming schemes exist for the stars in the M67 field: The F numbers (e.g. F108), and the quadrant numbers (e.g. II20). They are almost, but not completely, disjoint. A finding chart for the F numbered stars is in Johnson & Sandage (1955). A finding chart for the quadrant numbered stars is in Eggen & Sandage (1964). Four stars (of interest to this study) with F numbers, are not marked on the map of Johnson & Sandage (1955), and have also been assigned quadrant numbers by Eggen & Sandage (1964). These are: F93=I12, F106=I11, F128=I198, and F129=I199. The finding chart of Schild 1983, which covers a smaller area than that of Johnson & Sandage (1955), has these 4 stars on it with the F numbers. Also note, that *two* stars are labeled 124 (i.e. F124) in the map of Johnson & Sandage (1955). The bright one (the one most to the east) is F124, the other one is I10.

Finding charts for the PG1633+099 and the SA110 field are in Landolt (1992).

The standard star images were reduced in the same way as the galaxy images, i.e. trim, bias, fat zero, dark, shutter, and flat field, with the exception, that the height of the fat zero background box (`boxh`) was set to 3 pixels instead of 21 pixels. This worked better for the stars close to the fat zero columns. The flat field used for the Johnson V images was a dome flat – no sky flats were taken in this filter.

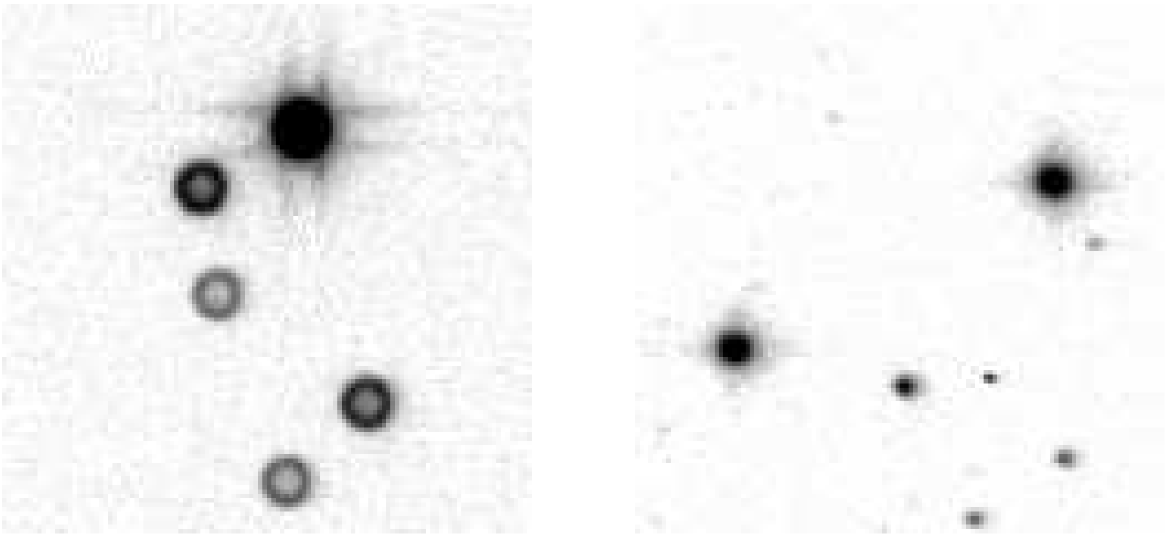

Figure C.1: Examples of defocused and focused star images. Both images are 120 pixels × 120 pixels (61″ × 61″) sections, in the Gunn r filter, displayed logarithmically, and have north down and east to the right. Left: Part of the M67 field, image d1534, display cuts: z1=0, z2=1500. The bright star is F108 (r = 9.3 mag), and the semi-bright star to the (lower) right is F111 (r = 12.7 mag). Right: Part of the SA110–503 field, image d1603, display cuts: z1=0, z2=1200. The bright star to the left is 499 (r = 11.5 mag), the one to the right is 502 (r = 11.4 mag).

Table C.1: Standard star observations, by night

Night	Field	Airmass	Exposure time [sec]				Image name (dfsc #)			
			GR	JV	JB	JU	GR	JV	JB	JU
1	M67	1.33	5	10	20	120	d1263	d1262	d1264	d1266
1	PG1633+099	1.43	10	20	120	300	d1322	d1318	d1320	d1321
1	SA110–503	1.67	4	7	20	240	d1325	d1326	d1327	d1329
1	SA110–503	1.16	3	6	20	90	d1349	d1350	d1351	d1352
2	M67	1.34	5	10	20	120	d1388	d1389	d1390	d1391
2	PG1633+099	1.38	7	20	120	300	d1464	d1465	d1466	d1467
2	SA110–503	1.67	4	7	20	120	d1472	d1469	d1470	d1471
2	SA110–503	1.15	4	7	20	120	d1494	d1495	d1496	d1497
3	M67	1.34	5	10	20	120	d1534	d1535	d1536	d1537
3	PG1633+099	1.42	10	20	120	300	d1597	d1598	d1599	d1600
3	SA110–503	1.68	4	7	20	120	d1603	d1606	d1605	d1604
3	SA110–503	1.15	4	6	20	120	d1632	d1633	d1634	d1635
4	M67	1.34	5	10	20	120	d1689	d1690	d1691	d1692
4	SA110–503	1.60	4	10	20	120	d1771	d1772	d1773	d1774
4	PG1633+099	1.29	10	20	120	300	d1785	d1781	d1782	d1783
4	SA110–503	1.15	4	7	20	120	d1797	d1798	d1799	d1800
6	M67	1.35	5	10	20	120	d1948	d1949	d1950	d1951
6	SA110–503	1.44	4	10	20	120	d2016	d2018	d2021	d2022
6	PG1633+099	1.29	10	20	120	300	d2023	d2024	d2026	d2027
6	SA110–503	1.16	4	7	20	60	d2044	d2045	d2046	d2047
7	M67	1.33	5	10	20	120	d2092	d2093	d2094	d2095
7	SA110–503	1.64	4	7	20	120	d2145	d2148	d2147	d2146
7	SA110–503	1.15	4	7	20	120	d2169	d2170	d2171	d2172

Notes: Only the images used to fit the parameters of the transformation equations are shown (i.e. the images in the output from `mkimsets`). Airmass is an approximate average for the 4 exposures. In the actual calculations, the exact airmass for the individual images has been used. The M67 images were defocused, the PG1633+099 and SA110–503 were focused. GR, JV, JB, and JU are the 4 used passbands: Gunn r, and Johnson V, B, and U.

Table C.2: Standard star observations, by field

Night	Field	Airmass	Exposure time [sec]				Image name (dfsc #)			
			GR	JV	JB	JU	GR	JV	JB	JU
1	M67	1.33	5	10	20	120	d1263	d1262	d1264	d1266
2	M67	1.34	5	10	20	120	d1388	d1389	d1390	d1391
3	M67	1.34	5	10	20	120	d1534	d1535	d1536	d1537
4	M67	1.34	5	10	20	120	d1689	d1690	d1691	d1692
6	M67	1.35	5	10	20	120	d1948	d1949	d1950	d1951
7	M67	1.33	5	10	20	120	d2092	d2093	d2094	d2095
1	PG1633+099	1.43	10	20	120	300	d1322	d1318	d1320	d1321
2	PG1633+099	1.38	7	20	120	300	d1464	d1465	d1466	d1467
3	PG1633+099	1.42	10	20	120	300	d1597	d1598	d1599	d1600
4	PG1633+099	1.29	10	20	120	300	d1785	d1781	d1782	d1783
6	PG1633+099	1.29	10	20	120	300	d2023	d2024	d2026	d2027
1	SA110–503	1.67	4	7	20	240	d1325	d1326	d1327	d1329
1	SA110–503	1.16	3	6	20	90	d1349	d1350	d1351	d1352
2	SA110–503	1.67	4	7	20	120	d1472	d1469	d1470	d1471
2	SA110–503	1.15	4	7	20	120	d1494	d1495	d1496	d1497
3	SA110–503	1.68	4	7	20	120	d1603	d1606	d1605	d1604
3	SA110–503	1.15	4	6	20	120	d1632	d1633	d1634	d1635
4	SA110–503	1.60	4	10	20	120	d1771	d1772	d1773	d1774
4	SA110–503	1.15	4	7	20	120	d1797	d1798	d1799	d1800
6	SA110–503	1.44	4	10	20	120	d2016	d2018	d2021	d2022
6	SA110–503	1.16	4	7	20	60	d2044	d2045	d2046	d2047
7	SA110–503	1.64	4	7	20	120	d2145	d2148	d2147	d2146
7	SA110–503	1.15	4	7	20	120	d2169	d2170	d2171	d2172

Notes: Same data as in Table C.1.

C.2 Aperture Photometry

To establish the transformation between instrumental magnitudes and standard magnitudes, we need to do photometry on the standard stars. Since the galaxy surface photometry is done as aperture photometry, we also need to do aperture photometry on the standard stars, as opposed to for example point spread function fitting.

The larger the aperture, the more of the flux from the star is within the aperture. But the larger the aperture, the larger is the error from the sky subtraction, and the more cosmic ray events will be within the aperture. Thus, the optimal aperture is one which is large enough to enclose most of the flux, but otherwise is as small as possible.

The correction for the finite size of the aperture is called the aperture correction. It is computed from a growth curve, i.e. a plot of magnitude within a given aperture versus aperture size. The aperture correction is simply the magnitude difference between the asymptotic magnitude and the magnitude at the given aperture.

The most straightforward way to determine the aperture correction is to measure it directly from a number of growth curves. A more advanced method is the DAOgrow algorithm (Stetson 1990), implemented in the task `mkapfile` in `digiphotx.photcalx`. It fits a five parameter (with usually only 3 of them free) stellar profile model to the growth curves for one or more stars in one or more images. It then computes the aperture correction from a given aperture to the largest aperture.

One of the five parameters in the model, R_i, represent the seeing radius for the individual images. The other four parameters are global for all the images. For more details, see Stetson (1990).

C.2.1 The Focused Images

Aperture photometry using the task `phot` (in `digiphotx.apphotx`) was done on the 5 standard stars in the PG1633+099 images and the 8 standard stars in the SA110–503 images (cf. Table C.11). As previously mentioned, these two fields were observed with the telescope focused. The apertures used were $2, 3, \ldots, 30$ pixels (1 pixel = $0.5073''$). The crucial sky fitting algorithm parameters (`fitskypars`) were set as follows: `salgorithm`=gauss, `annulus`=30.0 pixels, and `dannulus`=10.0 pixels, giving a background region of 30–40 pixels, or 15.22–20.29$''$. The length of the box within which the star is centered, `centerpars.cbox`, was set to 10 pixels.

`mkapfile` was used to determine the aperture correction from a number of apertures, $7, 8, \ldots, 14$ pixels to "infinity" (taken as the largest aperture, 30 pixels). The resulting aperture corrections versus the seeing is shown in Figure C.2.

The figure shows, as expected, that the size of the aperture correction decreases with increasing aperture size. It also shows, that the aperture correction (for most of the apertures used) is significantly seeing dependent.

It was decided, that an aperture of 9 pixels ($4.57''$) was optimal. The aperture correction versus seeing for this aperture only is shown in Figure C.3.

As can be seen, the dependence of aperture correction on seeing is very smooth. This is not totally surprising, since the seeing is calculated by `mkapfile` itself, and is one of the parameters it uses in the stellar profile model.

To further reduce the scatter, a 3rd order (`order`=4) Legendre polynomial was fitted to the points using `gfit1d`. The fit was very good, with residual no larger than 0.0008 mag, and typically 0.0002 mag. The final aperture corrections for the focused stars were calculated from the fit. The errors from `mkapfile` were used.

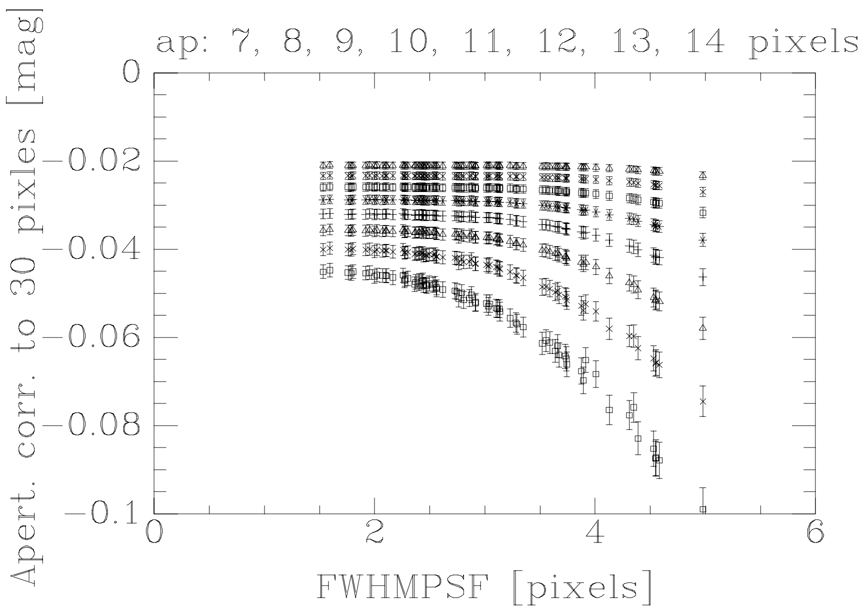

Figure C.2: Aperture corrections for different sized apertures, from 14 pixels (top) to 7 pixels (bottom). FWHMPSF is calculated as 2.355 times the seeing radius from `mkapfile`. For a Gaussian profile, 2.355 is the ratio between the FWHM and the standard deviation.

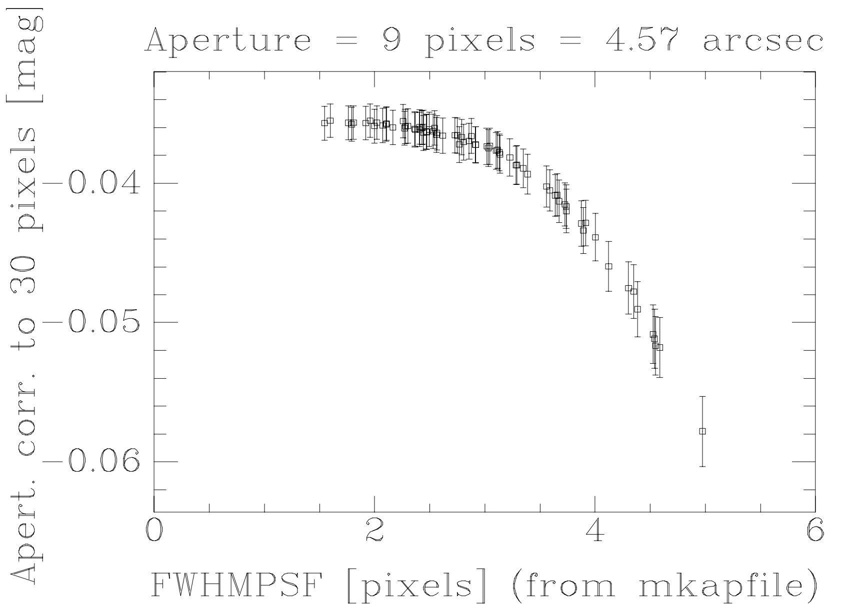

Figure C.3: Aperture corrections for the 9 pixels aperture. FWHMPSF is calculated as 2.355 times the seeing radius from `mkapfile`.

Seeing versus night is plotted in Figure C.4, right panel. The corresponding aperture correction variation with night is shown in Figure C.4, left panel.

Finally, `phot` was run again, this time with only one aperture: 9 pixels.

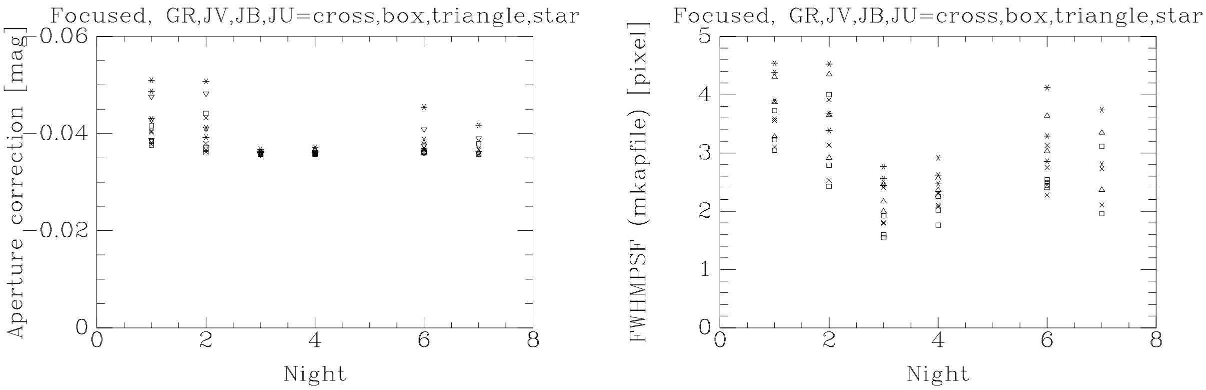

Figure C.4: Aperture correction and seeing versus night, same data as in Figure C.3. Left: Aperture correction versus night. Right: Seeing (FWHMPSF) versus night. FWHMPSF is calculated as 2.355 times the seeing radius from `mkapfile`.

C.2.2 The Defocused Images

`phot` was run on 4 well isolated stars (F81, F153, F170, & I27) in the defocused images, with apertures $5, 6, \ldots, 42$ pixels, and with `salgorithm`=gauss, `annulus`=42.0 pixels, and `dannulus`=14.0 pixels. Even though the defocused stars did not have a peak to define their centers, they were centered well using a somewhat large box, `centerpars.cbox`=15 pixels, which still was small enough to exclude the neighboring stars.

A large effort went into trying to get `mkapfile` to fit the profiles of the defocused stars, and compute the aperture correction. This did not succeed.

Instead, aperture corrections at 12 and 15 pixels were manually read from the growth curves that `mkapfile` produced. These growth curves, one for each image, were based on the above 4 stars. An example of such a curve is shown in Figure C.5. The resulting aperture corrections are shown in Table C.3, and plotted in Figure C.6, the two left panels. In the top right panel, the difference between the two is shown.

From the plots it can readily be seen, that the aperture correction is not the same for the 4 filters, and that it is not the same from night to night. Further, the difference between the aperture corrections at the two apertures is not the same for the 4 filters and from night to night.

The M67 field of this study had 23 stars in common with the standard stars of Jørgensen (1994). Besides of these standard stars, 36 stars were selected as "program" stars on the following three criteria: they should be somewhat bright (we required a peak > 500 ADU in the GR image d1262), they should not be too close to other stars, and they should have a unique name. The reason for including these program stars was: 1) the derived magnitudes for these stars could be useful in another context (they could perhaps serve as tertiary standard stars), and 2) the more stars, the better statistics for the test of the aperture correction, see below.

`phot` was run on these 59 stars, using two apertures: 12 and 15 pixels. `cbox` was increased to 20 pixels. The reason for using two apertures was to test the aperture corrections determined above at these two apertures. Since per definition

$$m(\text{total}) = m(12\text{px}) + \text{apcor}(12\text{px}) \quad (C.1)$$
$$= m(15\text{px}) + \text{apcor}(15\text{px}), \quad (C.2)$$

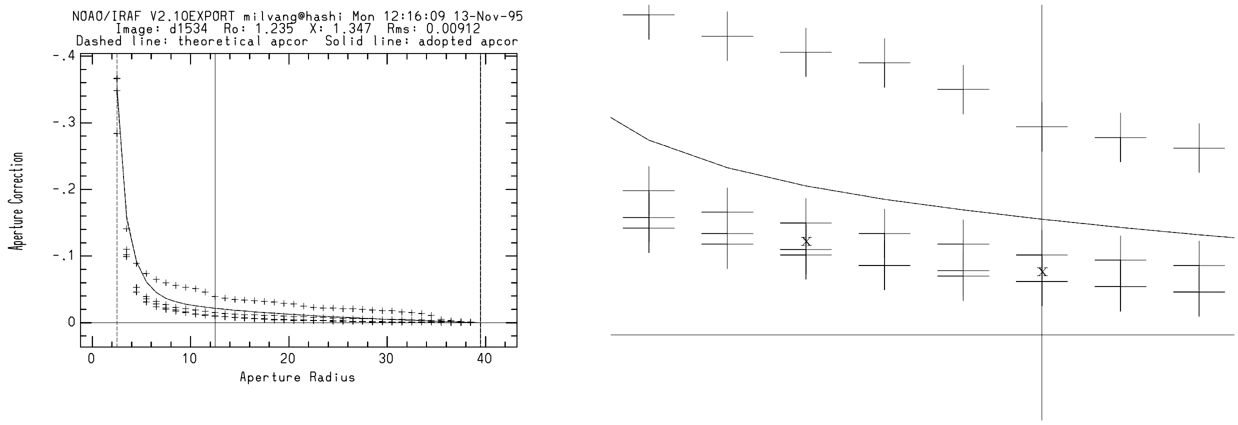

Figure C.5: Example of a growth curve (or *aperture correction curve*) made by `mkapfile`. The image is d1534, which is in Gunn r and from night 3.
Left: The entire curve. The x-axis is aperture radius minus 2.5 pixels. The y-axis is aperture correction with respect to the magnitude at 42 pixels. The dotted vertical line is at 5 pixels, the left solid vertical line is at 15 pixels, and the right solid vertical line is at 42 pixels. The curve is the fit, which was not used.
Right: A zoom around apertures 12 and 15 pixels. The "x"-s show approximately the values read by the user as the aperture correction to be used. As can be seen, the top point has been regarded as erroneous and omitted from the eye fit. The 15 pixels aperture is at the vertical solid line, the 12 pixels aperture is 4 "steps" to the left. The 3 "good" values at 12 pixels are -0.0150, -0.0160, -0.0210, with the eye fit mean of -0.0173. The arithmetical mean is also -0.0173. The estimated uncertainty on this is 0.002.

it follows that

$$m(12\text{px}) - m(15\text{px}) = -\left[\text{apcor}(12\text{px}) - \text{apcor}(15\text{px})\right]. \tag{C.3}$$

This only holds in the absence of contributions from neighboring stars and cosmic ray events. $m(12\text{px}) - m(15\text{px})$ for the above 59 stars for each image (with one image per night per filter) is shown in Figure C.7 for Gunn r and Johnson V, and Figure C.8 for Johnson B and U. The median value of $m(12\text{px}) - m(15\text{px})$ for each of the 24 images is shown in Figure C.6, bottom right panel. In the top right panel of the same figure is shown $-\left[\text{apcor}(12\text{px}) - \text{apcor}(15\text{px})\right]$.

As can be seen, the form of the "curves" is qualitatively the same, but there is a small offset. This offset is probably due to contributions from neighboring stars for the sample of 59 stars. This contribution is much less in the sample of 4 stars, since they were selected from being isolated. This can be checked by inspecting these 4 stars in Figure C.7 and C.8. They are almost always in the lower range of the 59 points. The mapping between names and serial ID number for these 4 stars is F81=ID1, F153=ID26, F170=ID28, and I27=ID38. F81 with and ID of 1 is particularly easy to locate. The conclusion is, that the manually determined aperture corrections pass the test of equation (C.3).

The M67 field is quite crowded. For example, F128/I198 and F129/I199 are 25 pixels (13″) apart, F129/I199 and F130 are 23 pixels (12″) apart, and F106/I11 and its fainter neighbor I10 are only 16 pixels (8″) apart. This also shows up in the magnitude difference plots in Figure C.7 and C.8. The mapping between names and serial ID number for these 4 stars is F128/I198=ID15, F129/I199=ID16, F130=ID17, and F106/I11=ID7. Especially F106/I11 is very contaminated. The above speaks in favor of a small aperture

Also, the images are quite defocused. Inspection of screen dumps of the images used in Jørgensen

Table C.3: The manually measured aperture corrections, by night

night	filter	image	apcor12	apcor15	delta
1	GR	d1263	–0.032	–0.018	0.015
1	JV	d1262	–0.027	–0.014	0.012
1	JB	d1264	–0.034	–0.019	0.014
1	JU	d1266	–0.048	–0.023	0.025
2	GR	d1388	–0.025	–0.017	0.009
2	JV	d1389	–0.020	–0.012	0.007
2	JB	d1390	–0.032	–0.020	0.012
2	JU	d1391	–0.044	–0.026	0.018
3	GR	d1534	–0.017	–0.012	0.006
3	JV	d1535	–0.015	–0.010	0.005
3	JB	d1536	–0.021	–0.016	0.006
3	JU	d1537	–0.043	–0.030	0.013
4	GR	d1689	–0.021	–0.014	0.007
4	JV	d1690	–0.017	–0.013	0.004
4	JB	d1691	–0.024	–0.015	0.009
4	JU	d1692	–0.040	–0.027	0.013
6	GR	d1948	–0.022	–0.017	0.005
6	JV	d1949	–0.017	–0.012	0.005
6	JB	d1950	–0.023	–0.015	0.008
6	JU	d1951	–0.038	–0.024	0.013
7	GR	d2092	–0.021	–0.015	0.006
7	JV	d2093	–0.016	–0.010	0.005
7	JB	d2094	–0.021	–0.014	0.008
7	JU	d2095	–0.038	–0.027	0.011

Notes: apcor12 and apcor15 are the aperture corrections for the defocused images at an aperture of 12 pixels and 15 pixels, respectively, in magnitudes. delta is minus the difference between the two, i.e. delta = –(apcor12–apcor15). The aperture corrections were manually measured from growth curves based on the 4 stars F81, F153, F170, and I27. Uncertainties were estimated from the scatter of the used individual points. Typical values are: GR: 0.002 mag, JV: 0.001 mag, JB: 0.002 mag, JU: 0.006 mag. When doing the eye fit, the JU values from night 4 was noted as uncertain, and a more realistic uncertainty for these values is probably 0.010–0.015 mag.

(1994) shows, that that these images were less defocused than the images of this study, despite that both used a defocusing of +200 encoder steps. This is probably because the filters are now placed in the DFOSC, instead in the instrument adapter as they previously were.

Jørgensen (1994) used two apertures for her defocused images, 7.52″ and 9.40″.

It was decided to use an aperture of 12 pixels (6.09″), and to use the corresponding aperture corrections listed in Table C.3. As previously mentioned, the background region was 42–56 pixels, i.e. 21.31–28.41″.

Finally, we can compare the aperture corrections for the focused and the defocused images. This in done in Figure C.9. The variation with night is quite similar for the focused and defocused images.

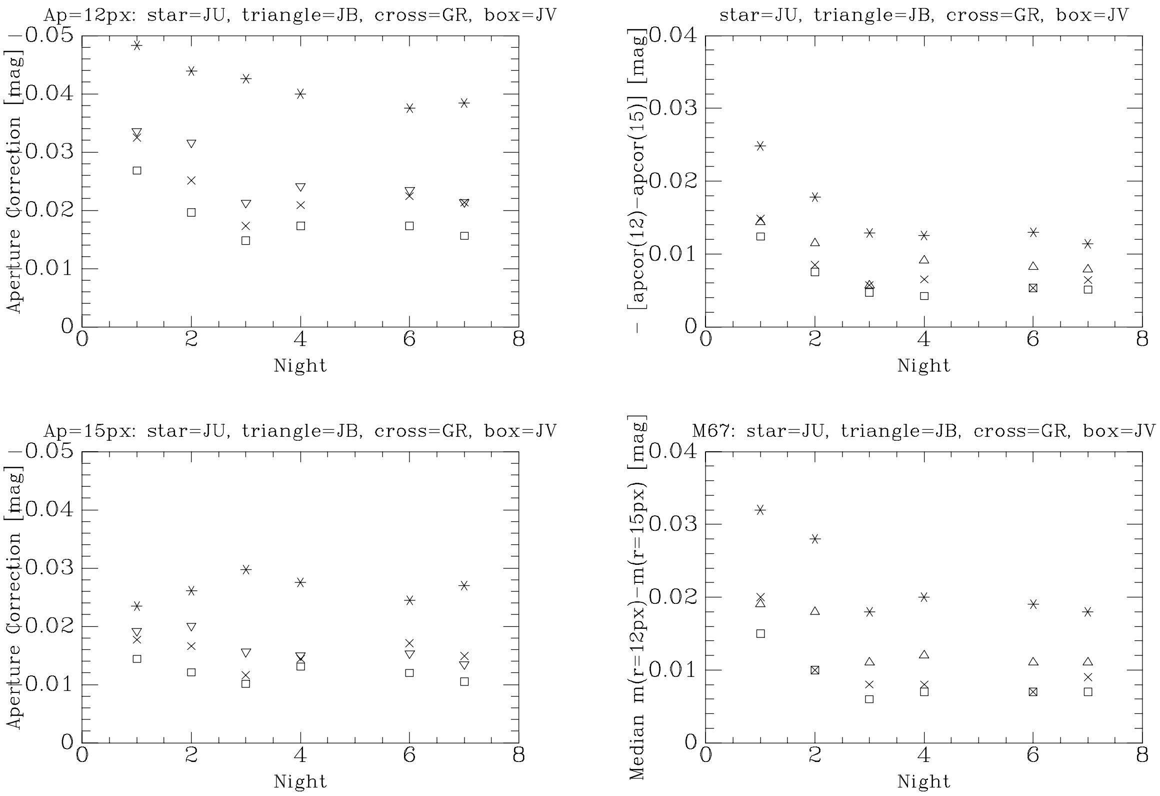

Figure C.6: The manually measured aperture corrections for the defocused images. Symbol legend: star: Johnson U, triangle: Johnson B, cross: Gunn r, box: Johnson V. Top left: aperture correction at 12 pixels. Bottom left: aperture correction at 15 pixels. Top right: difference between the aperture corrections at 12 and 15 pixels. Typical uncertainties on the manually measured aperture corrections are: GR: 0.002 mag, JV: 0.001 mag, JB: 0.002 mag, JU: 0.006 mag (night 4: 0.010 mag). Bottom right: difference between the magnitudes within 12 and 15 pixels (median value of 59 stars, cf. Figure C.7 and C.8).

Table C.4: Mapping between star names and ID numbers

ID	Name	Type	ID	Name	Type	ID	Name	Type
1	M67–F81	standard	21	M67–F141	standard	41	M67–I56	program
2	M67–F83	program	22	M67–F143	program	42	M67–I60	program
3	M67–F93/I12	standard	23	M67–F145	program	43	M67–II20	program
4	M67–F94	program	24	M67–F147	program	44	M67–II22	standard
5	M67–F95	standard	25	M67–F149	program	45	M67–II30	program
6	M67–F105	standard	26	M67–F153	standard	46	M67–III1	program
7	M67–F106/I11	standard	27	M67–F164	program	47	M67–III2	program
8	M67–F108	standard	28	M67–F170	program	48	M67–III7	program
9	M67–F111	standard	29	M67–I1	program	49	M67–III12	program
10	M67–F115	program	30	M67–I5	program	50	M67–IV2	program
11	M67–F117	standard	31	M67–I9	program	51	M67–IV3	program
12	M67–F119	program	32	M67–I14	program	52	M67–IV4	program
13	M67–F124	standard	33	M67–I15	standard	53	M67–IV6	program
14	M67–F127	standard	34	M67–I17	program	54	M67–IV12	program
15	M67–F128/I198	standard	35	M67–I20	standard	55	M67–IV13	program
16	M67–F129/I199	standard	36	M67–I24	program	56	M67–IV21	program
17	M67–F130	standard	37	M67–I25	standard	57	M67–IV34	program
18	M67–F132	program	38	M67–I27	standard	58	M67–IV35	program
19	M67–F134	standard	39	M67–I31	program	59	M67–IV59	program
20	M67–F135	standard	40	M67–I49	standard			

Notes: ID is the identification serial number which `phot` uses internally. It is also the number used in Figure C.7 and C.8.

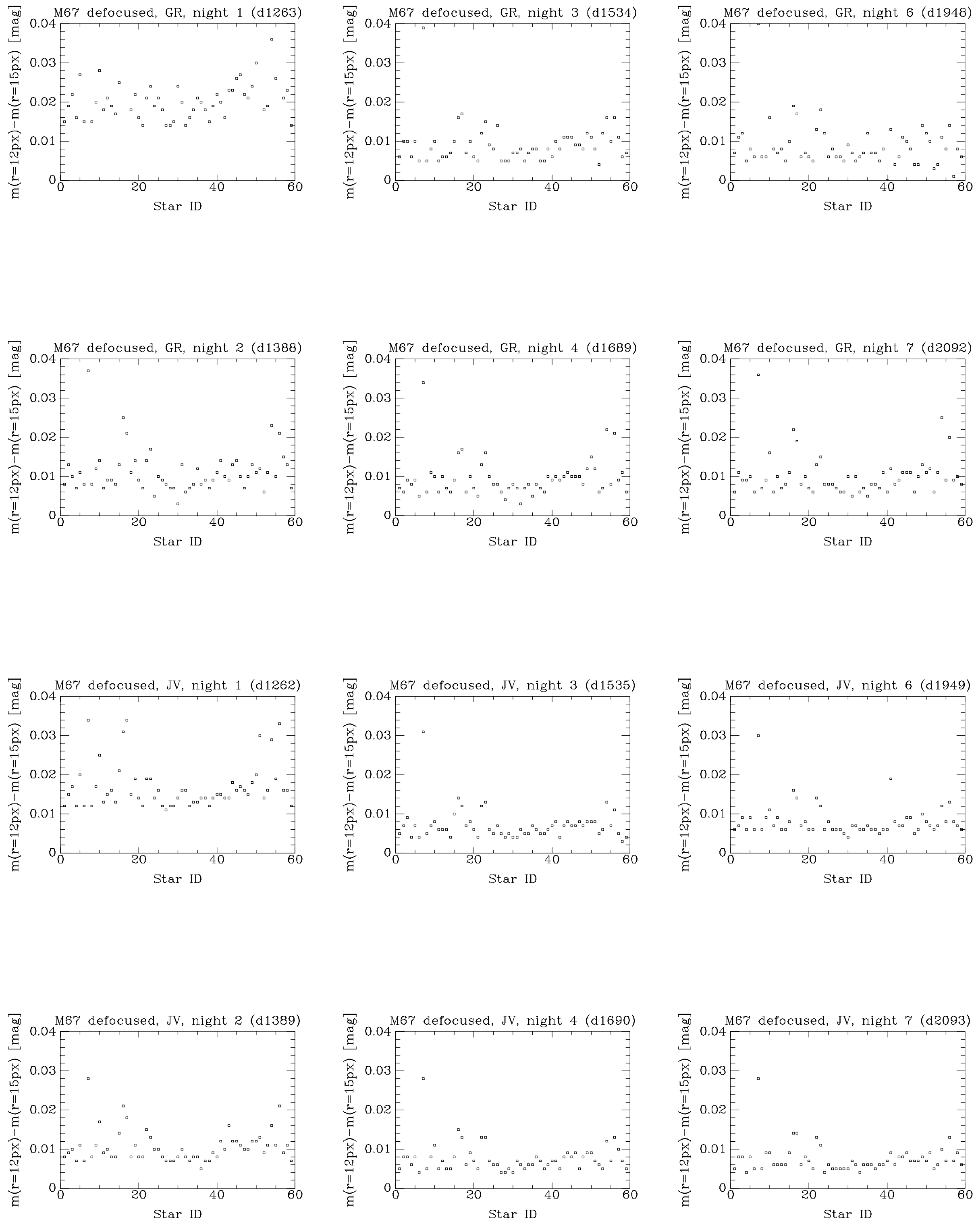

Figure C.7: Magnitude difference between apertures of 12 and 15 pixels. Top 6 panels: Gunn r. Bottom 6 panels: Johnson V. Along the x-axis is star ID number; mapping between this and star name can be found in Table C.4.

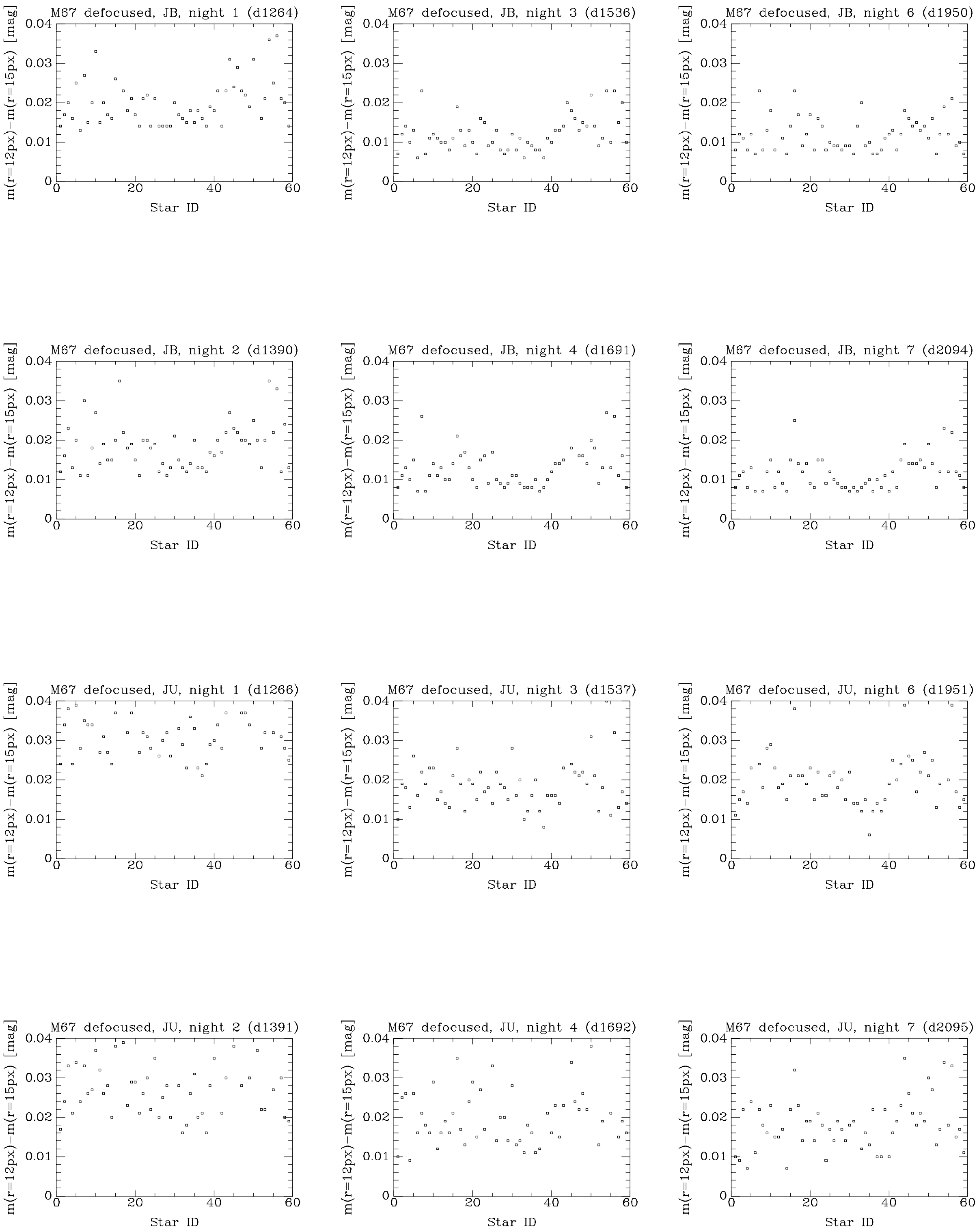

Figure C.8: Magnitude difference between apertures of 12 and 15 pixels. Top 6 panels: Johnson B. Bottom 6 panels: Johnson U. Along the x-axis is star ID number; mapping between this and star name can be found in Table C.4.

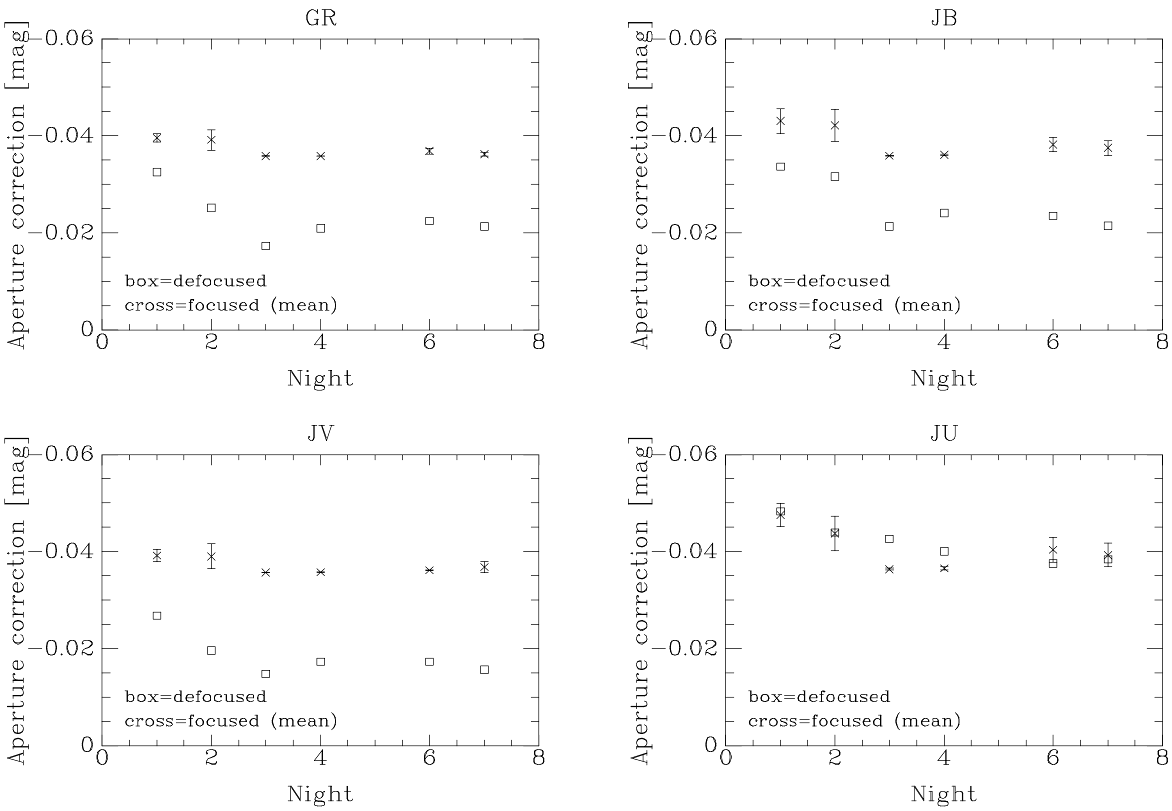

Figure C.9: Aperture corrections for the focused and defocused images. The focused data are the mean of the usually 3 images (2 SA110–503, and 1 PG1633+099) per night per filter, and are based on the data in Figure C.4, left panel. The aperture is 9 pixels ($4.57''$). The defocused data are the same as in Figure C.6, upper left panel. The aperture is 12 pixels ($6.09''$). Typical uncertainties on the aperture corrections for the defocused images are: GR: 0.002 mag, JV: 0.001 mag, JB: 0.002 mag, JU: 0.006 mag (night 4: 0.010 mag).

C.3 Extinction and Night Coefficients

As Table C.2 shows, the SA110–503 field was observed twice every night at different airmasses, typically 1.65 and 1.15. The extinction coefficient, k, can now be determined by fitting the relation $m = m_0 + kX$ to the two $(X, m(X))$ points for each night and filter. m is the observed magnitude, X is the airmass, and m_0 is the magnitude of the star outside the atmosphere. By the *observed magnitude* we mean the magnitude that `phot` outputs, m_{phot}, which in turn is given by

$$m_{phot} = \texttt{zmag} - 2.5 \log \left(\frac{I_{star+sky} - I_{sky}}{t_{exp}} \right). \tag{C.4}$$

`zmag` is the arbitrary zero point of the magnitude scale, $I_{star+sky}$ is the total number of counts (in ADU) from the star and the sky background within the aperture, I_{sky} is the equivalent number of counts (in ADU) from the sky background alone within the aperture, and t_{exp} is the exposure time (in seconds, say). `zmag` = 22 mag was used.

Since there are 8 stars in the SA110–503 field, we get 8 determinations of k for each image. The final k can then be calculated as the mean, with the possibility of rejecting points. This procedure is implemented in the task `stars.calext`. The package `stars` is written by IJ.

First, `mkimsets` was used to create an image set file for each night for the SA110–503 images.

Second, `mknobsfile` was used to create an observations file for each night for the SA110–503 images. `mknobsfile` inputs the APPHOT databases (the *image*`.mag.1` files) and the image set file, and outputs the observations file[1]. In the process of compiling the data of the multiple APPHOT databases into one file, it also does the aperture correction.

`calext` is given an observations file and a fields file. The first column of the latter contains the star names to be used. Optionally, in the second column it contains a color, e.g. (B–V). One can either fit k as a constant, or as a function of star color, $k = k((B - V)) = c_1 + c_2 \cdot (B - V)$, still for the same given filter.

`calext` was first run without a color term. The stars which seemed to deviate too much were deleted. The deleted stars are shown in Table C.5. No more than 3 of the 8 stars were deleted. Some of the deleted stars were inspected in the images; in some cases, there were cosmic ray events within the aperture, whereas in other cases, noting unusual could be seen. It should be noted, that the star SA110–502, which was deleted in 4 out of 6 cases in Johnson U, is very faint in that filter, U = 17.0 mag (cf. Table C.11).

Table C.5: Deleted Stars When Determining the Extinction

Night	GR	JV	JB	JU
1	–	496	502, 504	502
2	–	–	–	502
3	–	504	–	504
4	–	496	504	497, 504
6	497, 504	497	496	502, 497, 504
7	–	506	504	502

Notes: All stars are from the SA110 field. Magnitudes of the stars can be found in Table C.11.

[1] It should be noted, that the output from the `mknobsfile` in `digiphotx.photcalx` and from the `mknobsfile` in `digiphot.photcal` is not in the same format: the x version has eight columns with OTIME as the third, the non-x version has only seven columns, and does not have OTIME. Here, the x version was used.

The resulting nightly extinctions coefficients are shown in Figure C.10 and Table C.6. It can be seen, that there are variations from night to night. These variations are qualitatively the same in all the filters.

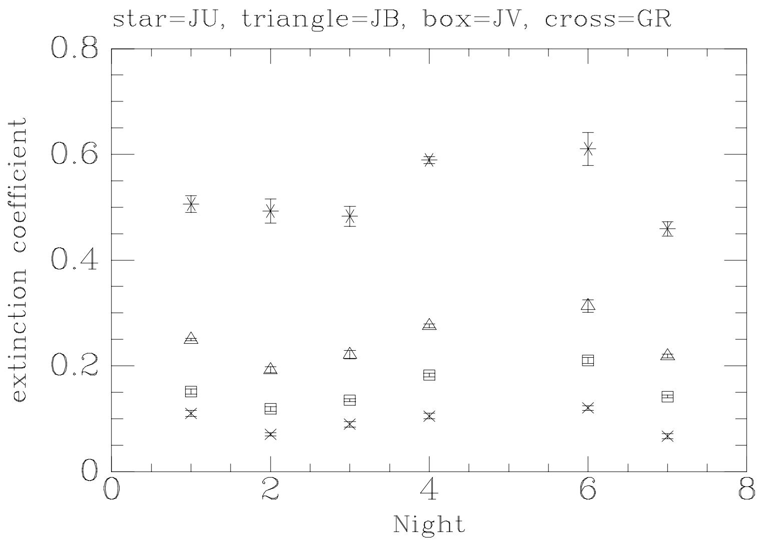

Figure C.10: The nightly extinction coefficients.

Table C.6: The Nightly Extinction Coefficients

Night	GR	JV	JB	JU
1	0.110	0.151	0.250	0.506
2	0.070	0.118	0.192	0.493
3	0.089	0.135	0.221	0.483
4	0.105	0.182	0.276	0.589
6	0.120	0.210	0.313	0.610
7	0.067	0.142	0.219	0.459

`calext` was also run fitting k as a function af (B–V), $k = c_1 + c_2 \cdot (B - V)$, with (B–V) taken from Landolt (1992). The stars which were deleted were the same as when fitting k without a color term, with three exceptions (night 1, JB: star 502 & 504 *not* deleted, night 2, JU: star 502 *not* deleted), and they were not very clear. The resulting color term coefficients, c_2, averaged over the 6 nights, were -0.007 ± 0.003, -0.001 ± 0.003, -0.012 ± 0.009, and -0.104 ± 0.043, for GR, JV, JB, and JU, respectively. At face value, these are different from zero at the 2.0, 0.5, 1.4, & 2.4 sigma level, respectively. For JU it was noted when doing the fit of $c_1 + c_2 \cdot (B - V)$ to the 8 values of k per night, that the scatter was very high, and that the mean c_2 for the given night was very sensitive to which stars were included in the fit, which in turn was not easy to decide. The 6 mean values of c_2 scatter a lot, too, from 0.00 to -0.27, with the latter value being for night 2 where the star 502 *was* included.

It was concluded, that if there was any color dependence it was small, and that it therefore was appropriate to use the color independent fit of k.

Now having determined the nightly extinction coefficients, we were ready to apply these to all the stars. `mkimsets` and `mknobsfile` (including aperture correction) were run on all the stars in the 3 fields, and the names were corrected to what they were in the standard catalog. All the magnitudes were then corrected for extinction (Table C.6) using the task `stars.magcorrect`. `magcorrect` can also apply night coefficients, but that function was not used at this step, the parameter `nitecoef` was set to `""`. The above was done separately for the focused and defocused images, and separately for the 6 nights.

Having corrected the magnitudes for extinction, they should in principle be consistent from night to night. However, this is usually not the case, so one brings them to the same relative system by *adding* so-called night coefficients. The night coefficient for night i with respect to night *ref* is given by

$$n(\text{night}\, i) = \langle m(\text{night}\, ref, \text{star}\, j) - m(\text{night}\, i, \text{star}\, j)\rangle, \tag{C.5}$$

where the mean is taken over all stars j observed on both of the nights. If a star has been observed more than once on a given night, $m(\text{night}\, i, \text{star}\, j)$ can be taken to be the mean value. Typically, night coefficients are of the order of a few hundredths of a magnitude.

Since night coefficients are relative, it is arbitrary which night is chosen as reference night. One might as well chose the night that would seem to be the most reliable one, e.g. the night with the most observations, or the night with the lowest extinction. Here, night 2 was chosen.

Calculations of night coefficients can be done by the task `stars.calnitecoef`. It calculates mean magnitudes using the task `stars.meanphot` (or, alternative, the user can do that directly first, and tell `calnitecoef` to use these mean magnitude files). The user can do the fitting of the mean of the individual night coefficients (one for each star in common) interactively.

Night coefficients with respect to night 2 were determined for the 6 nights, separately for the focused and the defocused images, using `calnitecoef`. The result is shown in Figure C.11.

As can be seen, the night coefficients are very large, indicating that something is wrong. It is also striking, that the variation of the night coefficients from night to night (Figure C.11) is qualitatively the same as the variation of the *nightly extinction coefficients* from night to night (Figure C.10). This suggests, that the nightly extinction coefficients are uncorrect.

The weather needs to be photometric in order to be able to determine the extinction coefficient. If the weather is not photometric, the stars will appear too faint.

If it is photometric when observing at low airmass, but not photometric when observing at high airmass, the determined extinction coefficient will be higher than the true value. If it is the other way round, the determined extinction coefficient will be lower than the true value. If it is not photometric neither at low nor at high airmass, anything can happen.

Notes about the weather was written by the observer usually on top of each page of the observations log, see Table C.7. These are the only notes about the weather in the log for the days in question. Only once it was stated, that the weather was not photometric for sure. A few places it was stated, that the weather might not be photometric.

If we assume, that the weather in fact was *not* photometric where it was stated that it *might* not be, we would expect, that the extinction coefficients were too high for night 3, and too low for night 6. In Figure C.10 one sees, that the night 3 extinction coefficients are not high compared to the values from the other nights, so it does not seem likely, that the night 3 values are actually *too* high. One also sees, that the night 6 extinction coefficients are high compared to the values from the other nights, so it does not seem likely, that the night 6 values are actually too *low*, either.

However, the above assumption might not be correct. It is difficult *per se* to precisely determine whether the weather is photometric, and since the observer is busy observing, he/she cannot spend all the time monitoring the weather. We will conclude, that it was not photometric all the time, but that we cannot say precisely *when*.

In any case, the night coefficients based on the nightly extinction coefficients are very large, and the variation does resemble that of the nightly extinction coefficients, so something with the latter must be wrong.

It was concluded, that the nightly extinction coefficients for night 4 and 6 were too high. It was decided to use the mean value of the nightly extinction coefficients for night 1, 2, 3, and 7 as *the* extinction coefficient for the given filter. Those 4 final extinction coefficients are shown in Table C.8. Also shown are the La Silla mean extinction coefficients. For JV, JB, & JU, the adopted values are 4–10% higher than the La Silla mean values. For GR, the adopted value is 30% higher than the La Silla mean value. However, the adopted value agrees very well (< 4%) with the values of run 1–3 of Jørgensen (1994), in which the very same filter (ESO #460) was used. These comparisons give confidence that the adopted values of the extinction coefficients are reasonable.

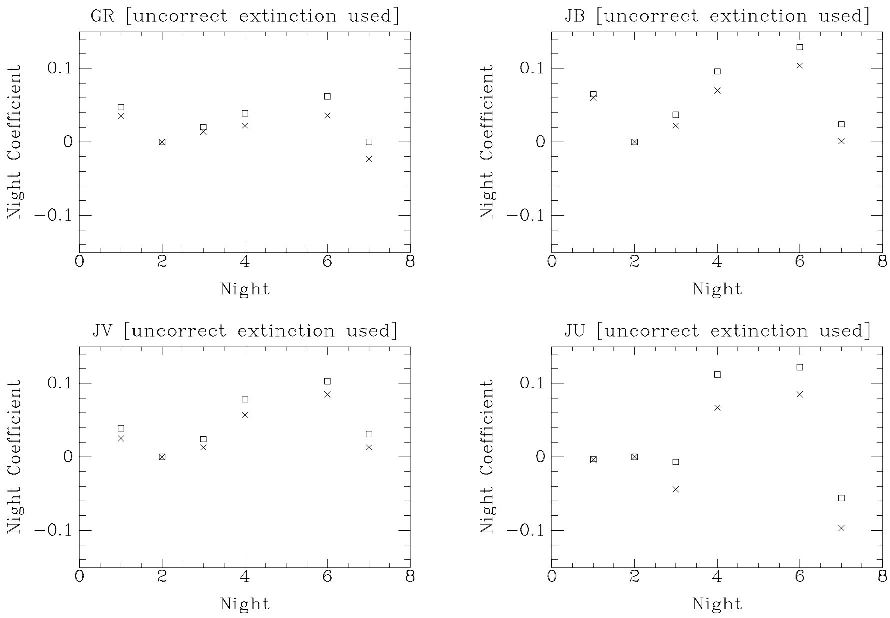

Figure C.11: The night coefficients based on the nightly extinction coefficients (Table C.6 and Figure C.10). The night coefficients are with respect to night 2. Legend: Boxes: defocused images. Crosses: focused images.

The observations were extinction corrected using the new extinction coefficients, and the night coefficients were determined again, still with respect to night 2. The result is shown in Figure C.12.

Now the night coefficients were of a more reasonable size, although still somewhat large. What is striking is, that the focused and defocused stars do not have the same night coefficients, except for the reference night, night 2, where they per definition are 0. This indicates, that night 2 is not representative – if another night had been chosen as reference night, this offset would have been smaller for more of the nights (and of course for night 2, it would be large and with opposite sign).

It was decided to proceed and to calculate night coefficients for the combined sample of focused and defocused stars. In doing this, the defocused stars were weighted more than the focused, as 59 stars to 13 stars. When fitting, it was sometimes obvious, that there was an offset between the focused and defocused individual night coefficients. Nevertheless, the mean was calculated more or less blindly, only throwing away points which seemed to deviate for other reasons. The result is shown in Figure C.12 and Table C.9.

Finally, the night coefficients were applied to the already aperture and extinction corrected

Table C.7: The Notes in the Observations Log About the Weather

Night	Page	Weather	Standard fields observed
1	1	Photometric – to be checked	
1	2	Photometric	M67
1	3	Photometric	
1	4	Photometric	
1	5	Photometric	PG1633+099, SA110 (high airmass)
1	6	Photometric	SA110 (low airmass)
1	7	Photometric	
2	8	Photometric	M67
2	9	Photometric	
2	10	Photometric	
2	11	Photometric	PG1633+099, SA110 (high airmass)
2	12	Photometric	SA110 (low airmass)
2	13	Photometric	SA110 (low airmass) continued
3	14	[nothing written]	
3	15	Photometric	M67
3	16	Photometric	
3	17	Photometric	
3	17	May not be photometric right now, check this	PG1633+099
3	18	Photometric (?)	SA110 (high airmass)
3	19	Photometric	SA110 (low airmass)
4	20	Photometric	
4	21	Photometric	M67
4	22	Photometric	
4	22	NON-photometric	
4	23	Photometric? check this	
4	24	Photometric	SA110 (high airmass)
4	25	Photometric	PG1633+099
4	26	Photometric	SA110 (low airmass)
6	25	Photometric	
6	26	Photometric	M67
6	27	Photometric	
6	28	Photometric	SA110 (high airmass)
6	29	Photometric (?)	PG1633+099, SA110 (low airmass)
6	30	Photometric (?)	
7	31	Photometric	M67
7	32	Photometric	
7	33	Photometric	SA110 (high airmass)
7	34	Photometric	SA110 (low airmass)
7	35	Photometric	

Notes: The weather was noted on top of each page of the log book, except for page 17 and 22, where it was also noted further down. On night 5, the first page number was set to 21 instead of 27 as it should have been, therefore the strange page numbers for night 6 and 7.

observations files using `magcorrect` again, this time setting `extcoef=""`. These magnitudes are called *instrumental magnitudes*. In short, they are given by

$$m_{inst} = m_{phot} + \text{apcor} - kX + n, \tag{C.6}$$

where k is the extinction coefficients for the given filter, X is the airmass for the given observation,

Table C.8: The Final Extinction Coefficients

Filter	GR	JV	JB	JU
Adopted ext. coeff.	0.084	0.137	0.220	0.485
La Silla mean ext. coeff.	0.065	0.125	0.212	0.459

Notes: The adopted extinction coefficient for a given filter is the mean of the nightly extinction coefficients for night 1, 2, 3, and 7 (cf. Table C.6 and Figure C.10). The La Silla mean values are taken from Jørgensen (1994). This author used the exact same filters as in this study, viz. ESO # 460, 451, 450, & 632, respectively.

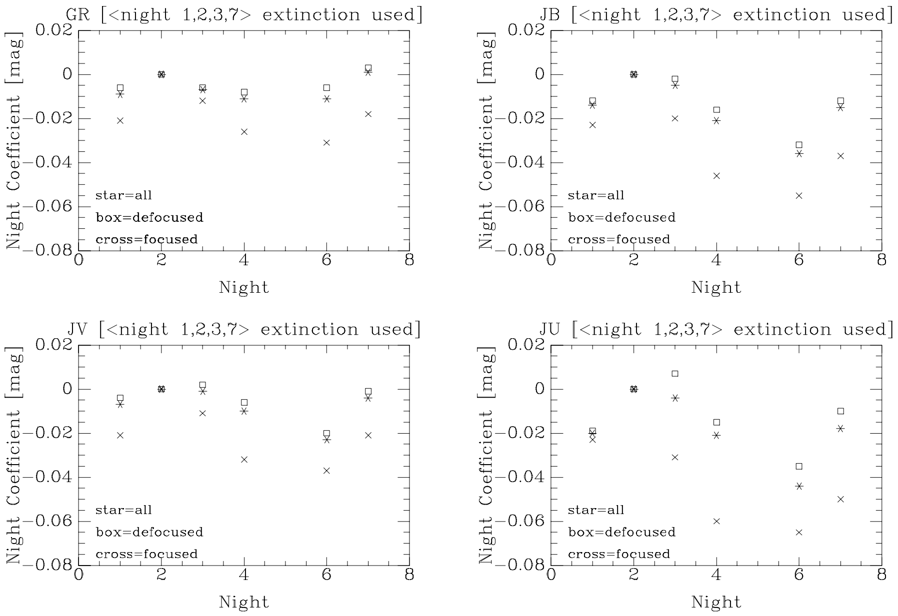

Figure C.12: The night coefficients based on the final extinction coefficients (Table C.8). The night coefficients are with respect to night 2. Legend: Boxes: defocused images fit alone. Crosses: focused images fit alone. Stars: defocused and focused images fit together.

and n is the night coefficient for the given filter and night. m_{phot} and apcor should correspond to the same aperture.

Table C.9: The Night Coefficients Based on the Final Extinction Coefficients

Night	GR	JV	JB	JU
1	–0.009	–0.007	–0.014	–0.020
2	0.0	0.0	0.0	0.0
3	–0.007	–0.001	–0.005	–0.004
4	–0.011	–0.010	–0.021	–0.021
6	–0.011	–0.023	–0.036	–0.044
7	0.001	–0.004	–0.015	–0.018

C.4 The Standard Catalog

A catalog of standard magnitudes was compiled as follows: For the SA110–503 field and the PG1633+099 field, Johnson V, B, & U magnitudes were taken from Landolt (1992). B and U were calculated from the listed (B–V) and (U–B) as follows:

$$B = V + (B - V) \tag{C.7}$$
$$\sigma(B) = \max\{\sigma(V), \sigma((B - V))\} \tag{C.8}$$
$$U = V + (B - V) + (U - B) \tag{C.9}$$
$$\sigma(U) = \max\{\sigma(V), \sigma((B - V)), \sigma((U - B))\} \tag{C.10}$$

Gunn r magnitudes were taken from Jørgensen (1994).

For the M67 field, Johnson V & B, and Gunn r magnitudes were taken from Jørgensen (1994). B was calculated from the listed (B–V) in the same way as for the Landolt stars, Eq. (C.7) and (C.8). U magnitudes were taken from Montgomery et al. (1993) for the 13 stars in common. U was calculated from the listed (B–V) and (U–B) in the same way as for the Landolt stars, Eq. (C.9), whereas the errors were somewhat arbitrarily set to 0.01 mag, since these authors do not list any errors. The stars were identified from Figure 7 in Montgomery et al. (1993), since these authors do not use the F or quadrant numbers. The established correspondence is shown in Table C.10.

The final catalog (called `DFC_std.dat`) is shown in Table C.11.

Table C.10: Identification for Stars in Montgomery et al. (1993)

Star	Fig ID
M67–F141	14
M67–F105	15
M67–F95	18
M67–F93/I12	19
M67–F124	20
M67–F127	21
M67–F130	22
M67–F129/I199	23
M67–F128/I198	24
M67–F111	25
M67–F108	28
M67–F81	29
M67–I20	30

Notes: Fig ID refers to Table 7 and Figure 7 in Montgomery et al. (1993).

Table C.11: Catalog of standard star magnitudes

Star	GR	σ(GR)	JV	σ(JV)	JB	σ(JB)	JU	σ(JU)
SA110–496	12.763	0.007	13.004	0.003	14.044	0.006	14.781	0.023
SA110–497	13.889	0.007	14.196	0.005	15.248	0.006	15.628	0.014
SA110–499	11.497	0.007	11.737	0.003	12.724	0.003	13.363	0.007
SA110–502	11.440	0.008	12.330	0.003	14.656	0.005	16.982	0.023
SA110–503	11.756	0.007	11.773	0.003	12.444	0.003	12.950	0.005
SA110–504	13.629	0.007	14.022	0.001	15.270	0.006	16.593	0.027
SA110–506	11.349	0.007	11.312	0.002	11.880	0.002	11.939	0.006
SA110–507	12.208	0.007	12.440	0.005	13.581	0.006	14.411	0.006
PG1633+099	14.799	0.018	14.397	0.002	14.205	0.002	13.231	0.005
PG1633+099A	15.104	0.018	15.256	0.004	16.129	0.005	16.449	0.009
PG1633+099B	12.772	0.017	12.969	0.002	14.050	0.002	15.057	0.007
PG1633+099C	13.004	0.017	13.229	0.003	14.363	0.003	15.501	0.004
PG1633+099D	13.711	0.017	13.691	0.002	14.226	0.002	14.201	0.005
M67–F81	10.392	0.006	10.030	0.008	9.947	0.008	9.556	0.010
M67–F93/I12	12.837	0.003	12.833	0.007	13.383	0.007	13.468	0.010
M67–F95	12.721	0.003	12.678	0.006	13.169	0.006	13.232	0.010
M67–F105	9.982	0.004	10.267	0.010	11.510	0.010	12.889	0.010
M67–F106/I11	13.064	0.003	13.062	0.005	13.625	0.005	–	–
M67–F108	9.310	0.003	9.662	0.006	11.024	0.006	12.623	0.010
M67–F111	12.736	0.003	12.741	0.006	13.297	0.006	13.357	0.010
M67–F117	12.517	0.003	12.632	0.005	13.411	0.005	–	–
M67–F124	12.184	0.003	12.129	0.007	12.584	0.007	12.605	0.010
M67–F127	12.789	0.003	12.785	0.007	13.338	0.007	13.365	0.010
M67–F128/I198	13.155	0.004	13.158	0.022	13.734	0.022	13.777	0.010
M67–F129/I199	13.169	0.003	13.174	0.010	13.761	0.010	13.831	0.010
M67–F130	12.954	0.004	12.895	0.022	13.349	0.022	13.356	0.010
M67–F134	12.254	0.003	12.265	0.008	12.832	0.008	–	–
M67–F135	11.216	0.003	11.428	0.008	12.480	0.008	–	–
M67–F141	10.245	0.004	10.442	0.011	11.527	0.011	12.586	0.010
M67–F153	11.559	0.011	11.280	0.015	11.385	0.015	–	–
M67–I15	11.635	0.007	11.563	0.010	11.961	0.010	–	–
M67–I20	13.440	0.007	13.444	0.010	13.996	0.010	14.038	0.010
M67–I25	12.643	0.007	12.669	0.010	13.273	0.010	–	–
M67–I27	11.492	0.007	11.333	0.010	11.614	0.010	–	–
M67–I49	13.447	0.005	13.465	0.007	14.046	0.007	–	–
M67–II22	12.766	0.011	12.911	0.015	13.809	0.015	–	–

C.5 The Transformation Equations

The following transformation equations were used:

$$r_{std} = r_{inst} + r_1 + r_2(B-r)_{inst} \tag{C.11}$$
$$V_{std} = V_{inst} + v_1 + v_2(B-V)_{inst} \tag{C.12}$$
$$B_{std} = B_{inst} + b_1 + b_2(B-r)_{inst} \tag{C.13}$$
$$U_{std} = U_{inst} + u_1 + u_2(U-B)_{inst} \tag{C.14}$$

"std" denotes standard magnitudes, and "inst" denotes instrumental magnitudes.

The fitting of the variables in the transformation equations to the data was done using the task `fitparams` (in `digiphotx.photcalx`).

At the very first it was tried to use transformation equations without a color term (i.e. with the subscript 2 variables set to zero). The rms scatter was so large, that it was concluded that a color term was needed. As will be seen in the following, the resulting color coefficients are indeed significantly different from zero at the 3 sigma level.

`fitparams` was run 3 times for the 4 filters:

1. On all the stars, focused and defocused, with the color term coefficient as a free variable. Plots showing $m_{std} - m_{inst}$ vs. instrumental color for the data points and the resulting fit are in Figure C.13–C.16. Note, that the aspect ratio of the 4 figures is the same, $\Delta y/\Delta x = 2/15$, so the color dependence can easily be compared.

2. On the focused stars only, with the color term coefficient fixed to the value from fit 1.

3. On the defocused stars only, with the color term coefficient fixed to the value from fit 1.

In all 3 fitting series, a number of stars were deleted (i.e. excluded from the fit) all together, that is, all the observations of the given star were deleted. These stars are listed in Table C.12. They were deleted for a number of different reasons:

- 3 stars (PG1633+099, M67–F81, & SA110–502) were deleted because they were either very blue ((B–V)$_{std} \sim -0.1$ mag) or red ((B–V)$_{std} \sim 2.3$ mag). Since we only need a transformation which is valid for the color range of E/S0 galaxies, say (B–V)$_{std} = 0.75$–1.1 mag (Jørgensen, private communication), this is perfectly justifiable. The remaining stars still span a sufficient range in (B–V)$_{std}$, from 0.1 (M67–F153) to 1.2 (SA110–504).

- 1 star (M67–F117) was deleted (in the Gunn r and Johnson V fits only) because it had a large scatter, i.e. the individual observations of this star were very scattered. This can be seen in Figure C.13 for Gunn r, and Figure C.14 for Johnson V. The reason for this was not further investigated.

- 3 stars (M67–F108, M67–F105, & M67–F141) were deleted (in the Gunn r and Johnson V fits only) because they deviated systematically from the fit. This can be seen in Figure C.13 for Gunn r, and Figure C.14 for Johnson V. These stars were the reddest and brightest of the defocused stars. The important question is, whether it is only these reddest and brightest defocused stars that behave differently, or if they are just the most extreme cases of a general trend that the focused and the defocused stars do not behave in the same way.

In addition, individual observations with uncertainties larger than 0.1 mag were deleted. This was only the case for Johnson U, for 9 data points, of which 4 belonged to SA110–502, which would

Table C.12: Deleted stars

Star	Deleted in				(B–r)	(B–V)	(U–B)	(B–V)	r	V	Reason for deletion
	GR	JV	JB	JU	instrumental, [mag]			standard, [mag]			
PG1633+099	x	x	x	x	0.24	0.87	1.26	–0.2	14.8	14.4	Very blue
M67–F81	x	x	x	x	0.41	0.95	1.88	–0.1	10.4	10.0	Very blue
SA110–502	x	x	x	x	3.96	3.02	4.86	2.3	11.4	12.3	Very red
M67–F117	x	x			1.69	1.69		0.8	12.5	12.6	Large scatter
M67–F108	x	x			2.44	2.16		1.4	9.3	9.7	Large res., bright
M67–F105	x	x			2.28	2.07		1.2	10.0	10.3	Large res., bright
M67–F141	x	x			2.05	1.94		1.1	10.2	10.4	Large res., bright

Notes: The instrumental colors are mean values for the individual observations of the given star. The standard color and magnitudes are taken from Table C.11. The instrumental colors are useful for locating the stars in the $m_{std} - m_{inst}$ vs. instrumental color plots, Figure C.13–C.16.
The above stars were deleted in the same way in the 3 fitting series: all stars with free color term, focused stars with fixed color term, and defocused stars with fixed color term.

have been deleted anyway. Also individual deviating observations were deleted. This also was only the case for Johnson U, for 3 data points.

The result from the 3 series of fit are shown in Table C.13.

Table C.13: Transformation equation coefficients

Type	Zero point [mag]	Color term	Scatter [mag]
all	$r_1 = +0.7718 \pm 0.0049$	$r_2 = 0.1244 \pm 0.0029$	rms = 0.0185
foc	$r_1 = +0.7816 \pm 0.0012$	$r_2 = 0.1244$ (fixed)	rms = 0.0124
def	$r_1 = +0.7624 \pm 0.0018$	$r_2 = 0.1244$ (fixed)	rms = 0.0187
all	$v_1 = +0.9380 \pm 0.0065$	$v_2 = 0.0861 \pm 0.0038$	rms = 0.0144
foc	$v_1 = +0.9406 \pm 0.0016$	$v_2 = 0.0861$ (fixed)	rms = 0.0164
def	$v_1 = +0.9353 \pm 0.0011$	$v_2 = 0.0861$ (fixed)	rms = 0.0117
all	$b_1 = -0.0523 \pm 0.0055$	$b_2 = 0.1253 \pm 0.0031$	rms = 0.0219
foc	$b_1 = -0.0518 \pm 0.0029$	$b_2 = 0.1253$ (fixed)	rms = 0.0291
def	$b_1 = -0.0526 \pm 0.0012$	$b_2 = 0.1253$ (fixed)	rms = 0.0139
all	$u_1 = -2.2369 \pm 0.0168$	$u_2 = 0.0187 \pm 0.0058$	rms = 0.0390
foc	$u_1 = -2.2404 \pm 0.0047$	$u_2 = 0.0187$ (fixed)	rms = 0.0461
def	$u_1 = -2.2320 \pm 0.0031$	$u_2 = 0.0187$ (fixed)	rms = 0.0256

Notes: "all": all stars fitted, color term free. "foc": only focused stars fitted, color term fixed. "def": only defocused stars fitted, color term fixed. The "all" coefficients are the final ones, i.e. the ones used to standard calibrate the surface photometry.

The reason for fitting the focused and defocused stars separately with forced same color dependence, was to be able to compare their zero points. These zero point differences are shown in Table C.14. There is a zero point difference in Gunn r at the 9 sigma level, and a zero point difference in Johnson V at the 3 sigma level.

That the focused and defocused stars behave differently in Gunn r and Johnson V can be seen

Table C.14: Zero point differences

Zero point def [mag]	Zero point foc [mag]	Zero point difference [mag]
$r_1 = +0.7624 \pm 0.0018$	$r_1 = +0.7816 \pm 0.0012$	$\Delta = -0.0192 \pm 0.0022$ (8.7σ)
$v_1 = +0.9353 \pm 0.0011$	$v_1 = +0.9406 \pm 0.0016$	$\Delta = -0.0053 \pm 0.0019$ (2.8σ)
$b_1 = -0.0526 \pm 0.0012$	$b_1 = -0.0518 \pm 0.0029$	$\Delta = -0.0008 \pm 0.0031$ (0.3σ)
$u_1 = -2.2320 \pm 0.0031$	$u_1 = -2.2404 \pm 0.0047$	$\Delta = +0.0084 \pm 0.0056$ (1.5σ)

Notes: "def" denotes the defocused stars, "foc" denotes the focused stars. "Zero point difference" is defined as "Zero point def" minus "Zero point foc".

in Figure C.13 and and Figure C.14. The question is what kind of difference it is. The figures could indicate, that it is not only a zero point difference, but also a difference in color dependence.

However, the rms scatter when fitting all the stars together (with the deletions previously mentioned) is still sufficiently low, less than 0.02 mag in both Gunn r and Johnson V. The conclusion is, therefore, to accept the result of the fit of all the stars together (Table C.15), and then to watch out for small differences in the derived galaxy magnitudes when compared with literature values.

Table C.15: Adopted transformation equation coefficients

Zero point [mag]	Color term	Scatter [mag]
$r_1 = +0.7718 \pm 0.0049$	$r_2 = 0.1244 \pm 0.0029$	rms = 0.0185
$v_1 = +0.9380 \pm 0.0065$	$v_2 = 0.0861 \pm 0.0038$	rms = 0.0144
$b_1 = -0.0523 \pm 0.0055$	$b_2 = 0.1253 \pm 0.0031$	rms = 0.0219
$u_1 = -2.2369 \pm 0.0168$	$u_2 = 0.0187 \pm 0.0058$	rms = 0.0390

Notes: These are the "all" coefficients from Table C.13, listed here alone for convenience.

Finally, we can check if the stars from night 4 and 6 have larger residuals than the stars from the other nights. Figure C.17 shows mean absolute residual for the 3 fields, with the SA110 field split up into the low and the high airmass observations. No such difference is seen, except for the SA110 high airmass observations in Johnson U, but it might not be significant due to the large random scatter of the data in this filter. Otherwise, these plots do not show any correlations with night and field/airmass, except that the night 2 and 3 residual in Gunn r are somewhat higher. The conclusion is still that the standard transformation we have arrived at is acceptable.

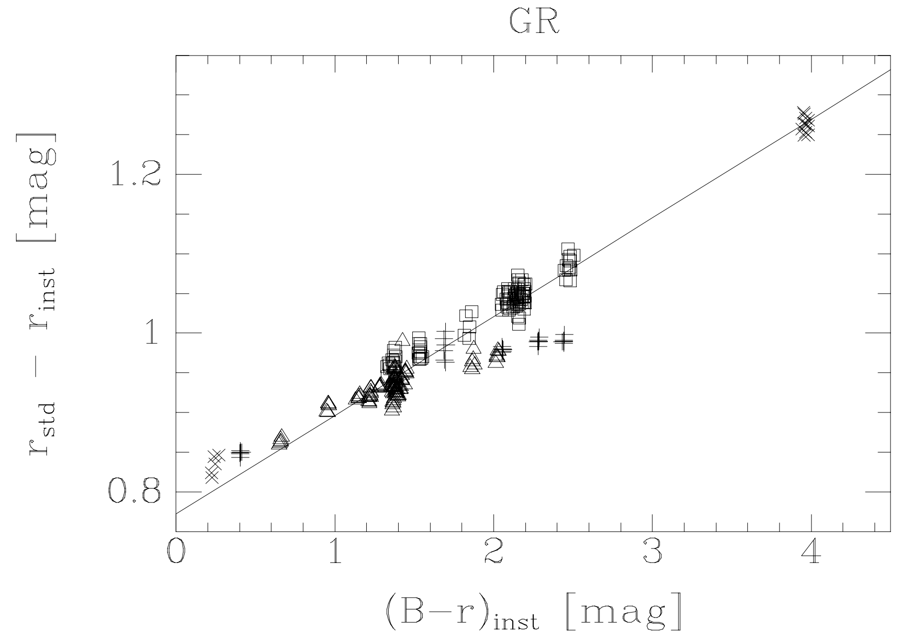

Figure C.13: $m_{std} - m_{inst}$ vs. instrumental color, Gunn r. Legend: box: focused & not deleted, triangle: defocused & not deleted, cross: focused & deleted, plus: defocused & deleted.

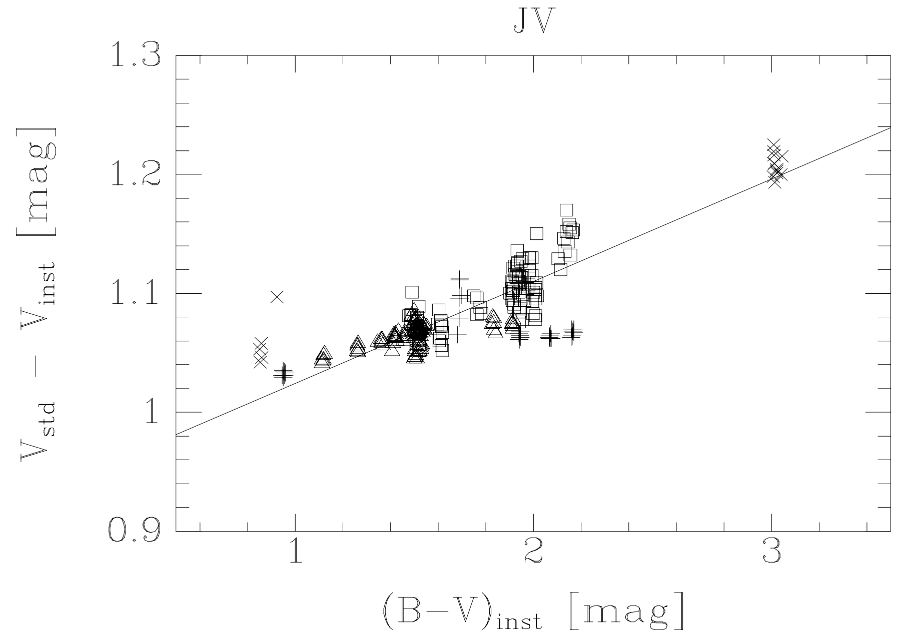

Figure C.14: $m_{std} - m_{inst}$ vs. instrumental color, Johnson V. Legend: box: focused & not deleted, triangle: defocused & not deleted, cross: focused & deleted, plus: defocused & deleted.

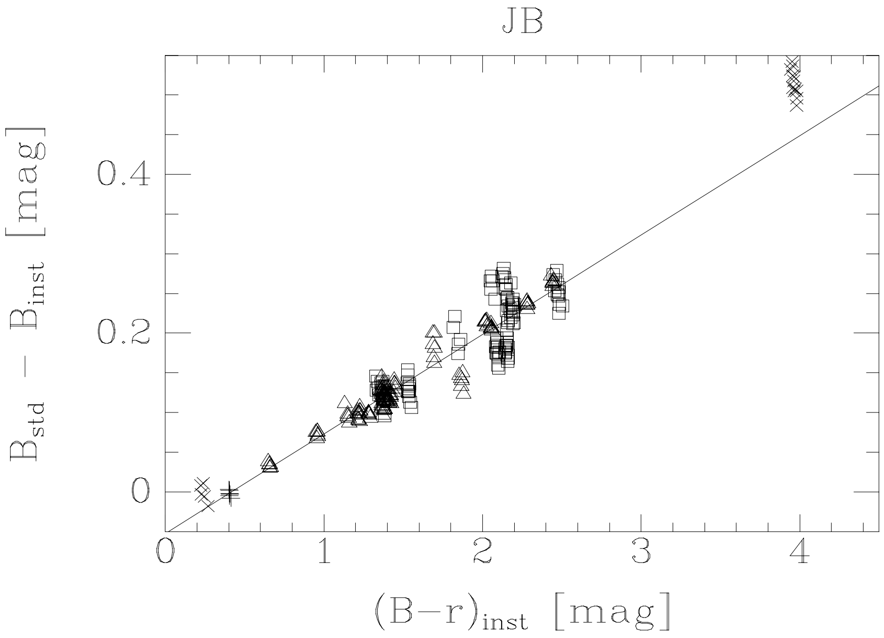

Figure C.15: $m_{std} - m_{inst}$ vs. instrumental color, Johnson B. Legend: box: focused & not deleted, triangle: defocused & not deleted, cross: focused & deleted, plus: defocused & deleted.

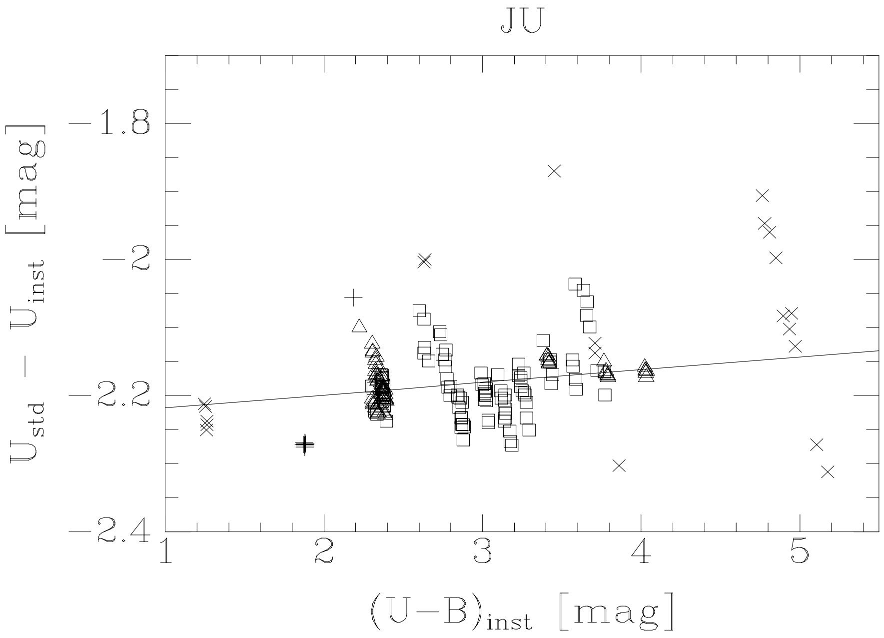

Figure C.16: $m_{std} - m_{inst}$ vs. instrumental color, Johnson U. Legend: box: focused & not deleted, triangle: defocused & not deleted, cross: focused & deleted, plus: defocused & deleted.

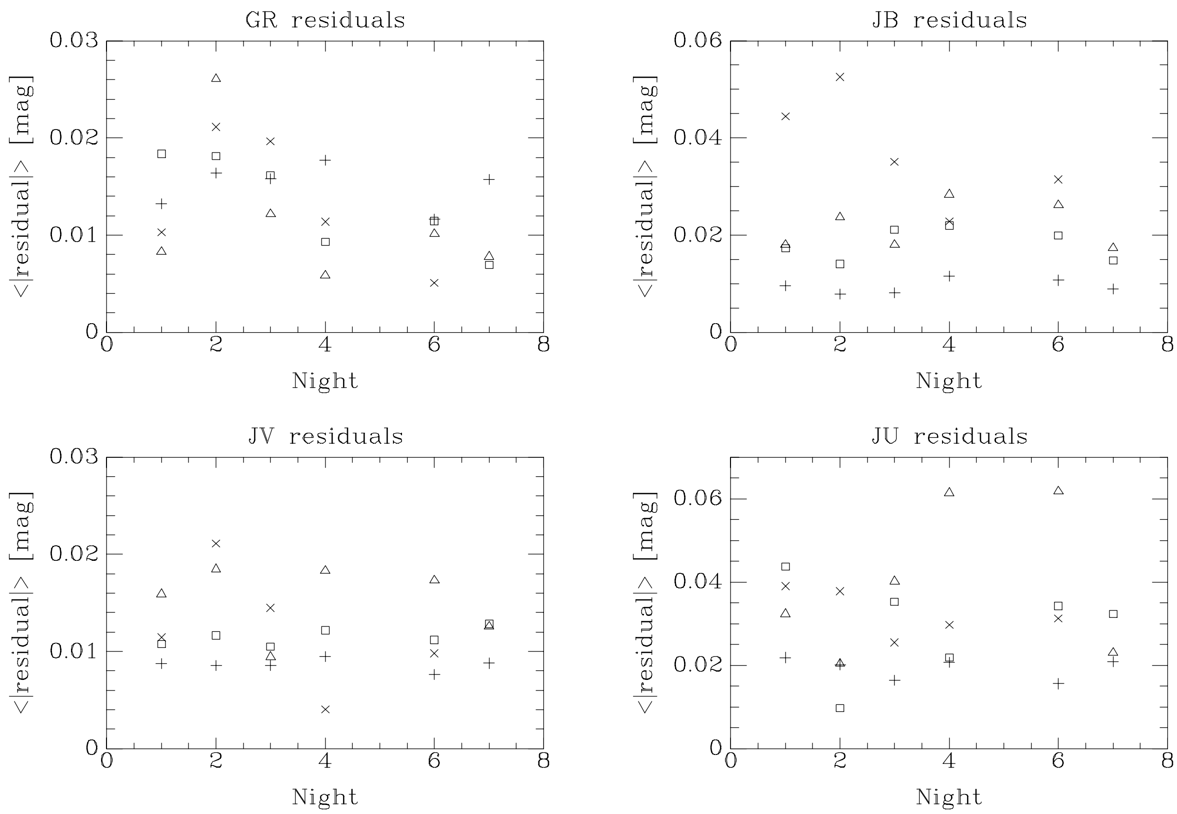

Figure C.17: Mean absolute residuals with respect to the final transformation equation fit. The mean is calculated for 4 disjoint groups: SA110 low airmass ($N = 7$), SA110 high airmass ($N = 7$), PG1633+099 ($N = 4$), and M67 ($N = 12$–22). Only points which were included in the transformation equation fit were used in this calculation. The typical numbers of points, N, is shown above; it can be deduced from Table C.11 (the standard catalog) and Table C.12 (the list of deleted stars). Legend: box: SA110 low airmass, triangle: SA110 high airmass, cross: PG1633+099, plus: M67.

Appendix D

Data for the Coma Cluster

The Coma data used for this work are given in Table D.1 (photometry) and Table D.2 (spectroscopy) below. Both tables have the same 116 galaxies.

The Coma data are described in Sect. 7.1.1 (p. 85).

TABLE D.1

COMA GLOBAL PHOTOMETRIC PARAMETERS, GUNN R

Galaxy		log r_e	$<\mu>_e$	ε_e	$\varepsilon_{21.85}$	c_4	$<c_4>$	$<c_6>$
D 13	···	0.72±0.03	19.67±0.10	0.30	0.249	0.020	0.004	−0.004
D 15	···	0.69±0.03	20.30±0.10	0.15	0.136	−0.007	−0.005	0.004
D 20	···	0.59±0.04	19.76±0.13	0.41	0.432	0.019	0.011	0.000
D 23	NGC4842B	0.41±0.03	18.91±0.10	0.23	0.397	0.020	0.016	0.002
D 24	···	0.63±0.02	19.06±0.08	0.14	0.040	0.009	0.001	0.003
D 27	···	0.66±0.04	20.17±0.14	0.16	0.147	−0.019	−0.002	0.004
D 30	NGC4842A	0.69±0.02	19.15±0.07	0.09	0.077	0.005	0.002	−0.004
D 31	NGC4839	1.47±0.03	21.18±0.07	0.42	0.344	0.004	0.001	0.000
D 33	···	0.44±0.02	18.64±0.09	0.25	0.379	0.011	0.006	−0.001
D 39	···	0.76±0.03	20.25±0.11	0.19	0.186	0.003	0.003	0.005
D 42	···	0.41±0.03	18.79±0.11	0.32	0.427	0.049	0.031	−0.002
D 43	NGC4853	0.59±0.02	18.18±0.06	0.18	0.137	0.006	0.005	0.000
D 46	NGC4840	0.81±0.02	19.35±0.07	0.18	0.144	0.008	0.006	0.003
D 49	NGC4926	1.04±0.03	19.79±0.10	0.13	0.121	−0.009	−0.001	−0.001
D 57	···	0.94±0.02	20.05±0.06	0.71	0.735	0.096	0.049	−0.017
D 58	NGC4854	1.15±0.03	21.13±0.09	0.27	0.202	0.004	0.000	0.003
D 62	···	0.77±0.04	20.66±0.12	0.43	0.428	0.027	0.019	0.001
D 65	···	0.82±0.03	20.55±0.11	0.45	0.435	0.008	0.000	0.003
D 67	···	0.38±0.03	18.81±0.12	0.20	0.403	0.058	0.020	0.004
D 68	IC3963	0.89±0.03	20.58±0.09	0.47	0.464	0.102	0.057	−0.003
D 69	IC3959	0.73±0.03	19.42±0.10	0.13	0.095	0.005	0.003	−0.002
D 70	IC3957	0.63±0.04	19.51±0.13	0.08	0.073	−0.004	−0.002	0.001
D 72	IC3947	0.52±0.03	19.00±0.11	0.28	0.322	0.028	0.020	−0.003
D 75	···	1.08±0.03	21.52±0.09	0.79	0.781	0.071	0.057	−0.012
D 78	NGC4923	0.93±0.02	19.88±0.08	0.17	0.183	0.010	0.002	0.000
D 79	NGC4919	0.76±0.02	19.30±0.08	0.31	0.431	0.010	0.000	0.000
D 80	···	0.85±0.04	20.81±0.13	0.25	0.357	0.009	0.002	0.003
D 81	···	0.82±0.04	20.70±0.13	0.21	0.212	0.004	0.003	−0.001
D 84	···	0.66±0.03	19.77±0.10	0.63	0.656	0.062	0.053	−0.008
D 87	···	0.48±0.04	19.79±0.16	0.07	0.074	−0.005	−0.001	−0.006
D 88	IC3976	0.47±0.03	18.58±0.10	0.41	0.532	0.026	0.017	−0.004
D 91	IC3946	0.65±0.02	18.98±0.07	0.31	0.479	0.044	0.035	−0.003
D 92	···	0.45±0.03	18.86±0.12	0.34	0.336	0.027	0.019	0.007
D 93	···	0.44±0.03	18.79±0.11	0.43	0.677	0.128	0.117	−0.019
D 98	···	0.72±0.02	19.78±0.08	0.62	0.662	0.031	0.035	−0.014
D101	···	0.56±0.03	19.42±0.11	0.30	0.435	0.063	0.038	0.008
D103	IC3973	0.64±0.03	19.06±0.10	0.23	0.252	0.016	0.000	0.000
D104	NGC4875	0.52±0.03	18.96±0.10	0.17	0.246	0.016	0.008	0.003
D105	NGC4869	0.88±0.02	19.74±0.08	0.13	0.096	−0.000	0.002	0.000
D106	···	0.39±0.04	18.99±0.13	0.05	0.256	0.007	0.002	−0.005
D107	···	0.75±0.04	20.55±0.14	0.41	0.415	−0.001	0.001	−0.001
D108	···	0.51±0.04	19.61±0.13	0.43	0.508	0.036	0.008	0.000
D109	IC3960	0.73±0.02	19.77±0.08	0.04	0.058	0.016	0.000	0.003
D110	···	0.71±0.04	20.46±0.13	0.29	0.289	0.026	0.021	−0.008
D111	···	0.81±0.03	20.15±0.09	0.25	0.274	0.005	0.003	−0.003
D116	···	0.85±0.03	20.62±0.10	0.16	0.210	0.032	0.019	0.002
D118	NGC4906	0.87±0.03	20.09±0.10	0.12	0.124	−0.005	−0.004	0.000
D119	···	0.62±0.03	19.87±0.11	0.17	0.280	0.012	0.001	−0.001
D120	NGC4898B	0.77±0.02	19.22±0.06	0.28	0.277	0.015	0.007	−0.001
D121	NGC4898A	0.30±0.02	18.39±0.08	0.06	0.116	−0.007	−0.003	−0.001
D122	NGC4894	0.68±0.03	19.93±0.11	0.53	0.586	0.067	0.039	−0.005
D123	···	0.97±0.04	21.43±0.12	0.32	0.437	0.043	0.015	0.000
D124	NGC4876	0.71±0.03	19.47±0.09	0.29	0.333	0.001	−0.001	−0.001
D125	···	0.18±0.04	18.06±0.14	0.05	0.100	0.010	0.005	0.001
D128	···	0.40±0.05	19.30±0.19	0.37	0.531	0.041	0.019	−0.003
D129	NGC4874	1.85±0.04	22.13±0.09	0.16	0.096	0.001	0.001	0.000
D130	NGC4872	0.48±0.03	18.53±0.11	0.06	0.232	0.018	0.006	−0.002
D131	NGC4871	0.92±0.04	20.24±0.12	0.43	0.414	0.030	0.014	−0.001
D132	···	0.61±0.04	20.24±0.14	0.30	0.318	0.026	0.021	−0.002
D133	NGC4867	0.49±0.03	18.53±0.10	0.25	0.246	0.002	−0.002	−0.002
D135	···	0.63±0.05	20.50±0.15	0.21	0.213	−0.006	−0.001	−0.002
D136	···	0.17±0.03	17.99±0.13	0.15	0.241	0.020	0.015	0.002
D137	NGC4850	0.67±0.03	19.07±0.09	0.21	0.127	0.009	0.002	−0.003
D143	IC4051	1.26±0.03	21.02±0.09	0.26	0.217	−0.005	−0.000	0.000
D144	IC4042	0.86±0.02	19.96±0.08	0.06	0.063	−0.011	−0.005	0.001
D145	IC4041	0.87±0.03	20.52±0.09	0.45	0.442	0.007	0.005	0.000
D146	···	1.05±0.03	21.31±0.10	0.29	0.291	0.164	0.100	−0.016
D147	···	0.95±0.04	21.19±0.11	0.54	0.543	0.033	0.020	0.001
D148	NGC4889	1.53±0.02	20.64±0.05	0.36	0.358	−0.008	−0.005	0.000
D150	IC4011	0.69±0.04	19.98±0.12	0.09	0.099	0.006	0.002	0.001
D151	NGC4886	0.97±0.03	20.38±0.09	0.02	0.024	0.005	0.003	−0.002
D152	IC3998	0.95±0.02	20.73±0.07	0.33	0.322	0.024	0.005	−0.001
D153	···	0.57±0.02	19.58±0.10	0.01	0.018	0.002	0.004	0.000

TABLE D.1—*Continued*

Galaxy		$\log r_e$	$<\mu>_e$	ε_e	$\varepsilon_{21.85}$	c_4	$<c_4>$	$<c_6>$
D155	NGC4873	0.87±0.02	20.09±0.08	0.25	0.269	0.008	0.006	−0.003
D156	···	0.51±0.05	19.96±0.16	0.21	0.252	0.006	−0.005	0.009
D157	···	0.49±0.03	19.48±0.12	0.24	0.380	−0.010	−0.006	0.003
D159	NGC4864	0.89±0.02	19.78±0.08	0.15	0.141	0.000	0.002	−0.007
D160	IC3955	0.91±0.03	20.36±0.08	0.44	0.434	0.070	0.030	−0.004
D161	···	0.91±0.03	20.07±0.09	0.12	0.119	0.011	0.008	−0.002
D167	NGC4908	0.85±0.02	19.60±0.08	0.31	0.308	−0.005	−0.002	0.002
D168	IC4045	0.64±0.03	18.79±0.10	0.33	0.316	0.014	0.011	0.000
D170	IC4026	0.86±0.03	20.38±0.09	0.18	0.181	−0.000	0.002	−0.001
D172	IC4021	0.51±0.03	19.02±0.10	0.10	0.107	0.000	−0.003	0.002
D173	···	0.53±0.05	19.52±0.19	0.26	0.385	0.034	0.028	0.001
D174	IC4012	0.33±0.04	18.23±0.14	0.16	0.220	0.002	−0.002	0.002
D175	NGC4883	0.84±0.02	19.91±0.08	0.20	0.245	0.012	0.005	−0.002
D176	···	0.49±0.03	18.98±0.11	0.43	0.509	0.045	0.034	−0.002
D177	···	0.56±0.04	19.98±0.13	0.34	0.394	0.018	0.000	−0.003
D179	NGC4865	0.71±0.02	18.77±0.06	0.41	0.512	0.016	0.008	0.000
D180	···	1.26±0.04	22.11±0.11	0.06	0.057	0.004	0.000	0.001
D181	···	0.51±0.03	19.45±0.13	0.24	0.534	0.147	0.123	−0.022
D190	···	0.63±0.02	18.96±0.08	0.52	0.649	0.103	0.073	−0.014
D191	···	0.36±0.04	18.95±0.14	0.41	0.598	0.071	0.062	−0.004
D192	···	0.77±0.03	20.15±0.12	0.74	0.768	0.098	0.077	−0.032
D193	···	0.62±0.03	20.04±0.12	0.17	0.151	−0.004	−0.005	−0.004
D194	NGC4860	0.93±0.02	19.64±0.07	0.15	0.171	0.004	0.002	0.001
D197	IC3943	0.67±0.02	19.24±0.08	0.48	0.595	0.057	0.044	−0.007
D198	···	0.78±0.04	20.76±0.12	0.40	0.411	0.035	0.028	0.003
D199	NGC4851	0.81±0.03	20.20±0.10	0.32	0.313	0.028	0.012	−0.004
D200	···	0.30±0.03	17.90±0.13	0.36	0.512	0.096	0.072	−0.006
D204	···	0.78±0.04	20.42±0.15	0.22	0.254	0.008	0.007	0.000
D206	NGC4895	1.00±0.02	19.86±0.06	0.58	0.614	0.041	0.014	0.011
D207	···	0.60±0.03	19.66±0.12	0.29	0.347	0.019	0.006	−0.002
D209	···	1.14±0.04	21.80±0.11	0.56	0.532	0.011	0.005	−0.004
D210	···	0.59±0.03	19.26±0.11	0.22	0.126	0.018	0.005	−0.002
D212	···	1.01±0.03	21.04±0.09	0.50	0.455	0.014	0.007	−0.002
D217	NGC4881	1.04±0.03	20.24±0.11	0.04	0.043	0.002	0.002	−0.001
D218	···	0.78±0.02	19.61±0.08	0.41	0.478	0.022	0.016	−0.003
D229	···	0.81±0.04	20.73±0.14	0.21	0.212	−0.012	−0.005	0.000
D230	···	0.89±0.02	19.72±0.06	0.40	0.434	0.011	0.006	−0.003
D231	···	0.49±0.03	18.74±0.12	0.39	0.395	0.019	0.015	0.001
D232	NGC4896	1.07±0.02	20.49±0.07	0.44	0.436	0.012	0.009	0.000
D238	···	0.40±0.03	18.94±0.11	0.20	0.216	0.017	0.011	0.002
D239	NGC4841B	0.93±0.03	19.88±0.09	0.04	0.035	0.005	0.001	0.001
D240	NGC4841A	1.25±0.02	20.39±0.07	0.16	0.167	−0.007	−0.004	0.000
D242	···	0.60±0.03	19.69±0.11	0.34	0.391	0.014	0.005	0.008

NOTE.— Galaxy IDs from Dressler (1980b). All data from JF94. $\log r_e$, $<\mu>_e$, and ε_e are the seeing corrected values given by JFK95a. r_e is in arcsec. Typical uncertainties on ε_e, $\varepsilon_{21.85}$, c_4, $<c_4>$, and $<c_6>$ are 0.006, 0.007, 0.004, 0.004, and 0.004, respectively; see also JF94.

TABLE D.2
Coma Global Spectroscopic Parameters

Galaxy		$cz_{\rm hel}$	log σ	Mg_2	< Fe >
D 13	···	5699	2.255±0.025	0.258±0.007	2.39± 0.23
D 15	···	4859	1.878±0.048	0.117±0.008	1.50± 0.28
D 20	···	7051	2.068±0.024	0.231±0.007	2.62± 0.22
D 23	NGC4842B	7261	2.175±0.034	0.255±0.009	2.62± 0.28
D 24	···	7455	2.347±0.033	0.305±0.013	··· ···
D 27	···	7825	1.997±0.022	0.264±0.013	··· ···
D 30	NGC4842A	7322	2.272±0.029	0.298±0.008	2.74± 0.24
D 31	NGC4839	7454	2.406±0.017	0.312±0.006	2.60± 0.22
D 33	···	5579	2.262±0.030	0.269±0.007	2.21± 0.23
D 39	···	5907	2.112±0.024	0.253±0.007	3.06± 0.23
D 42	···	6031	2.136±0.026	0.260±0.008	2.96± 0.24
D 43	NGC4853	7718	2.115±0.035	0.163±0.006	1.69± 0.21
D 46	NGC4840	5996	2.370±0.033	0.323±0.013	··· ···
D 49	NGC4926	7834	2.413±0.015	0.315±0.007	2.69± 0.27
D 57	···	8375	2.225±0.036	0.275±0.013	··· ···
D 58	NGC4854	8062	2.263±0.021	0.313±0.013	··· ···
D 62	···	8341	2.124±0.035	0.169±0.008	2.08± 0.27
D 65	···	6172	2.079±0.036	0.261±0.013	··· ···
D 67	···	6033	2.187±0.036	0.286±0.013	··· ···
D 68	IC3963	6812	2.129±0.036	0.278±0.013	··· ···
D 69	IC3959	7059	2.297±0.015	0.306±0.007	3.11± 0.25
D 70	IC3957	6364	2.180±0.025	0.296±0.013	··· ···
D 72	IC3947	5677	2.142±0.022	0.282±0.013	··· ···
D 75	···	6168	1.852±0.032	0.220±0.008	2.29± 0.26
D 78	NGC4923	5446	2.286±0.017	0.309±0.013	··· ···
D 79	NGC4919	7341	2.277±0.019	0.276±0.006	3.05± 0.18
D 80	···	6708	1.997±0.026	0.238±0.007	2.78± 0.23
D 81	···	5976	2.171±0.022	0.269±0.013	··· ···
D 84	···	6562	2.117±0.027	0.262±0.009	3.46± 0.27
D 87	···	7748	1.901±0.025	0.234±0.013	··· ···
D 88	IC3976	6838	2.418±0.036	0.327±0.013	··· ···
D 91	IC3946	5923	2.327±0.027	0.271±0.008	2.49± 0.24
D 92	···	7149	2.217±0.026	0.254±0.007	2.94± 0.23
D 93	···	6063	2.140±0.025	0.251±0.007	2.99± 0.22
D 98	···	6846	2.184±0.036	0.275±0.013	··· ···
D101	···	8062	2.118±0.036	0.278±0.013	··· ···
D103	IC3973	4717	2.337±0.036	0.308±0.013	··· ···
D104	NGC4875	8016	2.278±0.036	0.299±0.013	··· ···
D105	NGC4869	6787	2.313±0.025	0.321±0.013	··· ···
D106	···	5114	2.219±0.036	0.250±0.013	··· ···
D107	···	6429	1.838±0.025	0.238±0.013	··· ···
D108	···	6406	2.082±0.036	0.281±0.013	··· ···
D109	IC3960	6559	2.261±0.036	0.345±0.013	··· ···
D110	···	6969	2.090±0.044	0.249±0.014	2.77± 0.42
D111	···	5885	2.195±0.021	0.295±0.007	2.83± 0.20
D116	···	8414	2.132±0.036	0.256±0.013	··· ···
D118	NGC4906	7486	2.227±0.025	0.310±0.013	··· ···
D119	···	6965	2.204±0.036	0.289±0.013	··· ···
D120	NGC4898B	6371	2.151±0.025	0.264±0.013	··· ···
D121	NGC4898A	6869	2.308±0.025	0.275±0.013	··· ···
D122	NGC4894	4623	1.975±0.036	0.235±0.013	··· ···
D123	···	7728	1.979±0.030	0.224±0.008	2.45± 0.26
D124	NGC4876	6658	2.261±0.025	0.251±0.013	··· ···
D125	···	6898	2.231±0.025	0.273±0.013	··· ···
D128	···	8001	2.037±0.036	0.259±0.013	··· ···
D129	NGC4874	7206	2.415±0.016	0.310±0.007	3.17± 0.23
D130	NGC4872	7204	2.328±0.025	0.305±0.013	··· ···
D131	NGC4871	6757	2.243±0.036	0.290±0.013	··· ···
D132	···	7683	2.122±0.036	0.272±0.013	··· ···
D133	NGC4867	4807	2.350±0.025	0.312±0.013	··· ···
D135	···	8320	1.901±0.033	··· ···	··· ···
D136	···	5653	2.184±0.017	0.280±0.013	··· ···
D137	NGC4850	5995	2.227±0.022	0.272±0.013	··· ···
D143	IC4051	4981	2.344±0.018	0.332±0.006	2.89± 0.20
D144	IC4042	6363	2.228±0.036	0.283±0.013	··· ···
D145	IC4041	7070	2.142±0.036	0.292±0.013	··· ···
D146	···	7585	2.039±0.036	0.255±0.013	··· ···
D147	···	7728	1.993±0.028	0.223±0.007	3.23± 0.23
D148	NGC4889	6458	2.608±0.014	0.354±0.005	3.37± 0.17
D150	IC4011	7234	2.027±0.025	0.285±0.013	··· ···
D151	NGC4886	6349	2.178±0.017	0.253±0.013	··· ···
D152	IC3998	9403	2.210±0.036	0.281±0.013	··· ···
D153	···	6665	2.132±0.025	0.285±0.013	··· ···

TABLE D.2—*Continued*

Galaxy		$cz_{\rm hel}$	$\log\sigma$	$\rm Mg_2$	< Fe >
D155	NGC4873	5798	2.193±0.036	0.292±0.013	··· ···
D156	···	6665	2.001±0.022	0.235±0.013	··· ···
D157	···	6082	2.118±0.036	0.260±0.013	··· ···
D159	NGC4864	6812	2.297±0.025	0.290±0.013	··· ···
D160	IC3955	7642	2.276±0.036	0.309±0.013	··· ···
D161	···	7254	2.242±0.022	0.306±0.013	··· ···
D167	NGC4908	8712	2.325±0.036	0.274±0.013	··· ···
D168	IC4045	6944	2.328±0.025	0.310±0.013	··· ···
D170	IC4026	8152	2.164±0.036	0.298±0.013	··· ···
D172	IC4021	5717	2.204±0.025	0.304±0.013	··· ···
D173	···	7504	2.156±0.036	0.296±0.013	··· ···
D174	IC4012	7225	2.257±0.025	0.296±0.013	··· ···
D175	NGC4883	8132	2.252±0.036	0.306±0.013	··· ···
D176	···	6902	2.225±0.036	0.291±0.013	··· ···
D177	···	5619	2.016±0.036	0.265±0.013	··· ···
D179	NGC4865	4589	2.388±0.036	0.294±0.013	··· ···
D180	···	7834	2.116±0.031	0.232±0.007	2.62± 0.23
D181	···	6059	2.170±0.036	0.257±0.013	··· ···
D190	···	5821	2.294±0.021	0.286±0.007	3.42± 0.20
D191	···	6612	1.965±0.036	0.256±0.013	··· ···
D192	···	5423	1.975±0.036	0.231±0.013	··· ···
D193	···	7541	2.081±0.025	0.269±0.013	··· ···
D194	NGC4860	7934	2.390±0.017	0.347±0.013	··· ···
D197	IC3943	6821	2.262±0.023	0.276±0.007	3.02± 0.22
D198	···	6707	1.973±0.034	0.199±0.009	2.73± 0.29
D199	NGC4851	7895	2.128±0.026	0.249±0.007	2.80± 0.23
D200	···	7495	2.267±0.016	0.283±0.004	2.74± 0.13
D204	···	7667	2.102±0.033	0.272±0.013	··· ···
D206	NGC4895	8525	2.346±0.036	0.301±0.013	··· ···
D207	···	6764	2.187±0.017	0.258±0.006	2.97± 0.22
D209	···	7202	1.968±0.027	0.215±0.007	2.54± 0.23
D210	···	7245	2.225±0.033	0.274±0.013	··· ···
D212	···	8211	2.081±0.029	0.259±0.008	2.98± 0.26
D217	NGC4881	6705	2.314±0.017	0.299±0.013	··· ···
D218	···	8048	2.298±0.025	0.259±0.008	2.70± 0.25
D229	···	6941	2.008±0.033	0.214±0.009	2.73± 0.29
D230	···	7672	2.235±0.023	0.276±0.007	3.15± 0.21
D231	···	7928	2.106±0.025	0.261±0.007	2.68± 0.22
D232	NGC4896	5986	2.188±0.026	0.284±0.007	2.75± 0.22
D238	···	7339	2.013±0.022	0.240±0.013	··· ···
D239	NGC4841B	6527	2.304±0.019	0.289±0.007	2.91± 0.27
D240	NGC4841A	6765	2.412±0.017	0.315±0.006	2.69± 0.20
D242	···	7622	2.147±0.025	0.223±0.006	2.91± 0.20

NOTE.— Galaxy IDs from Dressler (1980b). $\log\sigma$ and $\rm Mg_2$ from Davies et al. (1987), Dressler (1987), Lucey et al. (1991b), and Guzmán et al. (1992) as compiled into a consistent system by JFK95b, and from Jørgensen (1997b, in prep.). < Fe > from Jørgensen (1997b, in prep.). The uncertainties on $\log\sigma$ and $\rm Mg_2$ for the data *not* from JFK95b and Jørgensen (1997b, in prep.) are based on the mean uncertainties quoted by the respective references.